

Optical atomic clocks

N. POLI⁽¹⁾, C. W. OATES⁽²⁾, P. GILL⁽³⁾ and G. M. TINO⁽¹⁾(*)

⁽¹⁾ *Dipartimento di Fisica e Astronomia and LENS, Università di Firenze*

INFN Sezione di Firenze, Via Sansone 1, 50019 Sesto Fiorentino (Firenze), Italy

⁽²⁾ *National Institute of Standards and Technology, Time and Frequency Division, MS 847, Boulder, CO 80305, USA*

⁽³⁾ *National Physical Laboratory (NPL), Teddington, Middlesex TW11 0LW, United Kingdom*

(ricevuto ?)

Summary. —

In the last ten years extraordinary results in time and frequency metrology have been demonstrated. Frequency-stabilization techniques for continuous-wave lasers and femto-second optical frequency combs have enabled a rapid development of frequency standards based on optical transitions in ultra-cold neutral atoms and trapped ions. As a result, today's best performing atomic clocks tick at an optical rate and allow scientists to perform high-resolution measurements with a precision approaching a few parts in 10^{18} . This paper reviews the history and the state of the art in optical-clock research and addresses the implementation of optical clocks in a possible future redefinition of the SI second as well as in tests of fundamental physics.

PACS 06.30.Ft – Time and frequency.

PACS 06.20.fb – Frequency standards.

PACS 37.10.Jk – Optical cooling and trapping of atoms.

PACS 37.10.Ty – Ion trapping.

1. – Introduction

The optical atomic clock, that is, a laser whose frequency is stabilized relative to that of an optical atomic transition, represents a revolutionary step forward in the evolution of atomic frequency and time standards [1, 2, 3]. For more than 60 years atomic frequency standards have played a critical role in basic science, precision measurements, and technical applications. During this period, the increasing need for more precise timing and synchronization, for a range of applications including navigation systems [4], telecommunications, VLBI telescopes [5], and tests of fundamental physics [6] has demanded

(*) corresponding author: Guglielmo.Tino@fi.infn.it

oscillators with higher frequencies and higher performance. Because of the experimental difficulties in counting high optical frequencies (several hundreds of terahertz in the infrared/visible domains), atomic and molecular optical standards have long been used mainly as length standards, but only rarely as frequency references [7]. Before the advent of optical frequency combs, the measurement of absolute optical frequencies was, in fact, a formidable task, requiring resources available only at large-scale laboratories [8, 9, 10, 11, 12].

However, recent advances in the field of femto-second laser technology, with the introduction of optical frequency combs, have enabled the possibility to cover in a single step the gap between optical frequencies and countable microwave frequencies [10, 13, 14]. As a result, the field of optical frequency metrology has, in some sense, become possible. Driven also by recent tremendous progress in the fields of atom manipulation and precise optical frequency control, the field of optical atomic clocks has, over the past decade, become a hot research topic. There are now dozens of labs worldwide working on various versions of optical atomic systems, based on neutral atoms or single trapped ions, and optical clocks have already significantly surpassed their microwave counterparts in terms of clock performance. Neutral atom-based and ion-based clocks each have their own advantages; neutral atom clocks benefit from their large signal-to-noise ratio due to large atom numbers, while single-ion clocks “tick” in a pristine environment, extremely well-isolated from external perturbations [3]. In fig. 1 we see that there has been a tremendous amount of activity and improvement in the field of optical standards, including both neutral atom and ion clock systems. The uncertainty in the ticking frequency of these standards (red circles) has been reduced by three orders of magnitude in a little more than a decade of research to the point where the best sources have absolute uncertainties below one part in 10^{17} , more than an order of magnitude below that of the best Cs microwave clocks (blue dots) that presently define the SI second. Additionally, there is spin-off research underway (especially that based on fs-laser combs), which takes advantage of much of the technology that was first developed with optical atomic clocks in mind. We emphasize, however, that optical clocks are still primarily research projects, less mature than Rb and Cs microwave standards, which regularly deliver time to the Bureau International des Poids et Mesures (BIPM).

In this review article, we will describe the science behind the explosion of activity and progress shown in fig. 1 for the field of optical atomic clocks, beginning with the physics that describes the inherent advantages of working at optical frequencies, followed by a description of the three key technologies that have revolutionized this field. We will then outline the physics that drives the design and ultimately limits the performance of optical atomic clocks, following this with a series of concrete examples of some of the most successful clock systems. To highlight the possibilities enabled by this new frequency/timing technology, we conclude with a description of how these clocks can be connected to the outside world, the applications these clocks could enable, and how such clocks may even one day be put in space to take advantage of a micro-gravity environment [18].

2. – The Optical Clock Revolution

At the heart of any good clock is a regular oscillatory phenomenon, whether it be the swinging of a pendulum, the spring-driven oscillations of a watch, or the voltage-driven oscillations of a quartz crystal. However, mechanical timepieces tend to be quite susceptible to environmental effects such as temperature changes, although ingenious

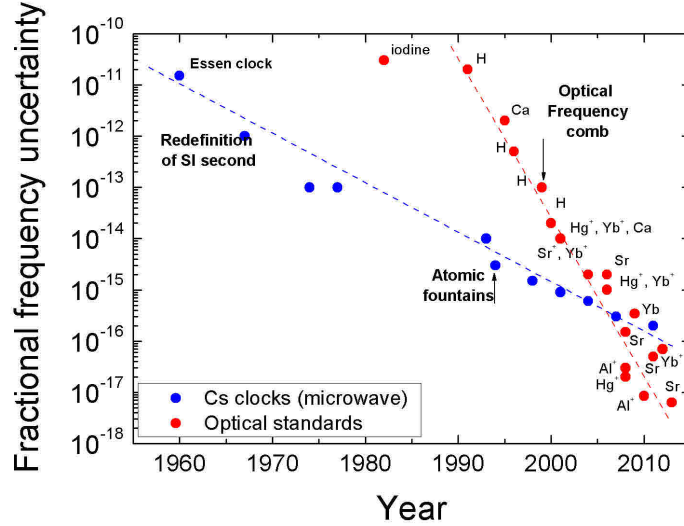


Fig. 1. – Evolution of fractional frequency uncertainties of atomic frequency standards based on microwave (Cs clocks)[15] and optical transitions. A fractional frequency uncertainty in the 10^{-18} region have been reported for two optical clocks respectively, the $^{27}\text{Al}^+$ single ion clock at NIST [16] and the ^{87}Sr optical lattice clock at JILA [17].

designs have led to some remarkable devices. Still the best performing clocks are those that use carefully chosen atomic transitions to steer the frequency of the oscillator. A typical atomic clock consists of an oscillator, either microwave or optical (*i.e.*, a laser) whose frequency is forced to stay fixed on that of an atomic resonance (see fig. 2). One of the most important parameters describing such a resonance is the atomic line quality factor, Q , defined as the ratio of the absolute frequency ν_0 of the resonance to the linewidth of the resonance itself $\Delta\nu$.

As we shall see, such resonances can have line Q 's many orders of magnitude higher than the best mechanical systems, and they can be isolated from environmental effects to a much higher degree. Atomic clocks have the added benefit that atoms are universal, in the sense that multiple clocks based on the same atomic transition should have the same oscillation frequency, thereby offering a degree of reproducibility not possible with mechanical devices.

For these reasons, atomic clocks have ruled the ultra-high precision timing world for the past 50 years or so. The famous 9.19 GHz hyperfine transition in Cs has served to define the SI second since 1967, and as we see in fig. 1, the absolute fractional frequency uncertainty for this transition has been reduced by about a factor of ten every decade. We emphasize that this remarkable rate of progress should not be taken lightly, as it has been the result of dedicated efforts and several ingenious advances, particularly in terms of atomic manipulation via laser cooling techniques. However, the present day state-of-the-art Cs fountain [19], which uses clouds of laser-cooled atoms that are tossed vertically through an interaction region, is nearing its practical limitations (astoundingly, the best Cs systems are approaching uncertainties of 10^{-16} with a system whose line Q is

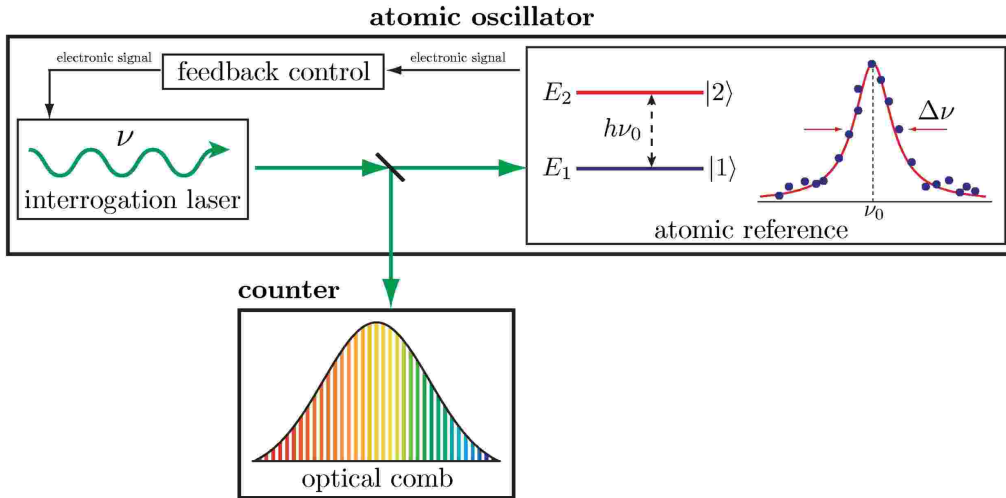


Fig. 2. – Schematic view of an optical atomic clock: the local oscillator (laser) is resonant with the atomic transition. A correction signal is derived from atomic spectroscopy that is fed back to the laser. An optical frequency synthesizer (optical frequency comb) is used to divide the optical frequency down to countable microwave or radio frequency signals.

only 10^{10}). For timing advances to continue to move forward, however, a new technology is required, and this is where optical clocks have come to the forefront.

To understand the advantage of going to a higher-frequency clock, we must first examine more explicitly what it means for a clock to be good. There are two principal characteristics that we consider when evaluating state-of-the-art clocks: stability and uncertainty. Stability is a measure of the precision with which we can measure a quantity (think of how widely scattered a group of arrows fired at target might be), and is usually stated as a function of averaging time since for many noise processes the precision increases (*i.e.*, the noise is reduced through averaging) with more measurements. The stability is usually set by the combination of the inherent frequency purity of the physical system (*e.g.*, the line Q) and the signal-to-noise ratio with which we can measure the system. In contrast, the (absolute) uncertainty for an atomic clock tells us how well we understand the physical processes that can shift the measured frequency from its unperturbed (“bare”), natural atomic frequency (think of how off-centre our group of arrows might be). Small absolute uncertainty is clearly an essential part of a good primary frequency standard and requires extensive evaluation of all known physical shifts (usually called “systematic effects”). We note that in order to be able to compare clocks with different oscillation frequencies fairly, we usually express the two main clock parameters, namely, stability (or its inverse, instability, as is commonly used in clock comparisons) and the absolute uncertainty, in fractional units.

With this understanding of the two essential clock properties, we can now understand the advantages inherent in moving from the microwave to the optical domain. Let us first consider the formula for clock instability, σ_y , in the regime where it is limited by fundamental (as opposed to technical) noise sources, such as atomic statistics based on

the number of atoms [20],

$$(1) \quad \sigma_y(\tau) \approx \frac{\Delta\nu}{\nu_0\sqrt{N}} \sqrt{\frac{T_c}{\tau}},$$

where $\Delta\nu$ is the spectroscopic linewidth of the clock system, N is the number of atoms or ions used in a single measurement, T_c is the time required for a single measurement cycle, and τ is the averaging period (see for example, [7]). This formula can be understood fairly intuitively, as $\Delta\nu/\nu_0$ is the inverse of the measured line Q , and the remaining terms combine to yield the signal-to-noise ratio as a function of averaging period. As expected, the instability is reduced for narrower lines ($\Delta\nu$) and shorter measurement cycles, and also benefits from a higher signal-to-noise ratio (\sqrt{N} , known as the atomic projection noise [20]). Moreover, in this projection-noise regime, which may extend from seconds to hours or even days and longer, the stability of the clock improves as the square root of the averaging period, as in the case of Gaussian noise processes. However, the term that is most relevant for this discussion is the appearance of ν_0 , the oscillator frequency, in the denominator, which states that fractionally it is advantageous to run a clock at higher frequencies. Alternatively, this can be thought of in terms of line Q , for which optical systems have demonstrated values as high as 10^{15} , five orders of magnitude higher than analogous microwave systems, giving optical clocks a tremendous advantage in terms of potential short-term and long-term frequency stability. From eq. 1, we see that for a transition linewidth, $\Delta\nu$, of 1 Hz, measured in an atomic sample of only 10,000 atoms, we can envision fractional instabilities as low as 10^{-17} in 1 second of averaging time, many orders of magnitude better than in other existing (non-optical) systems.

In terms of absolute frequency uncertainty, the second important clock characteristic, the advantages of the optical atomic clocks cannot be summarized in a single formula. Rather it is necessary to evaluate the systematic effects for different transitions and see how they compare with other optical and microwave clocks. However, the greatly enhanced stability possessed by optical systems enables the evaluation of the systematic effects much more rapidly and/or to a much higher precision, thereby enabling reduced uncertainty budgets. The most stable optical clock systems can presently measure shifts at the 1 part in 10^{17} level in less than an hour [21], while the best microwave systems would take ten days or more, almost prohibitively long to evaluate clocks systematics at this level.

While the inherent stability advantage of optical clocks was experimentally demonstrated quite early in the brief history of optical clock research, the absolute uncertainty took longer to catch up and surpass that of its microwave counterparts, principally because of the more painstaking nature of systematic uncertainty evaluations. However, as we see in fig. 1, around the turn of the millenium, the uncertainty of optical sources rapidly decreased, culminating in the landmark 2008 demonstration by the ion clock group at NIST, where they achieved fractional absolute uncertainties for the Al^+ and Hg^+ clocks of about one part in 10^{17} [6]. More recently, a neutral Yb lattice clock demonstrated a fractional instability (not uncertainty) of 1.8×10^{-18} for 25,000 s of averaging time [21]. As we will see in subsequent sections, many other optical clock systems are also now rapidly approaching this level, as this field continues to expand. So what happened around the year 2000? The short answer is that the femtosecond-laser frequency combs showed up on the scene, thereby providing the field of optical frequency metrology with an essential and long-awaited tool. A fuller answer would recognize that at the same

time optical frequency standards were also beginning to mature dramatically due to significant advances in laser stabilization and atom manipulation capabilities. Thus, these more precise optical standards were well primed to take full advantage of the possibilities enabled by the new optical frequency measuring devices. Let us now consider in more detail the three critical experimental capabilities that led to the revolutionary advances depicted in fig. 1; in this way we will be able to understand not only how these new timing devices have come so far, so quickly, but also how much further they might be able to go in the future.

3. – Key technologies for optical atomic clocks

3.1. Optical frequency synthesizers. – For many years the biggest unknown in the field of optical frequency standards and clocks was how to measure optical frequencies. The oscillations of the electric field for visible frequencies are too fast ($\sim 10^{15}$ per second) to detect directly, so there was no way to measure the absolute frequency of the optical clocks (*i.e.*, relative to the SI second defined by Cs) and no way to compare them to other clocks in the optical or microwave domains. There were a few heroic efforts to connect specific optical frequencies to the microwave domain through an array of phase-locked oscillators spanning many decades of the frequency spectrum [8, 9, 10, 11, 12]. What was needed instead was a more general and flexible solution to this problem. Nonetheless, many groups proceeded with their development of stable, accurate, optical sources, with the hope that one day this problem would be solved. Indeed in 1999, efforts in Th. Hänsch’s group and in J. Hall’s group basically solved this problem by developing methods to stabilize mode-locked femtosecond-lasers to such a high degree that they could play the role of a frequency divider with such versatility that one could use it to connect optical frequencies both to other parts of the optical spectrum and to the microwave domain [13, 22, 23]. For their efforts Th. Hänsch and J. Hall shared the Nobel Prize in 2005, a tribute to the significance of this technique [2, 1].

To see how a pulsed laser could perform the remarkable feat of linking the optical and microwave domains, let us first observe that a pulsed laser indeed contains frequencies in both domains (see fig. 3). The light is visible, but the repetition rate of the pulses occurs typically in the 100 MHz to 1 GHz regime. Thus, the trick here is to find some way to phase-lock the microwave repetition rate to the optical frequencies contained in the output spectrum. In fact, the method for doing this becomes clear when we consider the frequency spectrum for a femtosecond-laser. The Fourier transform for a regular sequence of pulses in time is simply a series (“comb”) of discrete visible frequencies (called “teeth”) spaced by the repetition rate. The range of frequencies is determined by the output spectrum of the laser, which is in turn determined by essential laser parameters such as the gain curve for the laser medium, the laser cavity mirrors, the laser pump source and intensity, etc. We can describe the resulting values, f_n , in the frequency “comb” with just two laser-based parameters: $f_n = f_o + n \times f_r$, where n is an integer (or mode number), f_o is the effective offset of the comb from zero frequency (physically, it results from the pulse-to-pulse phase shift of the light pulse relative to its pulse envelope), and f_r is the laser repetition rate.

Thus, simply stabilizing f_o and f_r then stabilizes the frequencies of all the visible modes as well as the microwave repetition rate. In order to stabilize these two parameters it is necessary to measure these quantities with sufficient precision and use feedback loops to control specific laser characteristics [23]. For f_o , it is customary to generate the feedback error signal by comparing one part of the comb to another. This is most

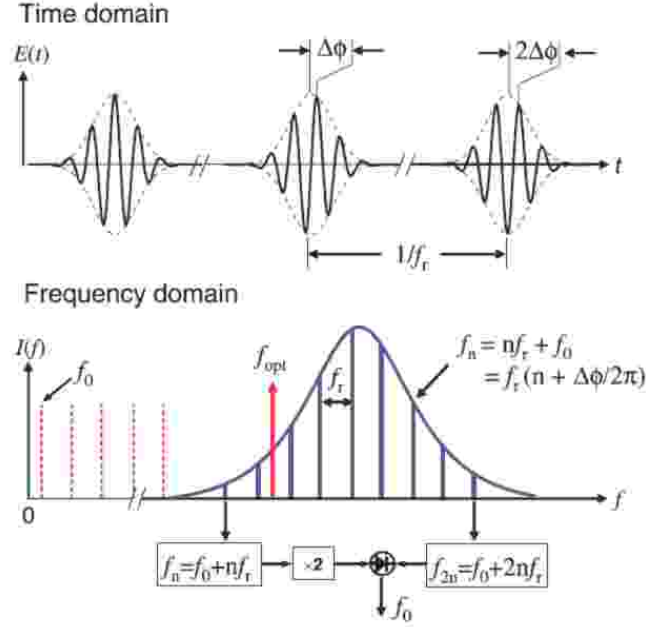


Fig. 3. – Representation of the output of a mode-locked femtosecond laser in time and frequency-domain. The frequency of emission of the pulses is f_r and due to dispersion in the laser cavity, the carrier advances with respect to the envelope by $\Delta\phi$ from one pulse to the next. In the frequency domain, the result of this phase slip is an offset common to all modes of $f_o = f_r\Delta\phi/(2\pi)$. $f - 2f$ technique for comb self-referencing is also shown. [7].

easily understood and readily accomplished by achieving a comb spectrum that spans a full octave. In this case, we can use nonlinear optics techniques (*e.g.*, a frequency-doubling crystal) to double the low-frequency end ($n \sim n_0$) of the comb and then beat it against the high frequency ($n \sim 2n_0$). The resulting beatnote will occur at the frequency difference, f_d , and is simply:

$$(2) \quad f_d = 2(f_o + n_0 \times f_r) - (f_o + 2n_0 \times f_r) = f_o.$$

The challenge, of course, is to generate a full octave (or a significant fraction thereof) directly out of the laser. Thus lasers with very short (femtosecond) pulses are desirable due to their broad output spectra, but still it is often necessary to complete the octave by passing the femtosecond-laser output through a highly nonlinear microstructure fibre [24], which can significantly expand the laser spectrum. An f_o error signal can then be generated by comparing the beatnote frequency to that of a stable microwave frequency (note that since the noise from this reference oscillator maps directly into the optical signal, it is fractionally reduced by 4 to 5 orders of magnitude, thereby reducing the requirements for the reference oscillator). The frequency of f_o can be then controlled in different ways such as through the pump laser power. For f_r , it is straightforward to measure the repetition rate directly with a photodetector and then generate an error

signal by comparing it with a stable microwave frequency. We can use the resulting signal to stabilize the repetition rate by feeding back to a parameter that controls the cavity length (*e.g.*, the position of a cavity mirror). However, in this case, the noise from the microwave reference is multiplied when we look at signals in the optical domain. Instead, the usual configuration for optical clocks is to generate the f_r error signal by superimposing light from the frequency comb with light from a stable optical clock frequency on a photodetector. If f_o is stabilized as described above, then forcing the comb repetition rate to keep the comb-clock beatnote fixed to a microwave reference frequency will fix f_r and the entire comb. In this way the stability of the optical source can be transferred to every comb tooth and the comb's repetition rate with a fidelity that has been confirmed to one part in 10^{19} [25].

Thus the formidable problem of measuring absolute optical frequencies and comparing optical and microwave frequencies is elegantly solved by the use of a single, stabilized, pulsed laser. Moreover, optical sources with very different frequencies can be compared directly by locking the comb to one source and measuring the beatnote between the other source and the comb tooth closest to it in frequency (see for example, [26]). Soon after the first demonstrations of stabilized frequency combs around 2000, these lasers became the standard tools in frequency standards labs for providing the clockwork. Not surprisingly, it turns out that a stabilized frequency comb also has very regular pulses in the time domain. As a result, there has been an explosion of new applications for frequency combs that have been developed in the past decade for use in both the time and frequency domains including the calibration of astronomical spectrographs for exoplanet searches, the generation of the world's lowest-noise microwaves, time-resolved femtosecond and attosecond spectroscopy, and precision mid-infrared spectroscopy (see [27] and references therein). In a similar way, there has been tremendous progress in the development of new femtosecond-laser frequency comb sources beyond the initial systems, which were Ti:Sapphire based, including compact fibre-based systems, and now even whispering-gallery mode-based "micro-combs" (for a review of this emerging field, see [28]).

3'2. Laser cooling and trapping of neutral atoms and single ions. – As we will see in more detail in sect. 4, the thermal motion of the atoms and ions used in optical atomic clocks presents tremendous challenges for clock scientists, because the effects are intrinsically enormous for the scale on which they operate. Room-temperature atoms can have a velocity distribution that yields Doppler shifts of 1 GHz or more - twelve orders of magnitude larger than the millihertz uncertainties towards which optical clock scientists aspire. As a result, the reduction and control of these effects have had a huge impact on the design of optical atomic clock systems. While various "sub-Doppler" techniques have been developed to resolve atomic resonances much narrower than those of the Doppler distributions, these methods were still plagued with shifts at the kilohertz level or more [29]; additionally, the second-order Doppler effect (associated with relativistic "time dilation" effects) approaches 1 kHz at room temperature, and so exquisite knowledge of the atomic velocity distribution is required to characterize this effect at the sub-hertz level [30]. Instead, through the past three decades or so, scientists have developed an array of tools using lasers and electric and/or magnetic fields to cool and trap atoms to very tight volumes with temperatures as low as 1 μ K and even below (see [31, 32, 33] and references therein). These techniques have led to amazing advances in atomic physics, including the generation of Bose-Einstein condensates [34] and ultracold Fermi gases [35], the trapping/cooling of molecules [36, 37], and a host of fundamental physics experiments

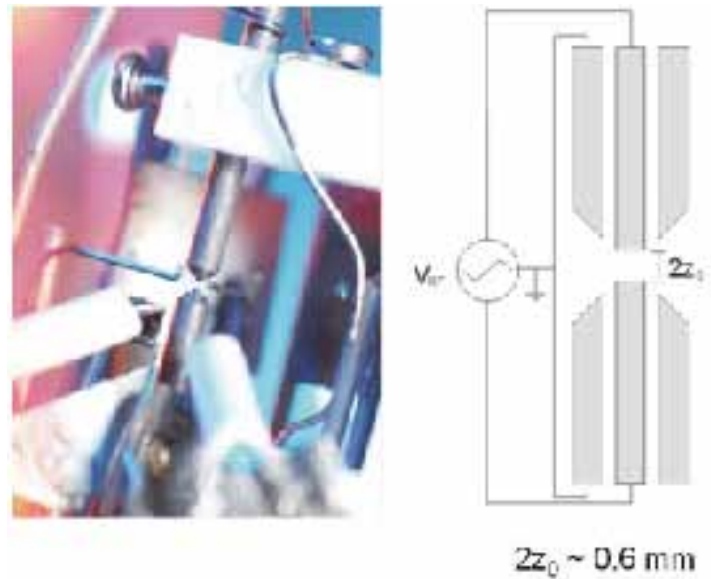


Fig. 4. – A typical single ion end-cap trap employed in high resolution clock spectroscopy (courtesy of National Physical Laboratory - NPL).

using clouds of atoms as quantum sensors.

Many of these techniques were first demonstrated with trapped ions, due to the long interaction periods and the exquisite control that the ion systems afford [38]. Due to their non-zero electric charge, ions can be trapped with oscillating electric fields (it turns out that static configurations cannot work for charge-free regions). There are several basic designs for ion traps, all of which use some combination of static and radio-frequency fields. Once confined in the trap, an ion can be cooled, that is, have its velocity reduced by illuminating it with laser light tuned just below (red) of a strong resonance. In this way, the ion preferentially absorbs momentum from the laser whose direction opposes its motion, and its velocity is reduced to the point where it fluctuates around zero velocity (see [39] for an early review of laser cooling with trapped ions). Trapped ions are now routinely cooled to temperatures of a few millikelvin, putting the ion predominantly in its motional ground state (see fig. 4). As a result the Doppler effects are not only reduced, but in fact the first-order Doppler effect is completely absent in spectroscopic signals. For this “tight confinement” regime (the so-called “Lamb-Dicke” regime [40]), in which the extent of the atomic motion along the probing direction is much less than the wavelength of the probe light, residual motional effects are transferred to spectroscopic sidebands, thereby leaving the carrier virtually unperturbed [41]. For temperatures at the millikelvin level, the residual time dilation effect is fractionally about 10^{-17} , manageable for even the most accurate systems. By about the year 2000, laser cooling techniques were fairly well developed for all existing optical clock systems based on trapped ions. More details on techniques employed in single ion trapping and laser cooling are described in sect. 6.

Because neutral atoms are more difficult to manipulate, it took a little longer (and more effort) to confine them to the required degree. The effects of resonant laser light on atomic motion was first demonstrated in 1982 [43], but it really wasn’t until the late

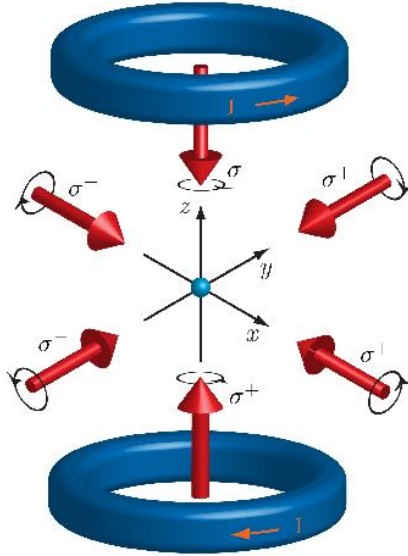


Fig. 5. – Sketch of the Magneto-Optical-Trap (MOT) setup. Three pairs of retro-reflected laser beams cross each others in the center of the trap. A pair of anti-Helmholtz coils provide the necessary quadrupole magnetic field for trapping. The atomic cloud is collected in the center of the trap (adapted from [42]).

1980's that microkelvin temperatures and magneto-optical traps were becoming routine for alkali atoms [44]. Magneto-optical traps for the species of atoms used in neutral atom clocks (*i.e.*, two-electron atoms) were not developed until 1990, due in part to the difficulty of generating tunable and high-power blue lasers required for cooling these atoms [45]. Magneto-optical traps (see fig. 5), which confine atoms through the combination of laser fields and magnetic field gradients, are efficient tools for collecting large samples of cold neutral atoms from background vapors or atomic beams. Typical trap geometries contain three intersecting orthogonal pairs of counter-propagating laser beams tuned just to the red of a strong cycling transition such as the $^1S_0 \rightarrow ^1P_1$ transitions in alkaline-earth and alkaline-earth-like atoms. The region of intersection, the “trapping region”, provides a three-dimensional optical molasses, so-called because the trap always supplies a net force opposing an atom's propagation direction. The addition of a magnetic field gradient (~ 0.6 T/m for alkaline earth atoms), supplied usually by a pair of anti-Helmholtz coils, adds a spatial component to this force, thereby forcing the atoms towards the centre of the trap. In this way, millions of atoms can be collected in a fraction of a second, with a resulting atom temperature of approximately 1 mK. The loading rate can be increased by slowing a portion of the atomic beam velocity distribution before the trapping region in order to accommodate the (usually) fairly low capture velocities of the MOT (~ 10 m/s). Such slowing can simply be accomplished by sending a laser beam counter-propagating to the atomic beam. Usually this beam is red-detuned by several hundred megahertz to compensate the large Doppler shifts of the oncoming atoms and to reduce asymmetry distorting the MOT. More efficient slowing can be accomplished by adding a magnetic field gradient along the atomic beam, designed to keep the atoms

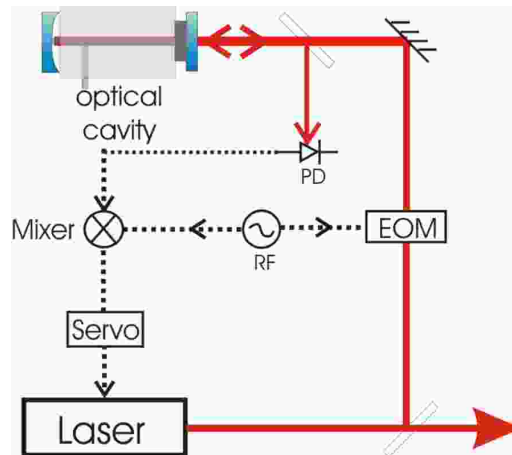


Fig. 6. – Typical scheme used for active laser frequency stabilization to optical resonators (Pound-Drever-Hall). EOM electro-optical modulator, PD photodetector, RF radiofrequency generator.

in resonance with the slowing laser beam throughout the slowing process [46].

Magneto-optical traps, however, do not present a suitable environment for precision clock spectroscopy because the trapping laser beams significantly perturb the clock transition. Additionally magneto-optical traps do not confine atoms sufficiently to reach the Lamb-Dicke regime, so residual Doppler effects still exist, which are at the megahertz level, even for atoms at millikelvin temperature. The solution was to employ optical traps [47] based on red-detuned standing waves of light (termed “optical lattices”), which could be loaded with very cold atoms. The atoms are drawn into the high-intensity regions of the lattice light and oscillate around the standing-wave anti-nodes, in a way similar to that of trapped ions, but with thousands or even millions of atoms confined simultaneously. By tuning the lattice light to a carefully determined wavelength, its effects on well-chosen clock transitions can be minimized [48]. In this way ultra-narrow, minimally perturbed spectra could be generated, and as we shall see, today such lattice clocks are leading the way for neutral atom clock research.

3.3. Frequency stabilization of laser sources. – Pushed by the extreme demands in high precision metrology experiments and optical clocks development, the field of frequency stabilization of laser sources has been undergoing something of a renaissance in recent years. In the early years, efforts in several labs, including those of J. Hall and Th. Hänsch, really tamed the laser through the use of exquisite optical reference cavities, making hertz-level lasers a reality [49] (see fig. 6). An optical cavity consists of a specialized glass spacer that separates two high-reflectivity (often as great as 99.999 %) mirrors that provide extremely sharp resonances that can be used to stabilize the laser on short to medium time scales (e.g., < 10 s). On longer time scales the cavities are subject to thermal and mechanical drifts, and the atomic signals are then needed to provide stable, accurate references. Early cavity research culminated in the benchmark result of J. Bergquist and colleagues in 1999, in which they achieved a laser linewidth of 0.22 Hz by carefully isolating ingeniously-designed cavities from environmental effects [50]. These results stood as the gold standard for more than a decade, despite the fact that many

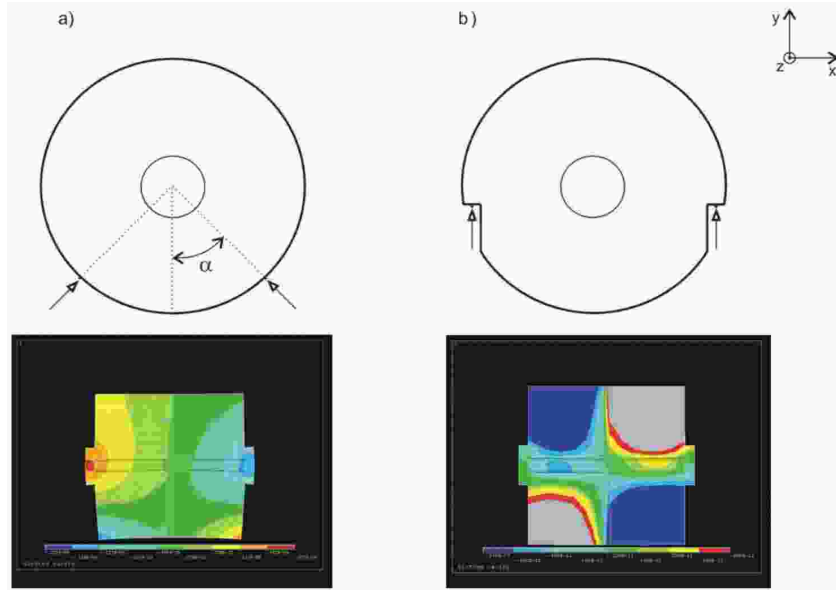


Fig. 7. – Example of FEM static analysis respectively on standard cavity mount in (a) and “slotted” horizontal cavity in (b) (see text for further details). The result of the FEM simulation shows the deformation (in false colours) of the cavity along the optical axis of the cavity due to a constant acceleration along the vertical axis. In case (a) the cavity deformation pushes the two mirrors far apart introducing also a relative tilt of the mirrors. In (b) the effect is compensated thanks to the modified spacer geometry and the optimum choice of supporting points.

scientists strove to push this research further, driven by the needs of the optical clock community and others. However in a paradigm-changing paper in 2004, it was recognized that the specialized cavities that were used to stabilize the lasers were in reality almost all limited by fundamental thermal noise processes in the cavity construction materials themselves [51], and that the cavities used in ref. [50] in fact minimized these effects quite well. As a result, modest improvements have since been achieved by choosing proper spacer and mirror material and carefully designing the cavity shape and spacer supporting points. However, it seems the next generation of cavities will need to use novel crystalline mirror coatings [52] and perhaps need to reduce the thermal noise directly by operating cavities at cryogenic temperatures [53]. Additionally, other approaches are underway as today’s best systems are still chasing the dream of a millihertz laser linewidth [49].

Why do the clocks put such stringent requirements on the laser stability? First, in order to perform spectroscopy at the highest resolutions (*e.g.*, $\Delta\nu < 10$ Hz) needed by many of today’s state-of-the-art clocks, it is necessary to pre-stabilize the probe laser systems. Second and equally important is the fact that in some of today’s state-of-the-art optical atomic clocks (especially those based on large numbers of atoms, for which the atom projection noise, $1/\sqrt{N}$, is low), the laser frequency noise actually determines the clock stability. Think back to Eq. 1, where we saw that optical clocks could enable stabilities at levels approaching 1 part in 10^{17} in a one second averaging period. But there we made the assumption that the clock was limited by fundamental noise sources,

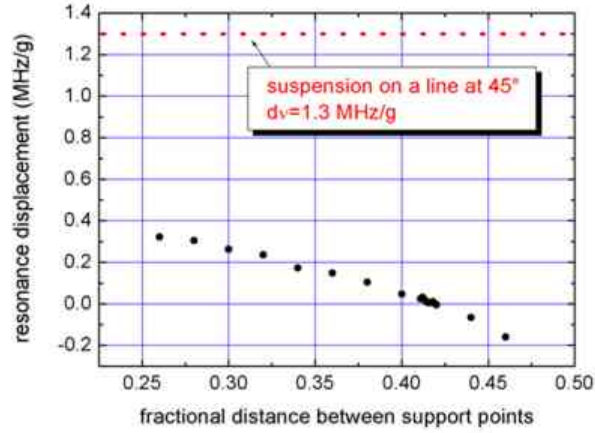


Fig. 8. – Resonance displacement $\delta\nu/\delta a$ for the two cavity geometries in fig. 7 calculated with FEM static analysis as a function of the supporting points position along the optical cavity axis. The support points (*i.e.*, 2 mm \times 2 mm areas) for the “slotted” cavity are chosen in order to reduce the sensitivity. With proper chosen support points, the sensitivity can be reduced by more than a factor of 100. Data from ref. [54].

and that technical noise sources (including laser frequency noise) were reduced below this level. In fact, this turns out to be a fairly ambitious assumption. How the frequency noise limits the atomic clock stability is a subtle issue, because in principle we can correct laser fluctuations with the atom signal-based servo loop. The problem is that the atom signal provides incomplete knowledge of the laser fluctuations because in virtually all clock systems, we can probe the atoms for only a fraction (typically 20 to 50 %) of the measurement cycle (see the descriptions of the various clocks, especially Sr, for more details). The rest of the cycle is spent preparing the atoms and detecting the excitation induced by the probe light. As a result, the clocks suffer from a sort of stroboscopic effect that aliases higher-frequency noise into low-frequency noise on the clock signal. The feedback system cannot null out the noise, effectively setting a limit for clock performance. This stroboscopic effect, known more formally as the Dick effect [55, 56, 57], contributes a noise level that is roughly the square root of the duty cycle times the frequency noise (for white frequency noise). To support a clock that has a 25 % duty cycle with a fractional stability that averages down as $10^{-15}\tau^{-1/2}$ requires a pre-stabilized laser with fractional frequency noise below 10^{-15} at 1 second. Thus for realizing better clocks, one important request is to minimize dead time in the measurement cycle and to reduce the laser frequency noise as much as possible.

While cycle-time optimization is quite system-dependent, laser stabilization is less so, thus it is possible to consider quite generally the challenge of stabilizing lasers at the sub-hertz level. Although most lasers have narrow fundamental (*i.e.*, Schawlow-Townes limited) linewidths, in reality, their outputs are quite broad (kHz-MHz) as a result of technical noise sources, such as vibrations, thermal effects, or noise in the laser pump sources. To reach the hertz level and beyond, it is therefore necessary to measure laser frequency fluctuations and correct them with a feedback loop connected to frequency-changing laser parameters (such as laser mirror position or the current in a diode laser). Measuring such fluctuations on a fast time scale with a high signal-to-noise ratio is a

challenging task. While several techniques have been developed to meet this challenge (*e.g.*, [58]), by far the most commonly used technique is locking the laser frequency to a cavity resonance. These cavities are typically made of ULE (ultra-low expansion) glass to minimize thermal drifts, and then have high-finesse (reflectivity) mirrors attached to either end, usually via optical contacting, again to minimize drifts. For typical spacer lengths of $L = 5$ to 30 cm, we then find a series of identical, sharp resonances, spaced by $c/2L \sim 1$ GHz, with linewidths as narrow as a few kilohertz. The laser is usually locked to the fringe nearest in frequency to the clock resonance and then the remaining gap is bridged with frequency-shifting devices such as acousto-optic or electro-optic modulators.

In order to achieve the highest performance levels, it is necessary to use sensitive techniques for generating the error signal that contains the laser frequency fluctuations relative to the cavity resonance. The preferred technique is to send a small amount of light ($< 100 \mu\text{W}$) to the cavity with modulation sidebands at ~ 20 MHz. We then detect the signal reflected from the input mirror of the cavity. In this way, we find that the error signal contains information on the laser frequency fluctuations for Fourier frequencies below the linewidth of the cavity resonance and laser phase fluctuations for Fourier frequencies higher than this cavity linewidth [59]. Moreover, the high modulation frequency encodes this information at a detection frequency well above that of most technical noise sources. When appropriately demodulated, the detected signal yields a high-bandwidth, high signal-to-noise error signal, which is then filtered and fed to the frequency correction devices. This well-known experimental design, the Pound-Drever-Hall technique, is used in almost all precision laser stabilization systems, and when used carefully (*e.g.*, minimizing effects such as residual amplitude modulation), yields laser stabilization results that are limited only by the reference cavity itself [59, 60, 61]. For this reason, current state-of-the-art research in laser stabilization is really about improving the reference cavities themselves. The goals here are quite extreme when we consider them; hertz-level laser performance requires that the cavity length (which maps proportionally into the laser frequency) be stable to less than 1 fm (about the radius of an atomic nucleus). Nonetheless, this level of performance is possible, but requires that extreme care be taken with both the isolation of the cavity from the surrounding environment and with the material used to construct the cavity itself.

Adequate isolation usually begins with putting the cavity inside an evacuated metal can (often with thermal shields) to minimize sensitivity to refractive index fluctuations in the path between the mirrors. The vacuum apparatus is then usually surrounded with a box that reduces coupling of acoustic vibrations to the system. Although optical cavities utilize a rigid spacer to hold the mirror spacing constant, no material is infinitely rigid, and as such is susceptible to elastic deformation. For the case of optical cavities, acceleration-induced deformation can result in cavity length changes that can seriously degrade both the short- and long-time scale frequency noise of the spectrum of the laser locked to the cavity. Thus, it is necessary to minimize external vibrations that can shake the cavity, thereby changing its length (principally around frequencies ranging from 1 to 100 Hz). Complicated methods for such vibration isolation have been used historically, including putting cavities in specialized rooms or supporting their platforms with long pendula [50]. However, today one can purchase more compact, active (or passive) vibration-isolation platforms that can support a cavity and its associated hardware. For best performance the cavity geometry and mounting systems are designed (see figs. 7 and 8) so as to minimize coupling of seismic vibrations to the cavity length [62, 63, 64, 65]. We note also an ingenious approach that minimizes the effect of vibrations on a symmetrically mounted cavity by measuring the vibrations on the cavity with an accelerometer,

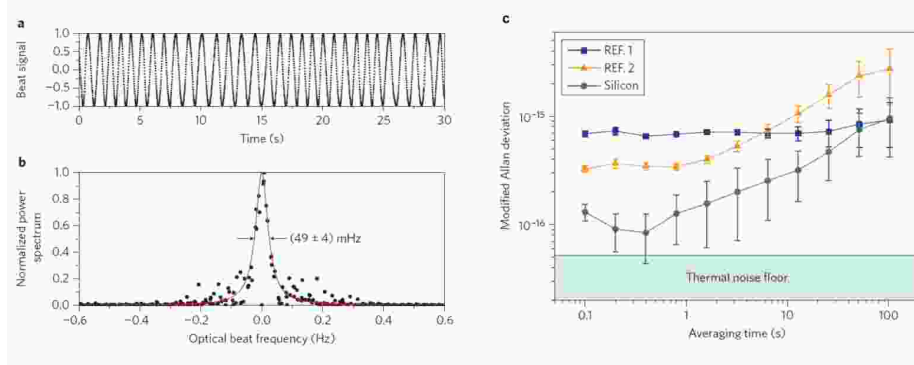


Fig. 9. – Optical heterodyne beat between a $1.5 \mu\text{m}$ laser stabilized to cryogenic silicon cavity and second laser system stabilized to a 25-cm long ULE-fused silica cavity. a, Beat signal mixed down close to d.c. and recorded with a digital oscilloscope. b, Normalized fast Fourier transform of the beat signal. A Lorentzian fit is indicated by the red line. The combined result of five consecutive recordings of the beat signal (black dots) is displayed here, demonstrating the robustness of this record-setting linewidth. c, Modified Allan deviation of each cavity-stabilized laser. The predicted thermal noise floor of $\text{mod } \sigma_y \sim 5 \times 10^{-17}$ for the silicon cavity system is indicated by the shaded area. Data from ref.[53].

then feeding forward frequency corrections to the light based on the cavity’s measured transfer function [66]. Additionally, today’s cavities are also designed to minimize a more fundamental limitation: that imposed by thermal noise due to the Brownian motion of the cavity itself [51], which exists even in a completely stable thermal environment. This effect manifests itself in all the components of the optical cavity: the spacer, the mirror substrates, and even the mirror coatings.

As a result, the materials used in cavity construction are chosen with thermal noise and thermal-sensitivity properties in mind. Specifically, this means choosing high mechanical Q materials (*i.e.*, with low loss angle) with low coefficients of thermal expansion (CTE). Usually the spacer is made from ULE glass (maintained near the zero-crossing temperature with residual CTE $< 10^{-9}/\text{K}$) because it represents the dominant contributor to cavity length, while the mirror substrates in modern cavities are often made of fused silica due to its high Q . Many such cavities have been constructed over recent years, each with their own advantages. Overall, for cavities longer than 25 cm, the noise floor limits the stability of the associated optical atomic clocks (with typical probe duty cycles) at about $10^{-16}\tau^{-1/2}$, a level that is already being challenged by the best optical clocks (see for example, [67]). Improving the cavity-stabilized laser stability significantly beyond this level is difficult, since at this point the coating noise is the dominant thermal noise factor. Pushed in part by the gravitational-wave community, other coating materials are under test, with some promising crystalline coating materials recently identified and demonstrated [52].

An alternative approach to reducing the Dick effect-limited instability is to increase the measurement duty cycle. In fact more stable reference cavities help here as well, since they enable longer probe times, thereby reducing, fractionally, the period during which the atoms are not being probed. Additionally there has been an original approach that uses non-destructive probing of the excitation, which enables recycling of the lattice-trapped atoms [68]. This reduces the reloading period, which is usually the dominant

contributor to the time during which the atoms are not being interrogated (often called the dead time). Alternatively, we can probe two independent atomic samples simultaneously [69], so as to make noise common-mode between the measurements. However, to make a single system that is virtually immune to the Dick effect we can use two systems in tandem, each one having at least a 50 % duty cycle, and then interleave their measurement cycles, so that the probe laser is always under evaluation by one of the atom systems [55, 70].

Because of the critical importance of laser stabilization to this field, other approaches to circumvent the thermal noise limitations of optical cavities are underway. Spectral hole-burning in cryogenically cooled crystals is a route that uses long-lived spectral holes induced by a narrow laser to serve as stable frequency references to stabilize further that same laser. Such systems have demonstrated fractional instabilities of 6×10^{-16} at one second, with a projected fundamental limit about another order of magnitude lower [71]. Other groups are pursuing high signal-to-noise signals in narrow, but not ultra-narrow (nor accurate), atomic transitions [72]. A different approach is to cool the cavity to reduce the thermal noise contribution. A set of experiments, initiated in the mid 90's with cryogenically cooled sapphire cavities [73], obtained a laser instability of 2.3×10^{-15} at a temperature of 3 K [74]. More recently a demonstration of a silicon cavity at 124 K reported an estimated thermal noise limit of only 7×10^{-17} [75, 53, 76], limited by mirror coating noise. Experimentally, it has been demonstrated that a $1.5 \mu\text{m}$ laser stabilized to this cavity had a record laser linewidth of < 40 mHz and stability of $< 1 \times 10^{-16}$ at short term (see fig. 9). It is worth emphasizing that even though this result was obtained with a laser at a wavelength unconnected to an atomic clock transition, it is possible to transfer this same level of stability to lasers at other wavelengths with the help of an optical frequency comb. For these reasons, though they are more complicated experimentally, cooled cavities may play an ever-increasing role as researchers seek ever more stable clocks.

4. – Systematic effects in optical clocks

The frequency of an atomic transition of an atom or single ion (quantum absorber) can be perturbed by many effects such as the presence of undesired electric and magnetic fields, the fact that the absorber is not perfectly at rest, collisional effects or even imperfect vacuum conditions. The influence of such systematic effects has been treated extensively, both experimentally and theoretically [77, 78, 79]. In this section the most important systematic effects that limit the performance of an optical atomic clock, for both the neutral atoms and ion cases, are discussed in detail, together with ways researchers have found to overcome them.

4.1. Doppler effect. – This effect results from the motion of the quantum system (*e.g.* neutral atoms or single ion) relative to the observer. From energy and momentum conservation in relativistic theory one can find that the frequency shift $\delta\nu = \delta\omega/2\pi$ of a photon emitted (or absorbed) by a two-level atom (or an ion) with a mass m , moving with a velocity \mathbf{v} with respect to the laboratory rest frame, can be written as [80, 81]

$$(3) \quad \delta\omega = \mathbf{k} \cdot \mathbf{v} - \frac{1}{2}\omega_0 \frac{\mathbf{v}^2}{c^2} \mp \frac{\hbar\mathbf{k}^2}{2m},$$

where \mathbf{k} is the wave vector of the photon emitted (absorbed) and $\omega_0 = 2\pi\nu_0$ with ν_0 unperturbed atomic transition frequency. The three terms in Eq. 3 represent respectively,

the first-order effect, the second-order Doppler effect, and the recoil effect.

In a sample of atoms in equilibrium at a certain temperature, due to the thermal statistical distribution of velocities, the first-order Doppler effect gives rise to an effective broadening of the optical transition lines. The Doppler profile of optical transitions is thus nearly Gaussian with a width related to the temperature of the cloud. At room temperature this effect produces a linewidth for an optical transition of the order of several gigahertz, and even at microkelvin temperatures (nearly the minimum that can be reached with laser cooling techniques), this effect still gives a broadening of several hundred kilohertz.

The second term in Eq. 3 is the second-order Doppler shift, which depends on the square of the velocity of the quantum emitter (absorber). In spectroscopy schemes adopted in atomic frequency standards, the asymmetry associated with second-order Doppler effects generally produces an asymmetry of the line profile and thus a shift of the line center. The size of this asymmetry is then typically evaluated starting from the knowledge of velocity distribution of the atoms for the spectroscopy scheme used [30]. For high-performance clocks, the reduction of the temperature of the atoms by means of laser cooling techniques is usually necessary to reduce this effect to a negligible level. For atoms or single ions cooled at millikelvin temperatures, the shift is small ($\approx 10^{-17}$), though not completely negligible, while at microkelvin temperatures the fractional frequency shift given by the second-order Doppler effect is below 10^{-20} .

The last term (recoil shift) in Eq. 3 depends on the frequency of the photon emitted (absorbed). While in the case of microwave clocks this term plays no significant role at the current clock accuracy ($\sim 2 \times 10^{-16}$ for Cs standard at 9 GHz), for higher-frequency quantum-based standards this effect gives a more important contribution (about 10^{-11} for Sr optical clock at 429 THz) and cannot be neglected.

To circumvent or at least minimize these limitations, several sub-Doppler or Doppler-free spectroscopy schemes have been developed, which have enabled the observation of electronic transitions with their natural linewidth: saturation spectroscopy, two-photon spectroscopy, Ramsey and Ramsey-Bordé [82] interrogation schemes in atomic beams. While theoretically these schemes all appear to remove at least the first-order shift, in reality, they don't remove it completely, due to effects such as imperfect laser beam alignment and wavefront distortions. Moreover, these techniques don't address the large second-order Doppler shifts. The laser cooling techniques described in sect. 3.2 seem well suited to address these problems simply by reducing the velocities of the atoms. However, even with laser-cooled samples, Doppler effects still play a significant role in the uncertainties [83, 84], due to asymmetries in the interrogation sequence (wave-front curvature and asymmetries in the intensity of the interrogating laser beams, asymmetries given by the incoherent signal of the background atoms, etc.), which can induce asymmetries in the center-line profile and consequently a systematic shift with respect to unperturbed atomic transition. Thus, for the most accurate systems, it is necessary for the atoms or ions to be confined to the Lamb-Dicke regime, for which the first-order Doppler and the photon recoil shifts disappear [41] (the recoils are absorbed by the trapping environment). Moreover, the second-order Doppler shift can be made negligibly small by sideband-cooling atoms down to the vibrational ground state of the trapping potential [85]. Under these conditions, whether for neutral atoms or single trapped ions in an rf trap, Doppler effects can be reduced to nearly negligible levels, although residual relative motion between the trapped atoms and probe optics still needs to be considered and at times compensated [86].

4.2. Interaction with magnetic fields: Zeeman effect. – Atomic states are coupled to static magnetic fields via their magnetic moment μ . The magnetic moment depends on the atomic state, and the interaction energy $\delta E = \mu \cdot \mathbf{B}$ is generally different for the ground and excited states of the clock transition. The differential energy shift causes a magnetic field dependency of the clock transition frequency,

$$(4) \quad \delta\nu(\mathbf{B}) = \frac{\delta E_e(\mathbf{B}) - \delta E_g(\mathbf{B})}{h}.$$

The magnetic moment of the atomic state is related to the corresponding total angular momentum \mathbf{F} (given by the orbital angular momentum of the electronic cloud \mathbf{L} , the electronic spin \mathbf{S} , and the nuclear spin \mathbf{I}). To first approximation, the energy shift is proportional to the projection of the total angular momentum along the quantization axis expressed by the quantum number m_F . In general, the clock frequency shift can be written as

$$(5) \quad \delta\nu = (g_e m_{F,e} - g_g m_{F,g})B + \beta B^2 = \alpha_{e,g}B + \beta_{e,g}B^2,$$

where g_e (g_g) represents the Landé factor for the excited (ground) state. By properly choosing transition states with $m_{F,g} = m_{F,e} = 0$ it is possible to avoid the first-order Zeeman effect. However, even for transitions between states with $m_F = 0$ a residual second-order energy shift is always present (quadratic Zeeman effect) due to interactions with nearby atomic states with non-zero magnetic moments (see Table I).

In general, fluctuations in the bias magnetic field may limit the clock stability, and the clock uncertainty can be limited by the uncertainty in either the Zeeman shift coefficients ($\alpha_{e,g}$ and $\beta_{e,g}$) or in the magnitude of the magnetic field. The standard solution, as in microwave atomic clocks, is to choose atomic transitions among states with $m_F = 0$, so that the linear Zeeman effect is absent, or among states with small g -factors, so that the α coefficient is small. Otherwise, it is common to interrogate sequentially two transitions with symmetric shift, such as $m_{F,g} = 0$, $m_{F,e} = \pm m$, so that the average frequency is immune to the first-order Zeeman effect.

For ultimate accuracy, the residual shifts must be properly accounted for by controlling the magnitude of the magnetic field and by measuring the Zeeman coefficients. The influence of magnetic fields on the clock performance is less critical than in the microwave case, since the absolute Zeeman shift of the atomic reference is typically of the same order of magnitude, and thus is proportionally much smaller for the optical case. With proper magnetic shielding it is possible to reduce the shifts due to residual magnetic fields and reaching relative accuracies below the 10^{-18} level. Higher-order effects are generally negligible.

4.3. Interaction with electric fields. – The influence of electric fields on the clock frequency is, generally, more important than that of magnetic fields. Electric fields affect the atomic energy levels through the Stark effect, and a variety of possible sources of DC or AC electrical fields can induce such shifts on the clock transition: stray static fields, motionally-induced electric fields for trapped ions, blackbody radiation and laser fields. In particular, we need always to consider the probe light field that excites the clock transition itself, as its interactions with off-resonant transitions can, at times, lead to non-negligible frequency shifts, especially for weak transitions such as those based on octupole or magnetically-induced moments. As we shall see in sect. 5.2, laser fields play

TABLE I. – *Linear (α) and quadratic (β) Zeeman shift coefficients for some optical clock transitions of neutral atom/ion.*

Atom/Ion	sublevels	Linear coefficient α (MHz/T)	Quadratic coefficient β (MHz/T ²)
²⁴ Mg	$m_F = 0$	0	164
⁴⁰ Ca	$m_F = 0$	0	64
⁸⁷ Sr	$m_F = \pm 9/2$	1.08	-23.3
⁸⁸ Sr	$m_F = 0$	0	-23.3
¹⁷¹ Yb	$m_F = \pm 1/2$	2.1	-7
¹⁷⁴ Yb	$m_F = 0$	0	-7
²⁷ Al ⁺	$m_F = \pm 5/2$	-82	-72
⁸⁸ Sr ⁺	$m_J = \pm 1/2$	5.6×10^3	3.1
¹⁷¹ Yb ⁺ quad.	$m_F = 0$	0	5.2×10^4
¹⁷¹ Yb ⁺ oct.	$m_F = 0$	0	-1.7×10^3
¹⁹⁹ Hg ⁺	$m_F = 0$	0	-1.9×10^4

an integral role in the operation and design of optical lattice clocks, in which these fields are used to confine the atoms during clock-transition excitation. Since atoms (or ions) do not possess a permanent electric dipole in a definite quantum state, the Stark effect is dominantly a second-order effect. In general, both clock levels have their energies shifted and the resulting transition frequency is changed by the differential shift

$$(6) \quad \delta\nu = -\frac{1}{2\hbar}(\Delta\alpha_{DC}E_0^2 + \Delta\alpha_{AC}(\omega)\langle E(\omega)^2 \rangle),$$

where E_0 and $E(\omega)$ are the static and dynamic electric fields applied, respectively, $\Delta\alpha_{DC} = \alpha_{DC,e} - \alpha_{DC,g}$ is the difference in static polarizabilities of the excited and ground states and $\Delta\alpha_{AC}(\omega)$ is the difference in dynamic polarizabilities for the same states. The general expression for the atomic polarizability $\alpha_{AC,i}(\omega)$ for a generic state i can be found from second-order perturbation theory

$$(7) \quad \alpha_{AC,i}(\omega) = \frac{1}{\hbar} \sum_{k \neq i} |\langle k | \hat{D} | i \rangle|^2 \frac{\omega_{ki}}{\omega_{ki}^2 - \omega^2},$$

in which the sum is performed on all k levels coupled by the \hat{D} dipole operator to the i level. It is worth noting that $\lim_{\omega \rightarrow 0} \alpha_{AC,i}(\omega) = \alpha_{DC,i}$.

With the help of these formulas a large number of theoretical atomic physics studies have been performed on the polarizabilities of atoms (see Table II). With improvements in atomic theory these can now be calculated very accurately, with errors at the few % level. However, this level of accuracy is not always sufficient, and recently, for specific clock transitions, atomic static polarizabilities [87, 88, 89] have been measured directly. Additionally, we re-emphasize that eqs. 6 and 7 pertain to shifts associated with dipole-allowed transitions. In fact as we shall see in sect. 7, many single ion optical clock transitions are based on quadrupole transitions to a D state that contains a quadrupole moment. Such moments can interact with residual quadrupole field gradients of the ion trap in a way analogous to the DC dipole moment and DC electric fields in Eq. 6 (along with a geometric factor based on the angle between the quadrupole field axis and a bias

TABLE II. – DC Stark coefficients and electric quadrupole coefficients for some ion clock transitions.

Atom/Ion	DC Stark coefficient (mHz/(V/cm) ²)	Electric quadrupole shift (mHz/(V/cm) ²)
²⁷ Al ⁺	-0.14	0
¹¹⁵ In ⁺	0.5	0
⁸⁸ Sr ⁺	-4	14
¹⁷¹ Yb ⁺ quad.	-6	60
¹⁷¹ Yb ⁺ oct.	1.2	1.5
¹⁹⁹ Hg ⁺	-1.1	-3.6

magnetic field) and lead to non-negligible shifts that need to be nulled or evaluated, as we shall see later in the sections on specific ion clock systems in sect. 7.

4.4. *Interaction with blackbody radiation (BBR).* – A type of Stark shift that is particularly relevant to state-of-the-art systems is given by the interaction with blackbody radiation emitted by the environment in which the the clock atoms or ion is trapped. The spectral density of energy emitted by a body maintained at a temperature T per unit volume has the well known Planck formula,

$$(8) \quad \rho(\nu) = \frac{8\pi\nu^2}{c^3} \frac{h\nu}{e^{h\nu/k_B T} - 1}.$$

From this it is possible to express the mean square electric field at temperature T as

$$(9) \quad \langle E^2 \rangle_T = \epsilon_0^{-1} \int_0^\infty \rho(\nu) d\nu \sim (8.319 \times 10^2 \text{ V/m})^2 \times (T/300 \text{ K})^4.$$

The distribution of electromagnetic fields can then shift the net frequency of an optical atomic transition via the quadratic Stark (and Zeeman effect). The temperature dependence of a given clock transition depends on the polarizability of its two levels. Since at room temperature the dominant frequencies of the BBR radiation are typically much lower than that of the first resonant transition coupling the excited and ground states, the dominant contribution comes from the static polarizabilities. As a result one can write the net shift, $\Delta\nu_{BBR}$, in terms of a differential DC Stark term, $\Delta\alpha_{DC}$, with a (much smaller) dynamic correction, η_T [90],

$$(10) \quad \Delta\nu_{BBR} = -\frac{1}{2h} \Delta\alpha_{DC} \langle E^2 \rangle_T (1 + \eta_T).$$

As pointed out in the previous section, it is possible to estimate both the static polarizabilities and dynamic correction coefficient η_T from ab-initio calculations [91, 92]. In table III we summarize the calculated relative shift at room temperature for some candidate optical clock transitions.

The BBR shift contributes in two ways to the clock uncertainty. First, because clock transition frequencies are traditionally defined at 0 K, it is necessary to extrapolate from the environmental temperature for the atom/ion system to 0 K. Such calculations require good knowledge of the coefficients in Eq. 10 and yield the values listed in columns two

TABLE III. – *Calculated BBR Shifts at $T = 300$ K for some optical clock transitions in neutral atoms and ions. In the third and fourth columns are reported the relative shift and estimated relative uncertainty with a temperature uncertainty of $\Delta T = 1$ K [91, 93, 94, 95, 96, 97].*

Atom/Ion	$\Delta\nu_{BBR}$ [Hz]	$ \Delta\nu_{BBR}/\nu_0 $	rel. uncertainty
Mg	-0.258(7)	3.9×10^{-16}	1.6×10^{-17}
Ca	-1.171(17)	2.6×10^{-15}	7.2×10^{-17}
Sr	-2.354(32)	5.5×10^{-15}	1.4×10^{-16}
Yb	-1.34(13)	2.6×10^{-15}	2.9×10^{-16}
Hg	-0.181	1.6×10^{-16}	5×10^{-18}
Al ⁺	-0.008	8×10^{-18}	3×10^{-18}
In ⁺	-0.0173(17)	1.36×10^{-17}	1.6×10^{-18}
Sr ⁺	0.249	5.6×10^{-16}	2.2×10^{-17}
Yb ⁺ quad.	-0.351	5.1×10^{-16}	2×10^{-17}
Yb ⁺ oct.	0.067(32)	1.1×10^{-16}	5×10^{-17}

and three of table III. Second, even with perfect knowledge of the atomic parameters, there is still an uncertainty in the environmental temperature, which affects the $\langle E^2 \rangle_T$ term above. Experiments currently estimate around one degree uncertainty for this term, which yields the relative uncertainty in the fourth column of table III.

An examination of the values of the fractional shifts in the third column reveals a wide variance. In particular, the value of Al⁺ is anomalously small and contributes in part to its being the most accurate clock to date. In other cases, the BBR coefficients are large enough to act as one of the dominant contributors to clock uncertainty. For these systems, more precise (and experimentally verified) knowledge of these coefficients is required. In particular, we see that the very promising lattice clock candidates, Sr and Yb, have comparatively large fractional shifts at room temperature, -5.5×10^{-15} and -2.6×10^{-15} , respectively. In both cases, direct, high-precision experimental evaluations of the static and dynamic coefficients have been performed (which agreed well with theory) [89, 87], leaving only the uncertainty in the temperature of the environment itself as the significant contributing systematic. This uncertainty in turn is being addressed in various ways, usually involving a specialized, temperature-controlled interaction chamber, which, if necessary, can be cryogenically cooled [98]. Operation at liquid nitrogen temperatures (77 K) substantially reduces the BBR shift, due to the T^4 dependence of the electric field intensity.

4.5. Collision & Pressure shifts. – Frequency shifts that result from interactions between colliding atoms have long been a serious concern in atomic standards. We note that for Cs fountain-based microwave clocks, these effects can actually limit clock performance [99], and indeed, they are important for optical clocks as well. While the idealized case of an atom or ion fully isolated from neighboring atoms can nearly be realized in single, trapped ion systems (only infrequent collisions with background atoms exist), for neutral atom optical clocks the situation is quite different. In both cell-based and trapped-atom-based clocks the atomic densities can be high enough that atomic interactions can lead to small, but not always negligible, shifts of the atomic clock frequencies. In cell-based systems these pressure shifts result principally from collisions with like atoms or molecules (typically around 1 MHz/Torr), but contaminants introduced during cell fabrication have also been seen to lead to frequency shifts between different cells (see for

example, [100]). For clocks using freely expanding atoms, either thermal or laser-cooled, the density-related collision shifts are too small to be measurable at their typical uncertainty levels, even at densities as high as $10^{10}/\text{cm}^3$ [101]. As we will see in more detail in sect. 5.3 and 5.4, collision effects for lattice clocks are more relevant, primarily due to their higher sensitivity. Moreover, since a large fraction of the lattice-trapped atoms are confined to identical motional states, the atom-atom interaction situation is further complicated by the quantum statistics of the absorbers (see [102] for a comparison between bosonic and fermionic clocks).

4.6. *Gravitational effect.* – A well-known consequence of general relativity is that the frequency of a clock $\nu(x')$ measured by an observer in the presence of a gravitational potential $U(x)$ will depend on the gravitational potential difference between the clock location and the observer location. This has the direct consequence that a comparison between two identical clocks operating at different locations x_1 and x_2 on Earth will show a difference in frequency proportional to the potential energy difference $U(x_1) - U(x_2)$. The change in clock frequency is directly related to the loss of energy of photons “climbing” the gravitational potential from x_1 to x_2 , which corresponds to a change in altitude, Δh , on Earth by (see, for example, [103] or [104] and references therein)

$$(11) \quad \Delta\nu/\nu_0 \sim g\Delta h/c^2.$$

In other terms, we may say that that clocks closer to massive bodies (*i.e.*, at lower gravitational potential) run slower, and for high-precision clocks, these differences can be large. A height difference of 1 cm yields an observed frequency shift of a part in 10^{-18} , so for clocks located at NIST in Boulder, CO, (altitude $\Delta h \sim 1600$ m with respect to the Earth geoid), the gravitational correction is about 2 parts in 10^{13} . For clocks to reach uncertainties at the 10^{-18} level, clearly detailed knowledge of the geoid will be required. This situation is further complicated by the fact that daily local fluctuations in altitude and hence gravitational field occur at the 10^{-17} level [105], so one day it may be necessary to locate our best clocks far from Earth’s surface. Or conversely, such clocks could actually be used to perform precision “relativistic geodesy” on Earth’s surface [103, 106].

4.7. *Locking errors due to technical effects.* – In addition to the effects already discussed in this section, which are mostly of a fairly fundamentally physical nature, there exists always an array of technical effects that can cause the probe laser to be stabilized just off the line center of the clock transition. Some are quite general to most clock systems, while others are more particular to a given clock apparatus. In general, these details are tucked away in articles on specific clocks and at times not mentioned at all. Here we give several examples of locking error that many clock systems need to consider.

One of the most important issues involves configuring the electronics to minimize “servo” error. Typically clock experiments operate with line quality factors of 10^{14} at best, yet they strive for performance at the part in 10^{17} level or better. This requires finding the center of the spectroscopic lineshape to a part in 1000 or better. In the past this meant controlling electronic offsets at the millivolt level or below, but well-designed digital servo systems have made this problem much more manageable (the Cs fountain microwave clocks now achieve a line splitting better than 1 part in 10^5 !). A second source of locking error results from unpredictable drifts of the probe laser reference cavity. Servo systems have limited correction capabilities, so a laser that is drifting too fast or

erratically can have offsets relative to the atomic transition to which it is stabilized. For this reason (among others) clock scientists go to considerable trouble to isolate the reference cavities (to which the probe laser frequencies are ultimately stabilized) from environmental effects such as temperature and vibrations. A third, less common (but particularly insidious) source of locking error results from uncompensated vibrations of the probe-laser optics that send the light into the apparatus containing the atoms or ions. If such vibrations are synchronized with the measurement cycle (for example, through the mechanical impulse caused by the electronic shut-off of magnetic field gradient coils), they can cause an effective and repeatable Doppler shift that leads to an offset in the locked laser frequency from the spectroscopic line center. Such effects can be detected (or even zeroed) by changing (or choosing) the time duration between, say, the coil shut-off and the probe time, but unfortunately such offsets can drift with time and temperature, so they can require considerable care. In one case, such vibration-induced effects drove one group to suspend their atom apparatus, pendulum-style, above the main optical table [107]. In the end, locking/servo errors rarely limit ultimate clock performance, but often require significant attention on the part of the researchers.

5. – Neutral atom optical clocks - general description

Neutral atom-based optical atomic clocks have attracted great interest for several reasons including comparative ease of construction and convenient wavelengths, but their principal advantage can be seen in Eq. 1. Here we see how the fractional instability depends inversely on the square root of the number of quantum absorbers in the system. For the systems we will describe in this section, N can be anywhere from 1000 to 50000. As a result, neutral atom systems have the potential to be 10 to 100 times more stable than systems based on a single quantum absorber. When used in conjunction with ultra narrow transitions such as those for intercombination lines of two-electron atoms, as are commonly used in neutral atom clocks, these large N systems can, in principle, have fractional instabilities well below $10^{-16}\tau^{-1/2}$ [108]. However, as we discussed previously in sect. 4, this potential advantage can be realized only in systems with frequency noise lower than this atom shot noise limit (given by Eq. 1). For this reason, neutral atom clocks were slow to capitalize on their large numbers of atoms, but as we shall see, recent experiments have demonstrated unprecedented levels of stability. The absolute frequency uncertainty obtainable with these systems is a more complicated issue. As we have seen in sect. 4, many effects must be considered when computing the uncertainty budget for a given clock, and the combined result depends greatly on the particular system. However, the dominant consideration, which has driven the design, and really the evolution, of neutral atom-based systems is how best to handle Doppler effects.

For this reason, neutral atom frequency standards and clocks have followed a fairly steady progression from thermal atom-based systems to laser-cooled atomic systems to those based on atoms trapped in optical lattices. Recall that sub-Doppler methods can greatly suppress these shifts for thermal and laser-cooled atoms; indeed we will describe in this section several clocks based on sub-Doppler spectroscopic techniques. However, these techniques rely on extreme parallelism between the counter-propagating beams (and almost perfect wavefronts). Various experiments have shown that this is hard to do at the microrad level (implying hertz-level residual shifts) [83, 107, 109]. Even the use of an optical cavity for the probe beams does not solve this problem, due to the mismatch between the beam waist and atom cloud size (and wavefront curvature away from the beam waist). Researchers thus had to conclude from these experiments

that it was unrealistic to expect sub-Doppler methods used in combination with freely expanding atomic clouds to achieve absolute uncertainties of much below 1 Hz (or 10^{-15} fractionally), even with laser-cooled atoms.

Thus, scientists have ultimately turned to optical lattice-based clocks to achieve the highest levels of performance. With clever choice of atomic transition and lattice wavelength, perturbations to the clock frequency induced by the lattice beams can be suppressed to the sub- 10^{-17} level [47]. Despite the considerable additional experimental complication required, optical lattice clocks now dominate the field of high-precision neutral atom clocks, with 15 to 20 existing worldwide and versions based on three different atomic species. In less than ten years, these clocks have gone from being a new idea to having achieved significant performance milestones, with demonstrated inaccuracy at the sub- 10^{-17} level and instability at the $3 \times 10^{-16} \tau^{-1/2}$ level.

Let us now examine in more detail the most influential neutral atom optical clock systems, with examples of clocks based either on freely expanding laser clouds (both at room and laser-cooled temperatures) or on laser-trapped atoms (*i.e.*, lattice clocks). In this way we will see how the combination of the atomic system, atom preparation, and excitation scheme determines clock strengths, limitations, and future prospects in terms of clock performance and potential applications.

5.1. Optical Clocks Based on Freely Expanding Neutral Atoms. – Due to their relative experimental simplicity, optical clocks and frequency references based on freely expanding (*i.e.* untrapped, in free fall) atoms have been popular systems for study for more than four decades. The atom source can be a cell filled with atom vapour, a thermal atomic beam, a laser slowed/cooled atomic beam, or even atoms released from a magneto-optical trap. With vapor cells, one usually employs a form of saturation spectroscopy (or optical heterodyne saturation spectroscopy [110], for higher precision), with overlapped counter-propagating laser beams to excite the atoms. Due to pressure-dependent collision effects and cell contaminants, the reproducibility between vapor cell frequency references is usually limited at the kilohertz level, making vapor cells less ideal for the highest precision optical clock research. Still, they are very convenient and compact sources, and fractional frequency instabilities as low as $5 \times 10^{-14} \tau^{-1/2}$ have been reported for a molecular iodine optical clock [111].

Cell limitations are overcome by using a thermal atomic beam (see fig. 10), usually fashioned by having an atomic vapor effuse from a crucible containing a small hole. In most cases it is necessary to heat the crucible to a temperature ranging from 600 to 1000 K, which produces an atomic beam with a most probable velocity, v_{prob} , of ~ 500 m/s. The atomic beam is typically collimated at the 10 % level, so there is significant Doppler broadening even for probe beams oriented orthogonally to the atomic beam (the usual geometry). Thus, sub-Doppler techniques using counter-propagating laser beams are required to reach sub-MHz spectroscopic resolution. Interestingly, due to the long lifetime of the excited state (~ 1 ms) of these ultra-narrow clock transitions, the counter-propagating beams can be spatially separated as the $1/e$ distance for decay from the excited state can be 30 cm or longer. This enables excitation with travelling waves rather than standing waves (and its associated spatial intensity dependence), thereby yielding more uniform excitation of the atoms. However, a single pair of counter-propagating excitation laser beams is not sufficient for high resolution as the fast-moving atoms pass through a typically sized laser beam in $\sim 10 \mu s$, limiting the resolution via transit-time broadening (essentially a Fourier effect that constrains resolved linewidths to be greater than the inverse of interaction time) to around 100 kHz.

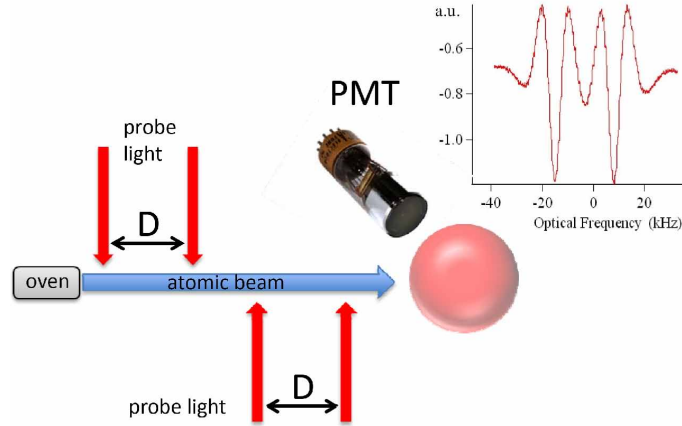


Fig. 10. – Schematic representation of Ramsey-Bordé spectroscopy on atomic beam with spatially separated interaction regions.

For this reason, high-resolution optical experiments employ instead a modified version of the Ramsey method of separated excitation zones [112], which has been used in microwave clocks for many decades. The resolution provided by the two-beam Ramsey geometry is determined by the separation of the beams, D , rather than the transit time through a single beam. The first interaction zone excites the atoms into a superposition of the excited and ground states. This superposition evolves in the dark zone between excitation fields, whose phase is then read out by the second field. Mathematically (and intuitively), this two-zone Ramsey excitation is analogous to the Young’s double slit experiment, in which the excitation zones play the role of the slits, and the atomic excitation plays the role of the light. Indeed, the resulting Ramsey excitation is an interference pattern with a period equal to the inverse of the transit time between zones. The optical version uses two pairs of Ramsey beams, with the second pair counter-propagating to the first, in order to suppress the first-order Doppler shift [113, 114, 115]. In this case the period of the Ramsey fringe interference signal is equal to $v_{prob}/2D$, due to the doubled length of the spectrometer. The analogy with Young’s double slit experiment goes further, as this optical Ramsey spectrometer is indeed an atomic interferometer as emphasized first by Ch. Bordé [116]. For this reason, four-beam optical geometries of this type are often termed “Ramsey-Bordé spectrometers” [117]. As we will see, such spectrometers can be used not only to generate high resolution spectra, but can also be used as atomic interferometric sensors to measure quantities such as rotation and Stark shifts [118]. This technique offers the additional benefit of high signal-to-noise ratios as the large effective Doppler coverage (due to transit broadening) of the small excitation zones excite a non-trivial fraction of the atomic distribution. However, due to the wide range of the velocities in the atomic beam, the source has a small degree of coherence, so usually only a few interference fringes are visible, and these usually come in two sets, one for each of the two “recoil” components [119, 84]. These recoil components are a by-product of performing spectroscopy with counter-propagating beams and yield a pair of resonances symmetrically located around (and close to) the unperturbed atom resonance. In fact only in high resolution work are the two features usually resolvable, since their separation is usually on the order of tens of kilohertz.

For accurate work, thermal beam-based Ramsey-Bordé interferometers have several drawbacks, not surprisingly Doppler related. First, we recall that the second-order Doppler shift is on the order of 1 kHz for typical thermal beam velocities, leading to uncertainties of tens of hertz or more. Moreover, these spectrometers have a sensitivity to the phase of the laser excitation laser beams that make them very sensitive to beam optics, and beam reversal techniques can only partially mitigate these effects [120]. For these reasons, the most accurate experiments employ laser cooling, either simply to slow the beams, or more commonly to collect the atoms in magneto-optical traps (MOTs, see fig. 11) [44] before releasing the millikelvin or microkelvin atoms for spectroscopy (the laser beams in a MOT distort atomic energy levels via the AC Stark effect too much to permit precision spectroscopy for the trapped atoms) [45, 121]. We note, however, one important exception to this rule: the most accurate measurement to date of a neutral atom transition with unconfined atoms was actually performed with thermal atoms and was made in more of a fundamental physics context than a clock context. Due to its calculability, the 1S-2S transition in H is fundamental in testing quantum electrodynamics and for the determination of such fundamental quantities as the Rydberg constant and the proton charge radius. Heroic experimental efforts led by the group of Th. Hänsch have achieved fractional uncertainties of 4.2×10^{-15} for this transition through careful evaluation of the second-order Doppler shift and the use of two-photon spectroscopy, which can reduce first-order Doppler effects [122, 123].

For MOT-based systems with atomic samples at millikelvin temperatures, the second-order Doppler shift becomes negligible, while residual first-order shifts are greatly reduced but still persist at the MHz level. Thus, it is still necessary to use optical Ramsey sequences, this time separated temporally, rather than spatially, to achieve high resolution signals [121]. In this case due to the much higher “coherence” of the atomic sample, a large number of fringes is usually visible (with a period of $1/4T$), thereby requiring some care in the identification of the central fringes (see fig. 12). In fact, each recoil component provides its own set of fringes, so for maximum signal contrast it is necessary to choose a fringe period that enables the two sets to add constructively.

Residual first-order Doppler effects (principally those associated with imperfect wavefronts and imperfect beam alignment) still limit the absolute uncertainty of systems based on millikelvin atoms to about 10^{-13} , so in some cases a second stage of cooling has been used to reduce the temperature by a factor of 100 to 1000, and the uncertainty in the clock frequency by a factor of ten or so [124, 125, 126, 127, 107]. But as we will see as with some specific optical atomic clock systems, it seems prohibitively hard to approach the accuracy of the best microwave clocks with optical transitions excited in freely expanding atoms. Nonetheless, these optical systems have demonstrated much higher stability than their microwave counterparts and as a result could find many important applications due to their relative simplicity in comparison with lattice-based clocks.

5.1.1. Ca optical clock. Calcium was the first element to be probed with kHz-level resolution in the optical domain. Calcium’s appeal for high resolution spectroscopy lies in its $^1S_0 \rightarrow ^3P_1$ intercombination line, which has a natural linewidth of only 400 Hz (due to its forbidden nature) at a convenient visible wavelength of 657 nm (see fig. 13). Additionally calcium has a convenient laser cooling transition at 423 nm. Landmark experiments by Barger and Bergquist used the “new” technique of optical Ramsey spectroscopy to resolve spectroscopic features with linewidths as narrow as 2 kHz (FWHM) [128, 129].

In the following decades, several groups, most notably those at PTB, Tokyo, and

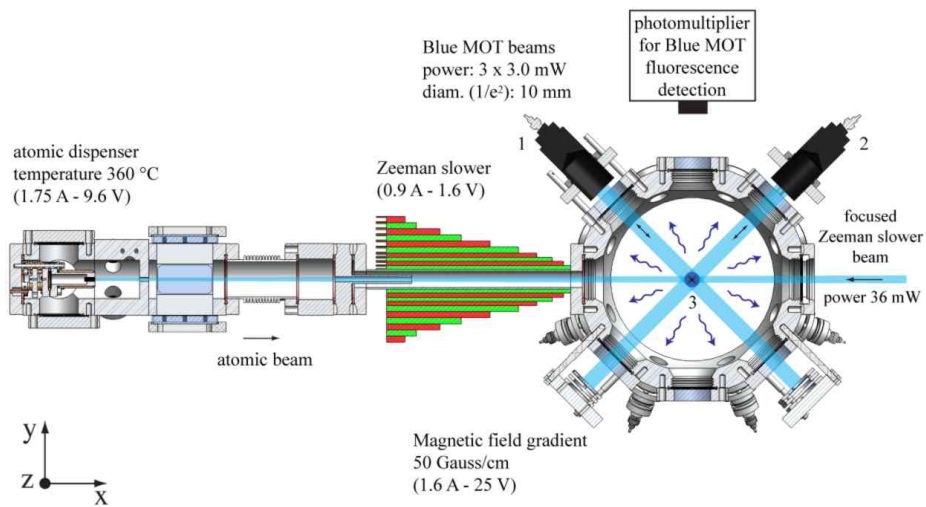
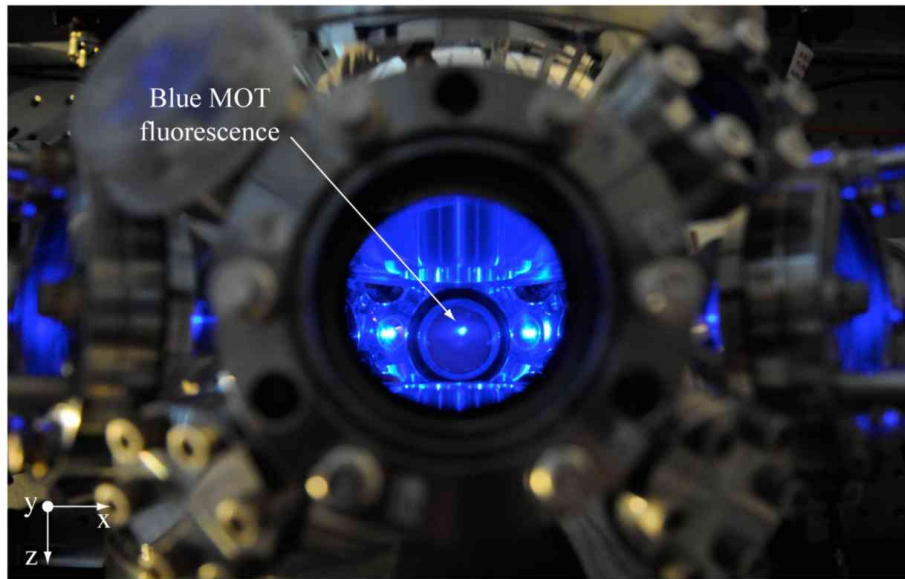


Fig. 11. – Typical alkaline-earth optical clock experimental setup. Atoms are evaporated in a high temperature oven, successively slowed longitudinally and finally trapped on the main chamber with MOT beams [adapted from [42]].

NIST, performed a large number of experiments based on this transition in ^{40}Ca (the most abundant isotope), some using it as an atom interferometer [118], while others were focused on its potential as a frequency standard [130, 131, 121, 107]. Early Ca experiments used thermal atomic beams and specialized vapor cells, while later experiments employed atoms released from magneto-optical traps in an effort to reduce Doppler-based

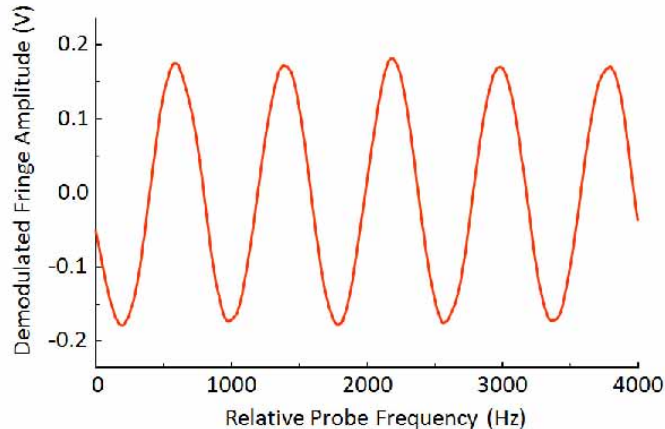


Fig. 12. – Bordé-Ramsey fringes with millikelvin Ca atoms. The resolution, 400 Hz, is comparable to the natural linewidth for this transition.

systematic effects. Such experiments used one and sometimes two stages of laser cooling, while Ca manipulation techniques culminated in the observation of a Ca Bose-Einstein condensate in 2009 [132].

Let us first consider atomic beam-based Ca spectrometers. The majority of experiments employed an apparatus similar to that used in the original NIST experiments [128]. Figure 10 shows how these experiments were laid out along the axis of propagation of the atomic beam. The atoms emerge from an oven held at a temperature of ~ 650 °C, which produces an atomic beam with a most probable velocity of ~ 640 m/s. Fluorescence is detected downstream with a photomultiplier tube. With a magnetic bias field of a few Gauss generated by a set of Helmholtz coils the first-order magnetically-insensitive $m_J = 0 \rightarrow m_J = 0$ transition can be excited. As discussed before, two recoil components are visible at resolved linewidths below the 23.1 kHz splitting for the Ca recoil components at 657 nm. In fig. 10 we show optical Ramsey fringes taken with a resolution of 5 kHz (resulting from an excitation beam spacing $2D = 9$ cm), which resolves cleanly the two recoil components. This spectrum is taken with an extended-cavity diode laser that is pre-stabilized to a high-finesse optical cavity. The laser has a fractional instability of 2×10^{-15} at 1 s, and an effective laser linewidth of about 1 Hz on a 1 s time scale [133].

To lock the laser frequency to the transition, one modulates the laser at ~ 300 Hz with a modulation depth equal to the full-width half-maximum of the spectroscopic feature (here 5 kHz). Subsequent demodulation yields an odd-symmetry error signal suitable for locking. Feedback with a loop bandwidth of ~ 10 Hz can yield a signal that yields a short-term stability of 5×10^{-15} at 1 s for a single laser system. Such systems could find a variety of precision timing applications, such as ultra-low noise microwave generation, in cases where stability is needed for tens or hundreds of seconds. Other applications arise from using the system to measure rotations via the Sagnac effect, DC electric fields via the Stark Effect, and AC Stark shifts via additional laser beams at different colors strategically located in the apparatus [118].

As discussed earlier, thermal systems will always be limited in terms of absolute uncertainty and even long term stability because of first- and second-order Doppler shifts. First order shifts lead to sensitivity to probe laser-beam alignment, while the second-order

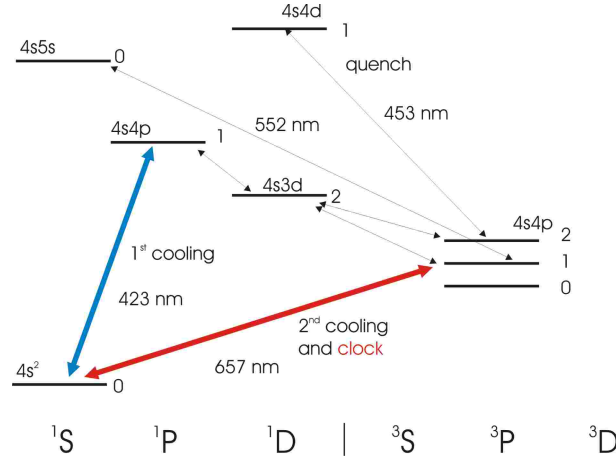


Fig. 13. – Energy levels and relevant optical transition for neutral Ca. The number near the level is the total angular momentum J .

effect leads to sensitivity to laser power fluctuations, oven-temperature fluctuations, and uncertainty in the velocity distribution. For these reasons, groups at Tokyo, PTB, and NIST (among others) used laser-cooling either with atomic beams or MOTs in an effort to make more accurate standards [45, 121, 107]. For Ca, the MOT-based systems loaded millions of atoms either from Zeeman-slowed beams or directly from laser-slowed atomic beams. Initial versions loaded atoms for a fraction of a second, then probed the atoms for up to a millisecond with a four-pulse optical Ramsey sequence [121]. A high signal-to-noise ratio resulted from normalized shelving detection based on earlier ion detection techniques (see, for example, reference [134]), which collects fluorescence from a strong transition (*e.g.*, the $^1S_0 \rightarrow ^1P_1$ cooling transition) rather than directly from the clock transition. A latter version used a much more rapid sequence that loaded for 2 ms, probed for 500 μs , and then quickly recaptured a majority of the atoms for a subsequent cycle [135]. The advantage of this approach is that the short cycle can yield high stability (4×10^{-15} at 1 s, 4×10^{-16} at 100 s) [133], but the disadvantage is that the magnetic field gradient needs to be left on throughout the whole sequence, yielding a large, though fairly steady systematic shift. For more accurate performance the longer cycle was used, for which the magnetic field could be well controlled and characterized.

Still, the best of millikelvin Ca clocks had absolute fractional uncertainties of $\sim 10^{-13}$, limited principally by the first-order Doppler effect, which includes non-parallelism of the counter-propagating laser beams and movement of the atoms through non-planar probe laser-beam wavefronts. Two groups pushed the performance further by implementing a second stage of laser cooling based on the $^1S_0 \rightarrow ^3P_1$ clock transition. However, the cooling force associated with this transition is too weak for efficient cooling, so these groups accelerated the cooling cycle with an additional “quenching laser”, either with the $^3P_1 \rightarrow ^1D_2$ transition at 453 nm [126] or with the $^3P_1 \rightarrow ^1S_0$ at 552 nm [127] (see fig. 13). Quenched cooling for calcium enables reduction of the atom temperature to 10 μK in three dimensions, and yields a distinctly different line shape due to the increased coherence of the atomic sample. With the reduced velocity the clock system attained an absolute fractional frequency uncertainty of 7.5×10^{-15} , still limited by motion of the

atoms in non-planar and non-parallel wavefronts [107]. Independent absolute frequency measurements of the Ca optical clock frequency agreed at the 1 part in 10^{14} level [83, 107]. While lattice clocks have attained a considerably smaller absolute uncertainty than that of Ca-based clocks, there is still interest in calcium in the clock world due to its potential as a simple system that can attain high stability and in even more exotic “Ca laser” experiments [136].

5.1.2. Mg optical clock. In many ways the development of clock spectroscopy with magnesium is similar to that of calcium, with several important differences that result from specific differences in their atomic properties. Early experiments, pioneered by W. Ertmer’s group in Bonn, were atomic beam-based and used the $^1S_0 \rightarrow ^3P_1$ intercombination line at 457 nm (analogous to the 657 nm transition in Ca shown in fig. 13).

This transition has a natural linewidth of only 31 Hz, and due in part to its higher frequency, it has a 5 to 10 times smaller blackbody shift than its strontium and ytterbium counterparts [91]. These potential advantages are somewhat offset by experimental complications associated with more challenging laser wavelengths and higher atomic velocities due to the comparatively light mass of $^{24,25}\text{Mg}$. The atomic beam clock experiments principally used the four-beam optical Bordé-Ramsey geometry with atoms emerging from an effusive oven whose induced fluorescence was detected downstream. The atoms fly through the probe beams with high velocity ($v_{prob} = 900$ m/s), thereby reducing the interaction periods and spectroscopic resolution. Nonetheless, spectra have been achieved with Mg thermal beams with resolutions sufficiently high to reveal clearly the 79.6 kHz splitting between the Mg recoil components [137]. In 2008 a thermal beam system was used to perform an absolute frequency measurement of the intercombination line with a fractional uncertainty of 2.5×10^{-12} , limited predictably by first- and second-order Doppler shifts.

A more precise measurement resulted from using laser-cooled atoms for atoms released from a MOT based on the strong $^1S_0 \rightarrow ^1P_1$ cooling transition at 285 nm. As a result of a larger Doppler width and a weaker line, only 1 % of the atoms in the cold (3 mK) sample could be excited on resonance, so a modified detection scheme based on optical pumping the atoms to the 3P_2 state from which they could be cycled on the 383 nm transition (with help from repumping from the 3P_0) enabled high signal-to-noise spectra to be obtained. In this way spectral linewidths as narrow as 290 Hz were resolved, and an absolute frequency measurement with an uncertainty of 7×10^{-14} was performed [138, 109]. Second-stage cooling has proved difficult in Mg [139], but there remain good prospects for use of Mg in an optical lattice (the magic wavelength for the $^1S_0 \rightarrow ^3P_0$ transition is predicted to be 463 nm) [140], where its smaller BBR shift could give it an advantage over existing lattice-clock systems.

5.2. Optical Clocks Based on Tightly Confined Neutral Atoms - Optical Lattice Clocks. – Despite their increased complexity, optical lattice clocks have become widespread tools for new clock research with neutral atoms due to two principal advantages: orders-of-magnitude higher resolution and greatly reduced systematics, especially those related to Doppler effects. The key aspect of a red-detuned optical lattice clock is the tight confinement that it provides along the propagation (or standing-wave) axis as a result of the attraction of the atoms to high light intensity. The one-dimensional standing wave (the vast majority of experiments have used 1-D standing waves, although we will mention a few that have employed higher dimensionality) forms a series of potential wells spaced by $\lambda/2$, where λ is the lattice wavelength (see fig. 14). To fill the lattice with atoms,

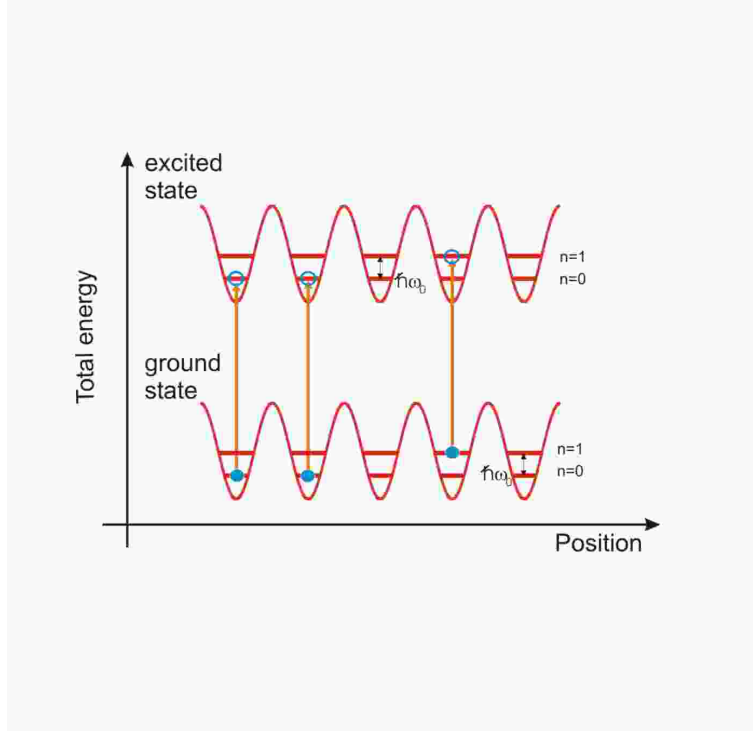


Fig. 14. – Schematic view of the excitation process in an optical lattice clock. Atoms are trapped in the minima of the periodical potential created by a standing wave in a region much smaller than the clock optical wavelength. Atoms are then excited on the narrow clock transition while the two clock states are equally energy shifted by the lattice potential. The index n represents the vibrational states of atoms in the lattice potential.

it is spatially overlapped with a magneto-optical trap that typically contains millions of atoms in roughly a cubic millimeter. This leads to filling of about 1000 potential wells, with 1 to 20 atoms per well on average. The wells contain ~ 5 -10 bound levels, with the $n = 0, 1, 2$ levels containing the vast majority of the atoms. Along the axis of tight confinement, the atoms oscillate at a frequency (50-100 kHz), 10 to 100 times higher than that of the atomic recoil frequency. In this so-called Lamb-Dicke regime, broadening and recoil effects are absent for near-resonant spectroscopy. Instead the motional effects are transferred to red- and blue-detuned sidebands, while the recoil effects are absorbed by the lattice itself. Under these conditions, the clock spectra can be as narrow as the probe laser itself, with several examples of sub-Hz lattice clock spectra existing in the literature. Spectra with widths of a few hertz have been used in conjunction with signal normalization (that is, normalizing the signal to the number of atoms in the lattice for the given measurement) to demonstrate fractional frequency instabilities well below 10^{-15} at 1 s [67, 141].

The key challenge in designing a lattice clock is handling the AC Stark effect associated with the lattice itself. The lattices need to have a depth, U_0/h , of at least 100 kHz-1 MHz in order to confine atoms with microkelvin temperatures, the coldest to which we can straightforwardly cool atoms. This means the ground-state energy level in the atom is

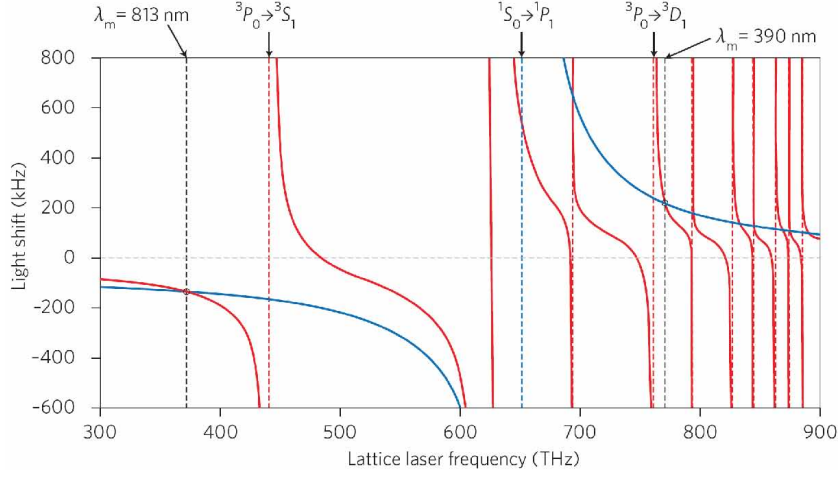


Fig. 15. – Estimated light shifts for the Sr 1S_0 (blue line) and 3P_0 (red line) states are plotted as a function of laser frequency for a laser intensity of 10 kW/cm^2 . The crossing points of blue and red lines indicate the magic wavelengths. Data from [144].

also shifted by roughly this amount. Such a shift seems at first glance unmanageable when we consider that we are striving to make clocks with millihertz accuracy. However, this drawback largely vanishes if we make a judicious choice of clock transition and tune the lattice wavelength to the appropriate value. In 2003, H. Katori and colleagues made the idea of lattice clocks feasible with their proposal to use the $^1S_0 \rightarrow ^3P_0$ transition in Sr [47] (soon after, the analogous transition was proposed for Yb [142]). The spherical symmetry ($J=0$) of both clock levels greatly reduces the clock sensitivity to lattice polarization fluctuations, and tuning the wavelength to its so-called magic value, at which both clock states experience identical shifts, suppresses its sensitivity to intensity effects. As a result the clock transition is left effectively unperturbed, minimally sensitive to lattice fluctuations. Perhaps surprisingly, even the magic wavelength is not that sensitive; holding the lattice frequency to within a range of 100 kHz is sufficient to keep fractional clock shifts to the low 10^{-18} level. In practice the magic wavelength requirement leads to lattice frequencies detuned far to the red, which in turn leads to shallow lattices even with a watt or more of lattice power focused to a waist of 30 to 50 μm . (Alternatively there have been proposals for blue-detuned, magic wavelength lattices, but these need to be three-dimensional, since the atoms are repelled by regions of high intensity [143]).

We note that this discussion is correct only to first order in intensity, for dipole-allowed transitions, which give the dominant part of the lattice shifts. We can re-write the lattice-induced shift in eq. 6 as:

$$(12) \quad \delta\omega = \alpha_0(\omega)I + \alpha_1(\omega)I^2 + \dots,$$

where α_0 is the differential polarizability for the 1S_0 ground and 3P_0 excited states (which includes both static and dynamic term), α_1 is the differential hyper-polarizability for these states, and ω is the frequency of the lattice light. By tuning ω to its magic value (usually in the near infrared, see fig. 15), α_0 goes to zero, but the higher-order terms, while in general very small, still persist [145]. In particular, the I^2 term, or

the hyper-polarizability, which corresponds to two-photon transitions, can cause non-negligible shifts that need to be evaluated, especially in the case of Yb. Additionally non E1 transitions, especially E2 and M1, can potentially contribute, sometimes in non-intuitive ways. Yudin et al. showed how in the standing-wave lattice geometry, such transitions can contribute with a \sqrt{I} dependence, although possibly at a negligible level [146].

With the lattice-induced shift effectively eliminated via lattice detuning, let us now consider how to excite what appears to be a heavily forbidden $^1S_0 \rightarrow ^3P_0$ transition. We note first that the $^1S_0 \rightarrow ^3P_1$ transitions are quite strong in heavy alkaline earth atoms due to mixing of the dipole-allowed 1P_1 state into the 3P_1 state (a result of the breakdown of strict L-S coupling rules). However, the 3P_0 state is still isolated from these allowed transitions, so further mixing is required. For even isotopes, the transition can be excited only with the inclusion of additional fields, either electric (AC) or magnetic, which mix a little of the 3P_1 state into the 3P_0 state, but also cause additional (although possibly manageable) systematic shifts to the clock system [147]. For the odd isotopes in Sr, Yb, and Hg, the situation is considerably more favorable. These isotopes have a nonzero nuclear spin that, through hyperfine mixing of the 3P_1 and 3P_0 levels, yields an almost ideal natural lifetime (10-100 s) for extreme clock applications. For such a lifetime, Hz-level spectroscopy is feasible with sub-microwatt power levels, leading to minimal probe-induced shifts. Moreover, the use of systems with non-zero spins yields multiple clock transitions split very weakly by a linear Zeeman effect. The use of transitions based on the two extreme m-values enables canceling of linear B-field effects (and very weak lattice polarization effects [47]) as well as simultaneous measurement of the B-field to evaluate the quadratic Zeeman shift. As we will see, while experiments have been performed on both bosonic (even isotopic) and fermionic (odd isotopic) systems, the majority of experiments now use fermions since they can be excited without external fields and have smaller systematic shifts to date.

The principal remaining systematic effects for lattice clock systems are (1) collision effects between atoms and (2) differential blackbody-based light shifts for the clock levels. In the original lattice clock proposals, collision shifts were thought to be almost insignificant because one would either use an under-filled 3-D lattice, which would effectively isolate the atoms from each another, or use a 1-D lattice with indistinguishable fermions, which would not collide (at least via the dominant s-wave mechanism) due to Pauli blocking [47]. However, three-dimensional lattices have been infrequently used due to power limitations and experimental complexity, and 1-D experiments in both Sr and Yb have in fact found non-negligible shifts (at the hertz level). As we shall see, these effects are now fairly well understood and have been minimized with experimental design. The blackbody effects, which are also at the hertz level, are easier to understand but harder to control. Control at the 1 K level seems straightforward in existing apparatus (corresponding to a mid 10^{-17} uncertainty), but specialized atom chambers may be required (and are being designed by several groups) for significant further reduction. While numerous atomic systems are under consideration for lattice clock research, to date three systems, Sr, Yb, and Hg, have been experimentally realized. In the following sections we will describe these three systems in more detail.

5.3. Sr optical lattice clock. – As with other alkaline earth atoms, spectroscopy on intercombination lines in Sr began with atomic-beam and cell-based investigations [148]. While there were some precision measurements made on the $^1S_0 \rightarrow ^3P_1$ transition [149], these investigations were somewhat hampered by the shorter lifetime (21 μ s) of the

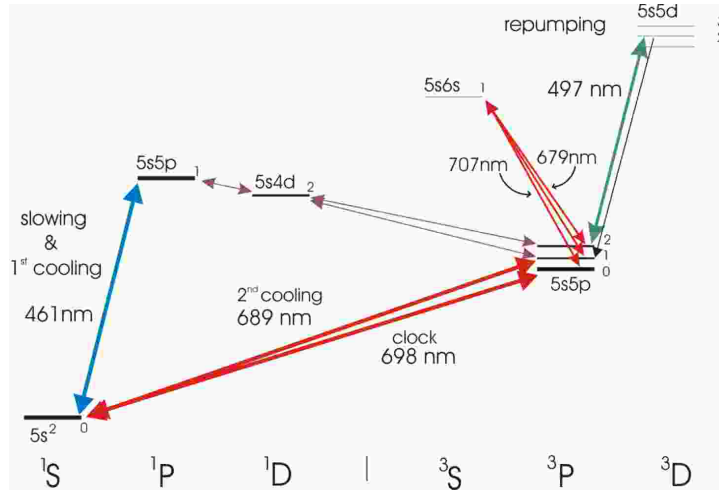


Fig. 16. – Energy levels and relevant optical transition for neutral Sr.

excited state. This lifetime, however, proved to be ideal for second-stage cooling to temperatures of $1 \mu\text{K}$ and below, which has helped propel Sr to the forefront of optical lattice clock research. Indeed, Sr was the first atom proposed for lattice research (by Katori and colleagues [47]), and the demonstration of spectroscopy with lattice-confined Sr atoms soon followed [48]. As a result, Sr lattice clocks are widespread throughout the community and have been used to achieve many of the seminal lattice results. Sr's suitability for this type of research comes from its particular electronic level scheme, presented in fig. 16.

The singlet-triplet structure found in alkaline earth atoms such as Sr provides strong singlet-singlet transitions for rapid atom cooling/trapping and weaker singlet-triplet transitions for more gentle atom manipulation and of course, clock spectroscopy. In Sr the $^1S_0 \rightarrow ^3P_0$ clock transition occurs at 698 nm, with a strong cooling transition at 461 nm, and the weak, but extremely effective, second-stage cooling transition at 689 nm. There is a convenient magic wavelength for the clock transition at 813 nm, well within reach of Ti:Sapphire and semiconductor laser systems. The most abundant isotopes (by far) are ^{88}Sr (82 %) and ^{86}Sr (10 %), which have zero nuclear spin, and ^{87}Sr (7 %), which has a nuclear spin of $9/2$.

Laser-cooled atomic clock systems such as those based on atoms confined to a lattice or on single-trapped ions must use a measurement cycle since the atoms/ions need to be loaded and/or cooled (and perhaps optically pumped) before being probed by the clock laser. Moreover, since the detection period following spectroscopy usually heats or depletes the sample, the full preparation-excitation-detection cycle must be repeated continually during clock operation. Here, to give the reader an example of how such cycle-based atomic clock systems work, we will describe the Sr lattice clock system in some detail, in terms of both its operational measurement cycle and (more briefly) its typical physical layout.

The heart of the Sr clock apparatus is the vacuum system that contains an atomic oven at one end connected by a tube to an interaction region at the other, which consists of a stainless steel chamber with multiple laser-grade windows to provide access for all

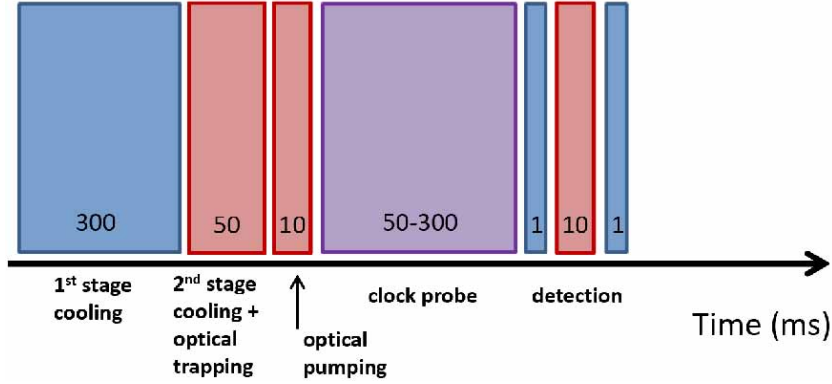


Fig. 17. – Typical optical lattice clock cycle.

the laser beams needed to manipulate and probe the Sr atoms. The measurement cycle for a typical Sr lattice clock (see fig.17) commences with ~ 300 ms loading period, during which a MOT based on the strong 461 nm cooling transition is loaded from a beam of Sr emerging from a hole in the Sr oven. The loading rate is usually enhanced with a counter-propagating slowing beam used in conjunction with a Zeeman slower. Transverse heating associated with the Zeeman slower can be compensated with transverse cooling beams upstream from the MOT [150]. This first-stage MOT can load as many as 10^8 atoms and cools the atoms to a few millikelvins, a bit above the Doppler cooling limit for this transition. A period (typically 50 ms long) of second-stage cooling based on the 689 nm intercombination $^1S_0 \rightarrow ^3P_1$ line reduces the atom temperature to near $1 \mu\text{K}$, well below that of typical Sr lattice depths ($\sim 10 \mu\text{K}$). The low temperature achievable with a second-stage Sr MOT is principally the result of the narrow width (7.5 kHz) of this cooling transition, which requires precise control of the laser detuning, frequency modulation, magnetic field gradient, and intensity. Additionally with odd isotopes, a second frequency source (sometimes called a “stirring” laser) is required to optically pump atoms back into the cooling cycle [151]. Careful overlapping of the lattice with the second-stage, red MOT leads to the accumulation of up to 10^5 atoms in the lattice, predominantly in the $n = 0$ and $n = 1$ motional states. We note that a different lattice loading approach, using an atomic “drain” has been demonstrated at SYRTE [152].

Spectroscopy of the clock transition is performed by precisely overlapping the traveling wave probe beam with the lattice beams in order to take advantage of the Lamb-Dicke confinement of the atoms. The frequency of the probe light is pre-stabilized on a narrow resonance of a high-finesse optical cavity (recall sect. 3.3), and an acousto-optic modulator is used to pulse the light (and stabilize the intensity) for a preset period of typically 10-200 ms to yield (usually) Fourier-limited spectra. The probe light usually excites some fraction of the atomic sample to the long-lived upper clock state. Near atom-shot noise-limited detection of the excitation fraction then results from the following detection sequence: (1) resonant 461 nm light (for a few milliseconds) is used to scatter many signal photons while simultaneously heating the ground state atoms out of the lattice, (2) lasers that connect the $^3P_0 \rightarrow ^3S_1$ and $^3P_2 \rightarrow ^3S_1$ transitions (see fig. 16) are used to pump (in a few ms) the still-excited atoms back to the ground state, and (3) the previously excited atom population is read out (for a period of a few ms) by again cycling

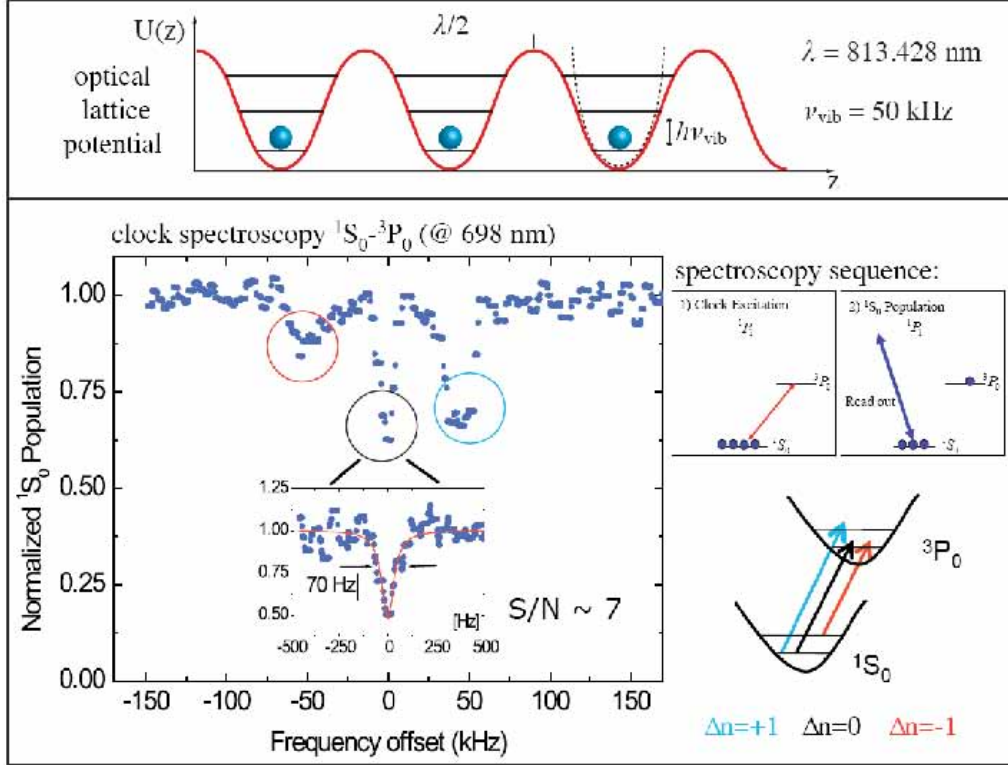


Fig. 18. – Lattice spectroscopy on 698 nm clock $^1S_0 \rightarrow ^3P_0$ transition of neutral Sr. Atoms are trapped in the minima of the optical lattice potential (upper part) while the clock transition is probed (lower part). Data from [153].

on the cooling transition. In this way a normalized shelving detection signal [134, 154] is generated, which is insensitive to shot-to-shot variations in the number of atoms in the lattice and can approach atom shot-noise-limited performance. Alternatively, we can make a dispersive, non-destructive measurement of the excitation in an effort to be able to recycle the atoms [68] more efficiently.

In any case, the detection period concludes the measurement cycle and yields a series of integrated PMT pulses, whose effective areas are read as voltages by a computer and then converted to a normalized excitation signal. We then use the computer to step the optical frequency via a frequency-shifting device such as an acousto-optic modulator and repeat the measurement cycle. In this way, we can generate a spectrum showing the excitation voltage as a function of laser probe frequency, with the frequency-axis points carefully referenced to the Fabry-Pérot cavity resonance to which the laser is locked. Moreover, since the computer receives the spectroscopic signals and controls the laser frequency, it can readily lock the laser frequency (seen by the atoms) to the clock transition through implementation of a modulation + digital servo scheme. Such schemes can be as simple as modulating back and forth over the half-maximum points of the spectroscopic signal and feeding back with a digitally integrated signal, or more sophisticated with a more complicated modulation protocol involving multiple resonances

and/or high-order loop filters.

As a brief aside, we note that the description of the Sr lattice clock system up to this point has included a fairly large vacuum apparatus, at least four laser systems, a computer control system, a Fabry-Pérot reference cavity, along with their implied supporting optics and electronics. Indeed, state-of-the-art optical clocks are complex experimental devices, which can easily fill two $1.5 \text{ m} \times 2.5 \text{ m}$ optical tables, along with several racks of supporting electronics and often a separate, vibrationally isolated miniature for the optical reference cavity. Certainly commercial or space-qualified versions will need to be built in a more compact and robust manner, and groups are already beginning to address these challenges (see sect. 8.2 for further discussion of this important issue).

Let us now look at the spectra that result from the Sr clock apparatus. A broader scan taken over a range of a few hundred kilohertz around the clock resonance reveals the key lattice spectroscopic features (see fig. 18). On either side of a narrow carrier, one sees the characteristic motional sidebands. These sidebands correspond to transitions that change the motional state (labeled by quantum number n) by $\Delta n \pm 1$ motional quantum, and reveal that the motional frequency is $\sim 70 \text{ kHz}$ (the splitting between the carrier and sidebands). From the ratio of the sideband heights we can determine the effective temperature of the lattice confined atoms, as the red sideband is reduced in height when more atoms are in the ground-state motional level ($\Delta n = -1$ transitions are forbidden from the ground state) [155]. If we focus on the carrier ($\Delta m = 0$ transitions), we see either a single feature for ^{88}Sr or a set of ten features for ^{87}Sr split by a weak magnetic field. In typical experiments with ^{87}Sr , the atomic sample is pumped to either of the stretched states ($m = \pm 9/2$) before clock spectroscopy is performed, and then the drift of the reference cavity is suppressed by fixing the laser probe frequency to the mid-point between the two features. As a result, the first-order magnetic field sensitivity of the transition and the vector light shift are suppressed. Due to the high multiplicity of its ground state, Sr also has a tensor light shift, which actually manifests itself as a shift in the magic wavelength that is the same for the two stretched states (see Reference [156] for details).

Evaluations of systems based on both ^{88}Sr [162, 102] and ^{87}Sr [163, 152, 159, 164, 161] have been performed, with ^{87}Sr looking considerably more promising due to its smaller quadratic Zeeman and probe light shifts. As a consequence the majority of research into systematic effects for Sr has focused on ^{87}Sr . In 2008, a seminal evaluation of this system was performed at JILA, which found a total fractional uncertainty of 1×10^{-16} [163] and was dominated by lattice light shift, blackbody shifts, and collision effects. Since then, the light shifts were investigated in detail through use of a build-up cavity for the lattice light in order to enhance (temporarily) the effects for more precise evaluation [165]. As a result, the magic wavelength was determined to higher precision, and the influence of higher-order effects was shown to be minimal. In this manner, the uncertainty for the lattice light shift term is now reduced to below 2×10^{-17} , fractional uncertainty [157]. Detailed collision studies have been performed on both ^{88}Sr [166] and ^{87}Sr [167], where systematic shifts as large as 1 Hz have been seen in both systems as well as distortions of the central feature. For ^{87}Sr , in particular, it was determined that the shifts were a result of non-uniform excitation of the trapped atoms, due in part to atoms in different motional states and to divergence in the probe laser. This non-uniform excitation degrades the indistinguishability of the atoms and enables s-wave interactions to occur. Studies with Sr atoms in two-dimensional lattices have offered further support for this picture and even showed how at high-enough density, paradoxically, the atom-atom interaction can be large enough to suppress the shift altogether [168]. There have

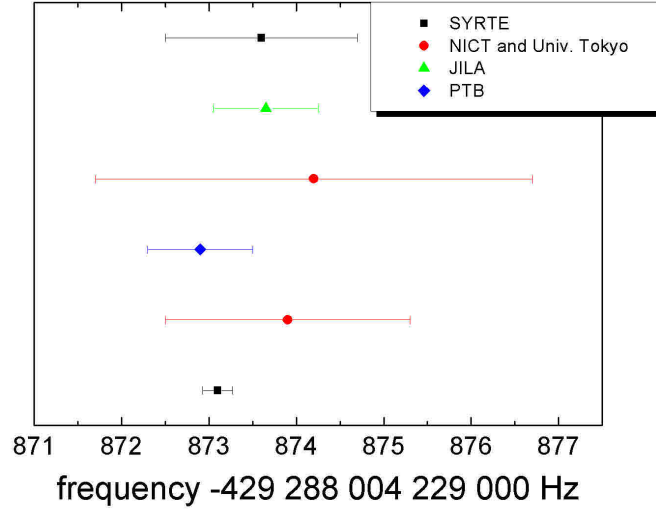


Fig. 19. – Frequencies of the ^{87}Sr clock transition measured by different laboratories: SYRTE, Paris (square, [152, 157]), JILA, Boulder (triangle, [158]), Tokyo Univ. and NICT (circle, [159, 160]) and PTB, Braunschweig (diamond, [161]).

been numerous absolute frequency measurements of the ^{87}Sr clock transition performed at the 10^{-15} level relative to Cs (see fig. 19), and their agreement displays the robustness of this transition to perturbations. More recently two ^{87}Sr lattice clocks in one lab at SYRTE showed agreement at the 1×10^{-16} level, and their agreement with three primary Cs standards was limited at 3×10^{-16} level by the microwave sources ($\nu_{Sr} = 429\,228\,004\,229\,873.10$ Hz) [157].

The most serious systematic remaining for the Sr lattice clock is the shift due to black-body radiation. Sr has the highest sensitivity to BBR of all of the most accurate optical clock candidates, with a room-temperature shift of 2 Hz (or 5×10^{-15} , fractionally). Thus, it is important to know the coefficient at the 0.1 % level, and to know and control the environment at the 0.1 K level for net clock performance in the mid- 10^{-18} at room temperature. By means of a moving lattice and a specialized DC Stark chamber, the differential DC Stark sensitivity was measured with a 28 ppm uncertainty [87], in good agreement with theory [169]. When combined with knowledge of the dynamic correction to yield the total BBR sensitivity, the fractional uncertainty for the BBR shift is now only a result of the uncertainty in the temperature of the environment, so several groups are now preparing specialized chambers, which can be cryo-cooled if necessary. Due to the T^4 dependence of the shift, operation of the clock at liquid-nitrogen temperature would reduce the shift to the 10^{-17} level with only modest knowledge of the temperature needed to reduce the uncertainty to 10^{-18} or below.

Recently a clock laser developed for Sr lattice clock spectroscopy at JILA has demonstrated stability at the 10^{-16} level due to advances in reference-cavity design. As a result, clean spectra with sub-Hz linewidths have been resolved, and when locked to the Sr signal, clock stability of $4 \times 10^{-16} \tau^{-1/2}$ level has been observed [141]. Together with

TABLE IV. – *Uncertainty budget for Sr optical lattice clock at JILA [17].*

Sources for shift	Shift (10^{-18})	Uncertainty (10^{-18})
BBR Static	-4962.9	1.8
BBR Dynamic	-346	3.7
Density	-4.7	0.6
Lattice Stark	-461.5	3.7
AC Stark (probe)	0.8	1.3
First-order Zeeman	-0.2	1.1
Second-order Zeeman	-144.5	1.2
Lattice vector shift	0	<0.2
Line pulling & Tunneling	0	<0.1
DC stark	-3.5	2
Background gas collisions	0.63	0.63
AOM phase chirp	-1	1
Second-order Doppler	0	<0.1
Servo error	0.4	0.6
Systematic total	-5922.5	6.4

similar performance demonstrated in Yb [67], these are the first clear demonstrations of the advantage that a large number of atoms can give, as previously the frequency noise (enhanced by the Dick effect) had masked the atom projection-noise limit. Such systems are capable of averaging down to less than 10^{-17} in tens of minutes (see fig. 21), making systematic evaluations at this level feasible, as evidenced by the record low uncertainty (6×10^{-18}) very recently reported by the JILA group [17] (see Table IV). Moreover, still further cavity advances are on the horizon, and instabilities well below $10^{-16}\tau^{-1/2}$ are anticipated. Sr clock's capabilities and reproducibility have been noticed outside of optical clock circles, and as a result, the Sr lattice clock is presently being considered as a prominent candidate for a possible redefinition of the second [157] or for use as a remote clock on the International Space Station [153, 42, 170].

5.4. Yb optical lattice clock. – While Ytterbium has long been an interesting candidate for parity violation [171] and degenerate gas [172] research, it became an optical clock candidate only recently with the advent of optical lattice clocks. This delay was due to the fact that its $^1S_0 \rightarrow ^3P_1$ intercombination line is much broader (187 kHz) than that of Ca, Sr, and Mg, making this transition unsuitable for high precision work, while its $^1S_0 \rightarrow ^3P_0$ transition did not become practical until the lattice clock proposal of Porsev et al. [142], soon after the first demonstration of the Sr lattice clock. It turns out that for optical lattice clock work, Yb is an excellent candidate. While in many ways very similar to Sr, Yb has some useful characteristics of its own, including an abundant spin-1/2 isotope and straightforward second-stage cooling. Yb is in fact a rare-earth element, but its two-valence electron structure leads to singlet/triplet manifolds similar to those seen in the alkaline earth atoms.

As shown in Figure 20, the Yb $^1S_0 \rightarrow ^3P_0$ clock transition is at 578 nm, with a natural linewidth of ~ 10 mHz, practically ideal for a lattice clock system. The initial cooling/trapping is performed on the $^1S_0 \rightarrow ^1P_1$ transition at 399 nm (natural linewidth ~ 34 MHz), while the previously mentioned $^1S_0 \rightarrow ^3P_1$ line at 556 nm is used for second-stage cooling. This second stage reduces the temperature from a few mK to $50 \mu\text{K}$, considerably warmer than one obtains with Sr, due to the 25 times broader linewidth of

the second-stage cooling transition. This has the consequence that the atoms loaded into the lattice also are warmer (typical temperature $\sim 10 \mu\text{K}$), thereby putting more atoms into motion levels above the ground state. The lattice magic wavelength for the clock transition occurs at 759.4 nm, and Yb also has repumping transition at 1.388 μm that is used to pump atoms from the excited state back to the ground state.

Early research geared toward the development of an Yb lattice clock took place at KRIS, the University of Washington, and NIST-Boulder [173, 174, 175], while more recent efforts are underway in Tokyo, Düsseldorf, Torino, Shanghai, and other laboratories [176, 177, 178, 179]. A typical Yb lattice clock apparatus looks similar to that of a Sr lattice clock described above. Atoms are typically loaded from a thermal, effusive beam (with or without the aid of a Zeeman slower) into a MOT at 399 nm, with millions of atoms loaded in ~ 300 ms. This can be achieved with only a few milliwatts per MOT beam and ~ 10 mW in a counter-propagating slowing beam. Due to its broad linewidth, the second-stage cooling transition makes transferring atoms from a first-stage MOT to a second-stage MOT very efficient ($> 80\%$ transfer), and the use of a “stirring” laser is not needed for odd isotope cooling. Some broadening of the cooling laser spectrum is employed initially in the transfer; then a single frequency cycle reduces the sample size to ~ 1 mm diameter and the temperature to $\sim 50 \mu\text{K}$ [180]. This matches the depth of the optical lattice, which is formed by tightly focusing ~ 1 W of power at 759 nm into a 30 μm waist, and then carefully overlapping a retro-reflected beam. Up to tens of thousands of Yb atoms with a residual temperature of 10 μK can be loaded into about 1000 lattice sites for a 1-D lattice.

The clock transition has been excited in both bosonic (^{174}Yb) and fermionic (^{171}Yb) systems for Yb. While magnetically induced laser excitation was first demonstrated in ^{174}Yb [180, 181], the majority of the most recent research has focused on ^{171}Yb , due to more straightforward excitation and reduced systematic effects. ^{171}Yb has an advantage over ^{87}Sr in that it is a spin-1/2 system, so it has only two ground-state sublevels, and optical pumping between these states is extremely efficient. Moreover, due to its low multiplicity, it has a zero tensor shift.

As was the case with Sr, it is important to work with an ultra-pre-stabilized laser to achieve the best results offered by the Yb system. Yb clock lasers have been stabilized to cavities with thermal noise limits as low as 10^{-16} and demonstrated stability at the 2×10^{-16} level for up to 5 s. Such lasers have been used to perform sub-Hz spectroscopy with the Yb clock transition, and for the NIST system (which has been at the forefront of Yb clock research), a < 5 Hz spectroscopic feature is regularly used for locking the laser in combination with a normalized shelving detection technique similar to that of Sr [67]. Recent comparisons between two similar Yb systems at NIST have demonstrated a clock stability of $3.2 \times 10^{-16} \tau^{-1/2}$, which averaged down to 1.6×10^{-18} at 25 000 s (see fig. 21), the highest clock precision to date [21]. Precision absolute frequency measurements of the Yb clock transition relative to Cs have been performed by three groups with good agreement within the uncertainties of the clocks [182, 176, 183]. At this point the absolute frequency of the ^{171}Yb clock transition, 518 295 836 590 865.2 Hz, is known with an uncertainty of 0.7 Hz.

The dominant systematic effects for the Yb lattice clock are basically the same as those for Sr: lattice light shifts, collision effects, and blackbody light shifts. The lattice light shifts are evaluated by changing the lattice intensity and wavelength while measuring clock frequency shifts. The situation for Yb is complicated by a much larger hyperpolarizability effect due to two two-photon transitions that are detuned only 0.3-1 nm from the magic wavelength. The effect of these transitions has been evaluated

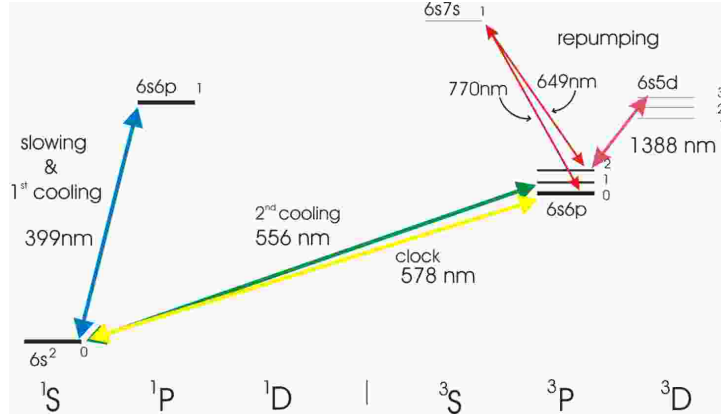


Fig. 20. – Energy levels and relevant optical transition for neutral Yb.

and contributed a fractional uncertainty of 7×10^{-17} to the clock uncertainty budget with excellent prospects for significant further reduction [184]. Detailed collision studies have been performed with Yb clocks in both 1D and 2D lattices [185]. These revealed a significant, even dominant, contribution from p-wave scattering, which early on was thought to play a small role in lattice clock atom-atom interactions due to the low atom temperatures. However the densities are high enough around the lattice anti-nodes to enable clock shifts as large as 1 Hz, but it was shown that with a judicious choice of pulse area Ramsey-style two-pulse excitation could be used to reduce the clock shift to $< 5 \times 10^{-18}$ for 1-D lattice samples of a few thousand atoms [186].

At this point, the most challenging obstacle to 10^{-18} accuracy for Yb optical lattice clocks is the blackbody radiation shift. While its shift is only half of that of Sr, until recently, the large uncertainty (10 %) in the knowledge of the blackbody coefficient led to a 3×10^{-16} contribution to the Yb uncertainty budget. A recent high precision measurement (20 ppm) of the DC differential polarizability for the Yb clock transition along with a reevaluation of the dynamic correction reduced the uncertainty in the knowledge of the blackbody coefficient to less than 0.1 % [89, 187]. These results are in good agreement with recent calculations [188]. Presently, the BBR uncertainty is limited by control and understanding of thermal environment, conservatively estimated ~ 1 K, corresponding to 3×10^{-17} fractional uncertainty. Progress much beyond this level will most likely require specialized interaction chambers, and indeed such hardware is presently under design for Yb clock systems.

5.5. Hg optical lattice clock. – While the Sr and Yb lattice clocks share many features and limitations, the third species of lattice clock demonstrated thus far, one based on the $^1S_0 \rightarrow ^3P_0$ transition at 266 nm in Hg, is quite different in several key ways. Perhaps its principal advantage is that, in part as a result of its higher clock transition frequency (in the UV), it has a BBR shift that is estimated to be more than an order of magnitude smaller than those of Yb and Sr [94]. Additionally, it can be trapped with a room-temperature source (further reducing BBR effects) and loaded into a lattice with a single stage of laser cooling/trapping. These advantages, however, are offset, at least in part, by the much-shorter-wavelength radiation required for the cooling/trapping, lattice, and probe lasers, making them considerably more difficult to develop, especially at high

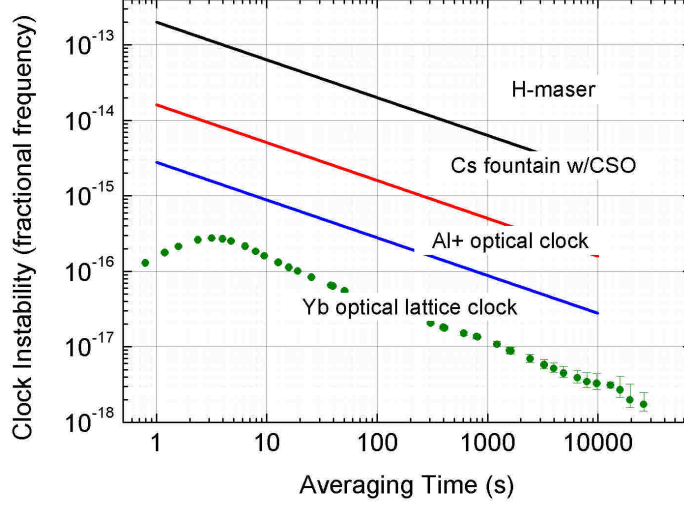


Fig. 21. – Comparison of lowest frequency instabilities achieved with different clock technologies (red line, high stability Cs fountain at SYRTE [189]; green line, Al^+ ion clock at NIST [16]; blue dot, Yb lattice clock at NIST[21]).

power.

Hg is a transition metal that has the two-valence-electron structure common to lattice clock atoms. The strong $^1S_0 \rightarrow ^1P_1$ transition used in other two-electron atoms for cooling and trapping is inaccessible for Hg due to its short wavelength (185 nm), but the $^1S_0 \rightarrow ^3P_1$ intercombination line (at 253.7 nm) that is used for second-stage cooling of Sr and Yb, is sufficiently strong in Hg (natural linewidth = 1.3 MHz) to enable trapping, while having a low Doppler limit to cool the atoms adequately for lattice-loading. The magic wavelength for the Hg lattice is 362.6 nm [190]. The radiation for the cooling and clock is typically generated by quadrupling infrared sources, while the lattice light requires a build-up cavity to reach the necessary intensity. The associated technical challenges have slowed development of the Hg lattice clock since its proposal in 2008 [94] and, in fact, there are only two groups aggressively pursuing Hg lattice clocks at this writing [94, 191]. Nevertheless, in recent years a successful demonstration of a Hg lattice clock has been reported [191] and impressive results have followed [190].

In the experimental apparatus of ref. [190], atoms are loaded from a source held at 233 K (the low temperature is characteristic of Hg's inherently high vapor pressure) into a 3-D MOT at 253.7 nm for 1.3 s. About 2500 atoms are transferred into a vertical lattice consisting of 3 W of intracavity build up power (120 μm waist yields a 9 μK lattice depth). Clock spectroscopy at 266 nm reveals a lattice-confined atom temperature of 4 μK , and central carrier features as narrow as 11 Hz have been generated. The absolute frequency of this transition was measured to be 1 128 575 290 808 162.0(6.4) Hz, with the uncertainty dominated by lattice light shifts and limitations in the precision with which the systematics could be measured [190]. To date, this system has demonstrated a fractional frequency instability of $5.4 \times 10^{-15} \tau^{-1/2}$, limited by the signal-to-noise ratio of

the system, which has yet to add normalization to the shelving detection process [192]. Since these limitations are basically technical in nature, there are good prospects for rapid improvement for the system, which, with its low BBR sensitivity, could lead to Hg being a leading player in future lattice clock research.

In Table V is reported the state-of-the-art of neutral atom optical-clocks.

6. – Optical clocks based on ions

A single ion confined in an electromagnetic trap, such as the Paul trap, has shown to be a powerful way of investigating very weak (or high- Q) clock transitions in the trapped ion, where environmental perturbations can be effectively controlled. Ions can be created by electron-beam ionization or photoionization of a weak atomic flux from an oven within an ultra-high-vacuum ($< 10^{-7}$ Pa) chamber whilst the atoms are within the trapping potential. Trapping of single ions to large clouds of ions (*e.g.* $N \sim 10^6$) can be achieved, dependent on trap geometries, but in the latter case, space-charge effects create significant perturbations for the ions. This is not so for the single trapped ion, where with appropriate parameter control, it can be isolated as a single particle within a low field environment, and laser-cooled to ~ 1 mK above absolute zero, whereby the thermal motion-induced Doppler broadening contribution to the spectral width of an absorption is minimized. Additionally, extended confinement times within the trap provide for long interrogation periods, also allowing environmental fields to be minimized, nulled and/or controlled. With these arrangements, the observation of a weak optical (clock) transition with natural linewidth ≤ 1 Hz from an ion virtually at rest in near-undisturbed conditions over extended periods (days) provides a high accuracy frequency standard.

6.1. *Single-ion clock operation.* –

6.1.1. Single ion trap designs. It is not possible to create a 3D potential well using just a static electric potential ϕ , and different trap designs have been developed to cope with this (see fig. 22). For single ions, these generally comprise a cylindrically symmetric potential of the form $\phi(r, z) = A(r^2 - 2z^2)$, where r and z are the radial and axial coordinates, respectively. The most common of these designs is the radio frequency (rf) Paul trap, which ideally has electrode structures with surfaces that match the hyperbolic contours of constant potential, resulting in a ring of inner radius r_0 and two end-caps separated by $2z_0$. Opposite polarity voltages applied to the ring and end-caps respectively, give rise to a saddle potential, which is confining in one direction only. However, by applying a large oscillating potential $V_0 \cos \Omega t$ combined with a small static potential U_0 between ring and end-caps, this has the effect of alternating the confinement direction between the axis and the radial plane, setting up a time-averaged pseudo-potential well where the trapping force is directed to trap centre on a timescale that is longer than the oscillation period, but fast enough to ensure that the ion(s) remain held within the potential, and strong enough to ensure that the ion's kinetic energy is unable to surmount the well. This leads to stable confinement of the ion(s) in the trap for certain values of applied AC and DC voltages, applied oscillation frequency (or micromotion frequency) $\Omega/2\pi$, and ion mass M . The ion motion can be derived as solutions to the Mathieu equation [193], giving rise to pseudo-potential oscillation frequencies ω_z, ω_r (secular motional frequencies) of the ion in the trap, which are of order of a factor 10 smaller than the drive frequency Ω .

In order to avoid strong perturbations from space charge due to multiple ions, the ion clock traps are operated with a single trapped ion. For this, miniature rf traps are used,

TABLE V. – Neutral atom optical clock species showing their associated state-of-the-art systematic uncertainties reported in the literature.

Atom	Nucl. Spin	λ_{cool} [nm]	Clock Trans.	λ_{clock} [nm]	$\Delta\nu_{nat}$ ($\Delta\nu_{obs.}$)	rel. uncertainty
^1H	1/2	-	$1S - 2S$	243 (2-ph.)	1.3 Hz (2 kHz)	4.2×10^{-15}
^{24}Mg	0	285	$1S_0 - 3P_1$	457	30 Hz (290 Hz)	7×10^{-14}
^{40}Ca	0	432, 657	$1S_0 - 3P_1$	657	375 Hz (250 Hz)	4.2×10^{-15}
^{87}Sr	9/2	461, 689	$1S_0 - 3P_0$	698	1 mHz (0.5 Hz)	6×10^{-18}
^{88}Sr	0	461, 689	$1S_0 - 3P_1$	689	7.6 kHz (14.5 kHz)	2.3×10^{-11}
^{171}Yb	1/2	399, 556	$1S_0 - 3P_0$	698	≈ 0 Hz (8 Hz)	2.9×10^{-15}
^{173}Yb	5/2	399, 556	$1S_0 - 3P_0$	578	10 mHz (1 Hz)	3.6×10^{-16}
^{174}Yb	0	399, 556	$1S_0 - 3P_0$	578	10 mHz (150 kHz)	8.5×10^{-11}
^{199}Hg	1/2	254	$1S_0 - 3P_0$	265.6	≈ 0 Hz (4 Hz)	1.5×10^{-15}
					100 mHz (11 Hz)	5.7×10^{-15}

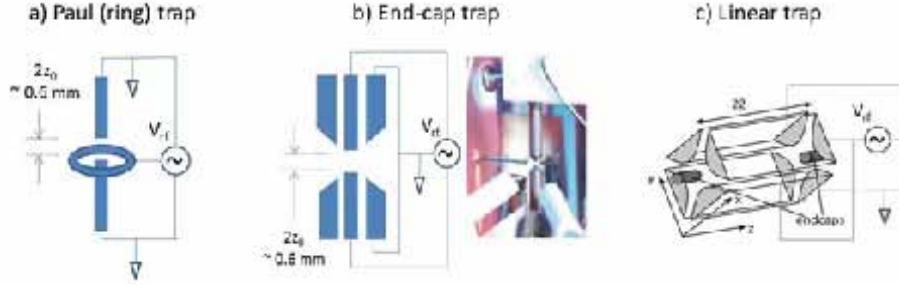


Fig. 22. – Common miniature rf Paul trap electrode configurations: a) ring trap, b) end-cap trap, c) linear trap. DC voltages not shown; typical end-cap electrode separation of 0.6 mm for ring and end-cap traps; linear trap end-cap separation dependent on 4-blade electrode length (typically a few mm) .

with ring diameters of ~ 1 mm, and applied oscillating voltages and drive frequencies of a few hundred volts at frequencies of 10 - 20 MHz. The ion exhibits 3D simple harmonic motion with secular frequencies ω_r and ω_z in the low MHz range, but with a high-frequency perturbation (micro-motion) at the drive frequency Ω . The magnitude of this perturbation depends on the average distance of the ion from the centre of the potential well, and small DC voltages are used to tweak the ion's position close to trap centre to minimise this micro-motion. In fact, these miniature trap designs have simpler, non-hyperbolic shaped electrodes. While these shapes are only approximations to the desired hyperbolic shape, this is not too critical for an ion located close to the trap centre. In addition to the ring trap, other common designs used for frequency standards also include the end-cap trap [194], where ring functionality is achieved by the use instead of two outer electrodes arranged co-axially around the end-caps, (see fig. 4), and the linear ion trap [195] where ions are confined in a linear string along the z-axis by means of AC voltages applied to two of four rod electrodes parallel to the axis and a DC voltage applied at each end. Various linear trap design have been applied to frequency standards, including the blade trap [196] and micro-fabricated segmented traps [16]. More recently, a micro-fabricated monolithic trap structure built into a silicon wafer with potential application to future ion clocks has been demonstrated [197].

6.1.2. Single ion generation. In order to create a single ion within the trapping potential, electron bombardment of neutral atoms emitted from a simple hot tubular oven of dimensions ~ 1 mm diameter \times 10 mm long was originally used to create singly-charged positive ions for ion trap experiments. This technique, however, was inefficient as it required both large atom fluxes and electron beam currents, which give rise to excessive coating of trap electrodes and surrounding materials and charge build up on insulating surfaces. These, in turn, generate patch potentials on the electrodes and variation in local surface charges, leading to increased micro-motion experienced by the ion and anomalous heating rates experienced by the cold ion. Moreover, the resulting micro-motion drifts over time, the more so with increased loading frequency, and requires frequent compensation using DC voltages as described earlier.

In recent years, photoionization techniques have been developed for loading single ions in order to mitigate these problems. These techniques have been shown to dramatically reduce the atom flux necessary, by a few orders of magnitude, to load a single ion under

near deterministic control. Photoionization loading of ion traps has been reported for all the common ion species used in ion clocks. By way of example, we consider the case of photo-ionisation for strontium. This requires two wavelengths at 461 nm and 405 nm. The 461 nm wavelength raises the atoms from the ground state to the 1P_1 resonance level (the same excitation as used for slowing and trapping Sr neutral atoms), with 405 nm further exciting the atoms into the continuum. This is simply achieved in Sr by single pass frequency doubling of DFB laser diode light at 922 nm in a periodically-poled KNbO₃ crystal (with typical output power of 300 μ W at 461 nm), where adequate control of a narrow-linewidth laser frequency allows tuning to the resonance transition frequency. A broad-linewidth ~ 1 mW 405 nm diode laser is sufficient for ionisation.

A refinement of this technique has demonstrated even more control [198]. Here a hot-plate is preloaded with Sr from the oven and is used as an atom source that can be operated at low temperatures of ~ 120 °C. With alternate photo-ionisation and detection periods of 70 ms and 30 ms respectively, where the detection is achieved by monitoring the 422 nm Sr⁺ $^2S_{1/2} - ^2P_{1/2}$ ion fluorescence used to cool the ion, the hot plate current can be turned off immediately after the particular detection period that indicates the presence of the ion fluorescence. This has the effect of minimising the atom flux used and subsequent generation of patch potentials, requiring less micro-motion compensation.

6.2. Laser cooling of single ions. – For simple Doppler cooling, repeated photon scattering of laser light red-detuned from line-centre of a strong transition of a single ion confined within the trap, reduces the ion’s velocity to about a metre per second, with corresponding temperature of ~ 1 mK, within a fraction of a second after a large number of scattering events. The rate of scattering is dependent on the upper level lifetime ($\sim 10^{-8}$ s). Ideally, this cooling would be a closed cycle. In fact, there is generally a branching decay from the upper level of the cooling transition to a metastable state, which will terminate the cooling process. In order to avoid this, a repump laser is used to empty the metastable state and return the ion to the cooling cycle. The Doppler cooling requires only a single cooling beam, since the driven motion will result in components of the cooling beam acting in all three orthogonal directions. Both the trap micro-motion and secular motion frequencies contribute series of sidebands to the ion’s Doppler linewidth. For a well-cooled ion, the secular sidebands are reduced to a few weak motional sidebands close to carrier and separated by the secular frequencies. However, for a strong cooling transition, the natural linewidth (*e.g.* ~ 20 MHz) masks these sidebands. For the weak clock transitions, the sidebands are clearly visible since the sideband spacing is much larger than the clock transition natural linewidth. With efficient Doppler cooling, the ion is confined to a dimension (< 100 nm) much less than the laser wavelength. In this Lamb-Dicke limit, the spectrum is free from first-order Doppler broadening, although a small second-order Doppler shift remains.

In some cases, such as the Al⁺ quantum logic clock described in the following, it is necessary to cool well below the Doppler cooling limit, and close to the ground state of motion in the trap. In this case, the additional cooling strategies of Raman or resolved sideband cooling are required.

Confirmation of single ion operation and detection of the state of the ion is through observation of its cooling wavelength fluorescence. This is achieved via a high numerical aperture imaging lens and photomultiplier. With a fluorescence rate of $\sim 10^8$ photons s⁻¹, solid-angle detection efficiencies $\sim 10^{-4}$ and photomultiplier efficiencies of ~ 0.1 , single ion fluorescence rates of a few $\times 10^3$ counts s⁻¹ can be achieved for a cold ion at trap centre.

6.2.1. Quantum jump detection of the clock transition. High- Q weak clock transitions with ≤ 1 Hz natural linewidth are extremely difficult to detect directly above the background laser scatter rates. This is surmounted by making use of the technique of electron shelving or quantum jumps [199]. This relies on the widely differing cooling fluorescence rates observed when the clock probe laser is on or off resonance with the clock transition, which is connected to the cooling transition via a common ground state. On probing the weak absorption, the ion is driven to the metastable upper clock level, remaining “shelved” there for a period corresponding to the long natural lifetime of the clock transition, before decaying back to the ground state via spontaneous emission. During this period, the ion is not available to undergo fast ($\sim 10^{-8}$ s) cooling absorptions, and thus the cooling fluorescence level drops to zero until re-established by the decay or recovery from the metastable level. Weak clock transitions in a single ion can thus be detected with virtually 100 % efficiency. This quantum jump technique is key for generating a single trapped ion optical frequency standard. The spectral profile of the weak clock transition is built from the statistics of the number of quantum jumps as the frequency of the very-high-finesse cavity-stabilised clock probe laser (with *e.g.* 1 Hz linewidth) is stepped across it. A repeated pulse sequence of cooling, state preparation via optical pumping, clock-probing, state detection and clock-state clear-out is undertaken at each frequency position, with a single sequence time of tens to hundreds of milliseconds. Ideally, the clock probe pulse should be as long as possible, allowing Hz-wide Fourier-limited probe linewidths. With a knowledge of the experimental clock transition profile, the clock laser can be servoed to the profile line centre by stepping it back and forth across the profile between half-intensity points and generating a frequency discriminant by detecting any quantum jump imbalance between these points.

6.2.2. Ion clock computer control. A major requirement of any clock system is to be able to operate continuously over long periods in order both to achieve clock stability performance offered by extended averaging periods and to apply this capability to measurement problems that can benefit from this increased stability, precision and accuracy. Current goals for optical clock stability and systematic uncertainty are of order 10^{-17} to 10^{-18} . With typical ion clock stabilities of a few $\times 10^{-15} \tau^{-1/2}$, averaging times of hours to days are needed to reach these values. Thus, it is paramount that the clock system operates autonomously over such long measurement campaigns, and auto-control algorithms are being introduced to provide monitoring and correction of multiple sub-system processes over a wide range of time scales from the sub millisecond up to several days. The pulse probe sequence that forms the basic routine to provide frequency lock requires time resolution at the 1 ms level (see fig. 23). Each probe sequence is repeated ~ 10 times at each side of the clock transition, resulting in 10 to 20 s to make a correction to the probe laser frequency. Real-time systematic uncertainty determination can require B-field or Zeeman-component pair switching to null the quadrupole (E2) shift, laser intensity switching for AC Stark shift extrapolation, and 3D micromotion monitoring and correction on the minute-to-hour periodicity to allow reaching best performance.

In addition, it is necessary to monitor the various laser servo-lock signals and automatically re-acquire lock in the event of loss of lock. It is also necessary to monitor the continued normal operational characteristics of the ion within the trap (eg expected cooling rates, fluorescence levels, minimised micro-motion) and to be able to diagnose the causes of non-adherence to expected values and initiate the relevant re-acquisition procedure. Loss of the ion from the trap, for example, as a result of loss of servolock of the cooling laser due to a mode hop, and subsequent heating of the ion, will require

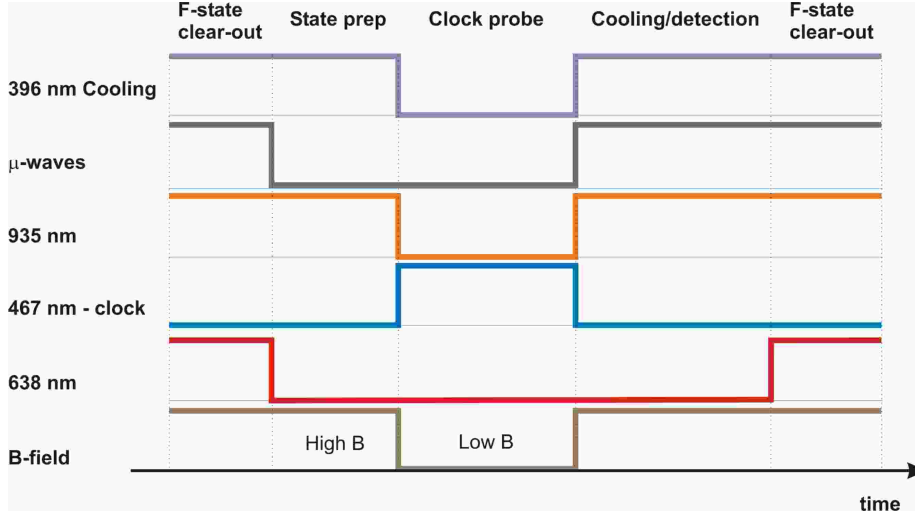


Fig. 23. – Generic pulse sequence showing cooling, magnetic field state preparation, clock probe and detection and F-state clear-out pulses for probing the $^{171}\text{Yb}^+$ 467 nm octupole clock transition.

reload of a single ion and re-adjustment of compensation voltages.

For auto-control of cavity-stabilised clock and cooling lasers, monitoring of the cavity fringe, fluorescence signal, quantum jump rate and wavemeter reading allow fault diagnosis and determination of the correct re-acquisition procedure for probing and cooling of the ion. The repumper and clear-out lasers operate at lower frequency resolution levels, and can be controlled effectively from the wavemeter readings. Flags are generated between the short periods of lock loss and re-acquisition to inhibit data-taking during these periods. Control algorithms are already in routine use for comparisons between two ion clock systems over periods of days [200].

7. – State of the art of ion clocks

Here, we examine recent results for a number of single ion clocks. The most common clock transition across the various ion species is the quadrupole transition, which has been the subject of research in $^{199}\text{Hg}^+$, $^{171}\text{Yb}^+$, $^{88}\text{Sr}^+$, $^{40}\text{Ca}^+$ and $^{135}\text{Ba}^+$ ions. There has also been a significant amount of research on the $^{171}\text{Yb}^+$ highly-forbidden octupole clock transition, and the $^1\text{S}_0 - ^3\text{P}_0$ transitions in $^{27}\text{Al}^+$ and $^{115}\text{In}^+$. The $^{27}\text{Al}^+$ system resulted from the development of the quantum logic clock concept, which has led to leading optical clock performance over recent years.

7.1. $^{199}\text{Hg}^+$ quadrupole clock. – The $^{199}\text{Hg}^+$ $^2\text{S}_{1/2}$ ($F = 0, m_F = 0$) - $^2\text{D}_{5/2}$ ($F = 2, m_F = 0$) electric quadrupole transition at 282 nm (see fig. 24), with a natural linewidth of 1.7 Hz, was the first ion clock transition to have a reported absolute total fractional frequency uncertainty of below 1 part in 10^{15} . Laser radiation at 194 nm is used to cool and prepare the ion, with subsequent probing of the clock transition with 120 ms pulses at 282 nm. With this arrangement, a Fourier-transform-limited cold ion linewidth of 6.5 Hz has been demonstrated, corresponding to a Q of 1.5×10^{14} at an optical frequency

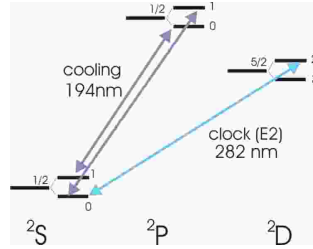


Fig. 24. – Partial energy level scheme for $^{199}\text{Hg}^+$.

of 1.06×10^{15} Hz. The absolute total fractional uncertainty relative to the NIST Cs primary standard was 7×10^{-16} , of which the Hg^+ ion systematic uncertainty comprised 7.2×10^{-17} [86]. This has since been reduced to 1.9×10^{-17} [201], with a reported frequency instability of $2.8 \times 10^{-15} \tau^{-1/2}$.

As regards systematic frequency shifts due to external fields, the $m_F = 0 \rightarrow m_F = 0$ Zeeman component of the $^{199}\text{Hg}^+$ quadrupole clock transition is chosen for a standard, on account of there being no linear Zeeman shift. However, there are shifts, for example, as a result of the second-order Zeeman effect and Stark effect. More significant is the electric quadrupole shift resulting from the interaction of the D-state atomic quadrupole moment with static electric field gradients such as those induced by charge build-up on the trap electrodes. In the recent measurement of the Hg^+ to Al^+ frequency ratio, the Hg^+ quadrupole shift was nulled to the level of 1×10^{-17} by a series of transition frequency measurements with the magnetic field oriented in three orthogonal directions [6]. The Hg^+ system is operated within a cryostat at liquid-helium temperatures in order to mitigate loss of the ion at room temperature after relatively short periods (a few minutes) by charge exchange and dimerization. This has the effect of rendering the blackbody shift negligible, but at the expense of increased complexity of cryogenic operation.

7.2. $^{88}\text{Sr}^+$ quadrupole clock. – The $^{88}\text{Sr}^+ \ ^2\text{S}_{1/2} - \ ^2\text{D}_{5/2}$ quadrupole clock transition at 674 nm (fig. 25) has a 0.4 Hz natural width. The ion is laser-cooled on the strong $^2\text{S}_{1/2} - \ ^2\text{P}_{1/2}$ transition at 422 nm. Two repumpers at 1092 nm and at 1033 nm are needed respectively to repump the ion back to the cooling cycle and to recover the ion to the ground state once the clock transition is driven. Research at NPL [202] and NRC [203] led to experimental Fourier-limited cold ion linewidths of 9 Hz (100 ms probe pulse) and 4.4 Hz (200 ms probe pulse) respectively. One drawback of the $^{88}\text{Sr}^+$ even isotope transition is the lack of hyperfine structure and hence a magnetic-field-insensitive $m_F = 0 \rightarrow m_F = 0$ transition. The applied magnetic field of a few μT splits the clock transition into five pairs of Zeeman components, with each pair being distributed symmetrically about the line centre. In order to take account of this linear Zeeman shift, symmetrical pairs of Zeeman components are probed, where each component of the pair experiences an equal and opposite linear shift to the other component. In this case, the quantum jump imbalance for each component of the pair is alternately and repeatedly monitored, and frequency corrections made, after each imbalance determination. This gives rise to a “virtual” magnetic-field-insensitive transition, and is now used extensively for both ion (*e.g.* $^{27}\text{Al}^+$) and atom (*e.g.* ^{87}Sr) clock transitions without intrinsic first-order magnetic-field insensitivity. By adopting this arrangement, we are then left with a

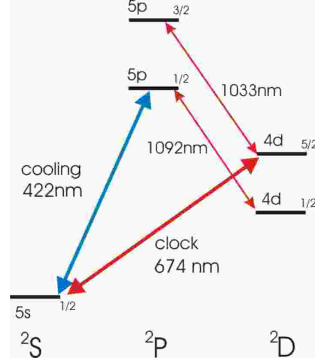


Fig. 25. – Partial energy level scheme for the $^{88}\text{Sr}^+$ ion.

very small second-order Zeeman shift of order a few mHz/mT^2 .

Frequency stability measurements have been made between two independent Sr^+ ion clock systems, giving rise to a single trap stability fitted to $1.6 \times 10^{-14} \tau^{-1/2}$ ($30 \text{ s} < \tau < 5000 \text{ s}$) for interrogation periods of 40 ms and 40 % peak excitation probability in the absence of optical pumping [200]. For 90 % peak excitation and 100 ms probe periods, this converts to $2.5 \times 10^{-15} \tau^{-1/2}$ or 2.5×10^{-17} at 10^4 s . Cycle periods required to make a frequency correction are of the order of 20 s. Once the excess micromotion is fully reduced in all directions, the impact on the second-order Doppler shift and Stark shift contributions to the clock frequency uncertainty are in the range $10^{-18} - 2 \times 10^{-17}$. However, these shifts need to be monitored during long measurement periods. The major systematic uncertainties then relate to the electric quadrupole shift and blackbody radiation Stark shift. The former (together with the tensor Stark component) can be nulled effectively by making centre-frequency measurements of three Zeeman component pairs, which give an average value with the quadrupole shift nulled out [204]. With these arrangements, the blackbody shift becomes the dominant effect. The uncertainty in this shift has contributions from the effective temperature of the trap surroundings, the emissivity of these surroundings (particularly the electrode surfaces in close proximity to the ion) and the uncertainty in the calculated blackbody shift coefficients [205]. Temperature rises of a few degrees for the electrodes are typical for small traps with rf drive voltages in the low hundreds of volts, but the effect of the electrode contribution to the blackbody field can be mitigated by use of highly polished electrode surfaces, where the emissivity is very low. With current calculated coefficient uncertainties, the overall blackbody uncertainty is $\sim 2 \times 10^{-17}$ [206].

The 674 nm $^{88}\text{Sr}^+ \ ^2\text{S}_{1/2} - \ ^2\text{D}_{5/2}$ quadrupole clock transition absolute frequency (see fig. 26) has previously been measured using the NPL Cs fountain-referenced femtosecond comb, with a relative fractional uncertainty of 3.4×10^{-15} [207]. More recently, another absolute measurement has been made via a comb referenced to the NRC hydrogen maser, itself calibrated via GPS precise point positioning (PPP) and BIPM Circular T [206]. This gave an overall uncertainty of the clock frequency of 2×10^{-15} , with an ion systematic uncertainty of 2×10^{-17} . The offset between the NPL and NRC values is $\sim 2 \times 10^{-15}$, well within the combined uncertainty of the two measurements.

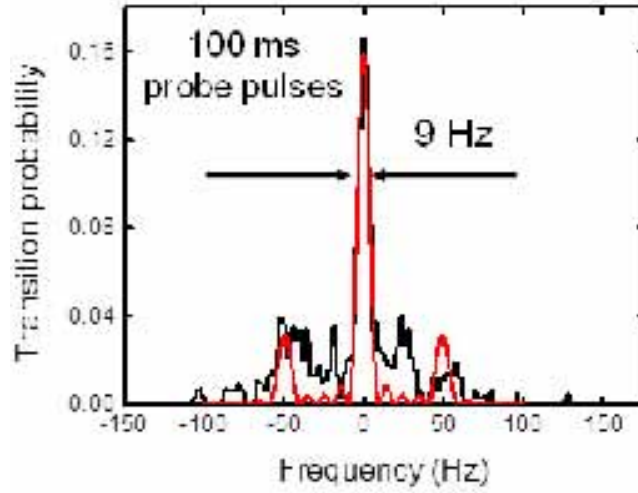


Fig. 26. – $^{88}\text{Sr}^+$ $2S_{1/2}$ ($m=1/2$) - $2D_{5/2}$ ($m=1/2$) 674 nm clock transition, showing a 9-Hz transform-limited linewidth. Black line, expt data; red line, fit to sinc function [202].

7.3. $^{40}\text{Ca}^+$ quadrupole clock. – The $^{40}\text{Ca}^+$ clock transition is the electric quadrupole transition $4s\ 2S_{1/2} - 3d\ 2D_{5/2}$ at 729 nm, which has a lifetime of 1.17 s and a corresponding natural linewidth of 0.2 Hz. This has been investigated at the University of Innsbruck, the Wuhan Institute of Physics and Mathematics in China and NICT in Japan. The Innsbruck trap is a linear rf trap with four blades separated by 2 mm and two end-cap tips separated by 5 mm. The Wuhan and NICT traps are miniature ring traps (the Wuhan trap has a ring radius of 0.8 mm). Ions are produced by photo-ionisation of neutral calcium via 423 nm + 374 nm, and laser cooled at 399 nm. A repumper at 866 nm is used to maintain the cooling cycle.

The first measurement of the 729 nm clock frequency was made by the Innsbruck group. This gave a fractional uncertainty of 2.4×10^{-15} via a comb measurement referenced to the LNE-SYRTE transportable fountain clock [196]. A subsequent measurement at Wuhan with fractional uncertainty of 3.9×10^{-15} agreed with the Innsbruck value at a level of 5 parts in 10^{16} . In the latter case, the optical clock transition was measured by a frequency comb referenced to a hydrogen maser. The maser was calibrated via UTC (NIM) using GPS and PPP.

In contrast, the measured Ca^+ clock transition at NICT was observed to be discrepant from the mean of these previous measurements by 5.3 Hz, where the NICT uncertainty was 1.2 Hz, or 3×10^{-15} [208]. This was derived from UTC (NICT) and Circular-T via microwave link. NICT also measured the frequency ratio between their Ca^+ and Sr neutral lattice standards, which was consistent with the Sr and Ca^+ absolute values. NICT also reported a frequency stability between the Sr and Ca^+ standards of $2.4 \times 10^{-14} \tau^{-1/2}$ ($100\text{ s} < \tau < 8000\text{ s}$), where the Ca^+ frequency is considered to be the dominant instability.

7.4. $^{171}\text{Yb}^+$ quadrupole clock. – Similar to the $^{199}\text{Hg}^+$ case, the odd isotope $^{171}\text{Yb}^+$ has complicating hyperfine structure, but also has an advantageous 1^{st} order magnetic-field-insensitive Zeeman component $m_F = 0 \rightarrow m_F = 0$ of the quadrupole clock transition.

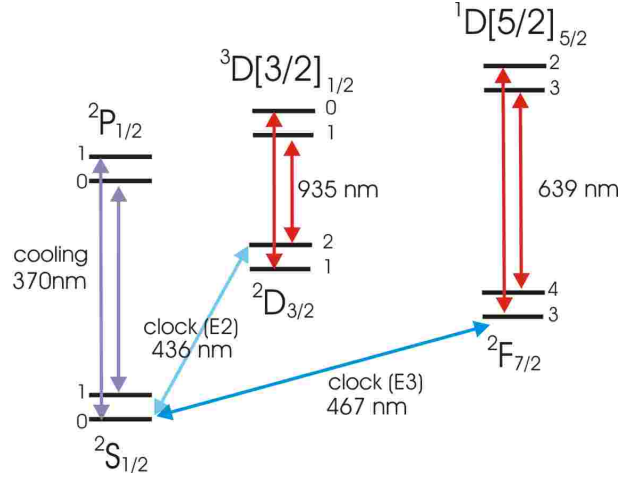


Fig. 27. – Partial term scheme for $^{171}\text{Yb}^+$.

The $^2\text{S}_{1/2} - ^2\text{D}_{3/2}$ quadrupole transition at 436 nm, with a natural linewidth of 3.1 Hz, is chosen as the clock transition (see fig. 27), rather than the more normal $^2\text{D}_{5/2}$ transition. This is on account of existence of the extremely long-lived low-lying $^2\text{F}_{7/2}$ metastable energy level to which the $^2\text{D}_{5/2}$ can readily decay.

However, use of the $^2\text{S}_{1/2} - ^2\text{D}_{3/2}$ quadrupole transition is also not straightforward in that the $^2\text{D}_{3/2}$ level is also accessed during the laser cooling cycle. The cooling is effected by cycling on the $^2\text{S}_{1/2} - ^2\text{P}_{1/2}$ 370 nm dipole transition via frequency-doubled diode laser at 740 nm or direct generation of 370 nm with a UV diode laser, with occasional decays from the $^2\text{P}_{1/2}$ level into the $F = 1$ $^2\text{D}_{3/2}$ metastable level with a branching ratio of $\sim 0.7\%$. The ion is recovered to the cooling cycle by driving out of level this $^2\text{D}_{3/2}$ level with a 935 nm diode laser. A frequency-doubled extended-cavity diode laser at 872 nm, stabilized to a high-finesse reference cavity, is used to probe the 436 nm $^{171}\text{Yb}^+$ $^2\text{S}_{1/2} (F = 0) - ^2\text{D}_{3/2} (F = 2)$ quadrupole (E2) clock transition, thereby decoupling the clock transition from the cooling transition to first order. However, it is also possible for the 935 nm repumper laser to off-resonantly drive out of the $F = 2$ level, so this needs to be both weak intensity and spectrally narrow to avoid prematurely emptying the $F = 2$ level during the clock-interrogation quantum jump detection period. Nevertheless, a small background of false counts is generally encountered. Further, there is a small probability of the ion accessing the extremely long-lived $^2\text{F}_{7/2}$ level by means of collisional interactions, with the need to clear the ion from this level back to the ion $^2\text{S}_{1/2}$ ground state by use of diode laser light at 639 nm or 760 nm.

The 436 nm $^2\text{S}_{1/2} - ^2\text{D}_{3/2}$ quadrupole transition natural linewidth of 3.1 Hz corresponds to an upper state lifetime of ~ 52 ms, which compromises the use of increased interrogation pulse times to improve the experimental line Q of the clock transition. Experimental linewidths of 10 Hz have been demonstrated for the clock transition, with measured frequency stabilities between two single Yb^+ ion systems of $1 \times 10^{-14} \tau^{-1/2}$. The clock transition has been measured to a fractional uncertainty of 1.1×10^{-15} but without correction for the blackbody shift[96], where the major contribution to the uncertainty is the systematic uncertainty of the Cs fountain reference. The contribution to

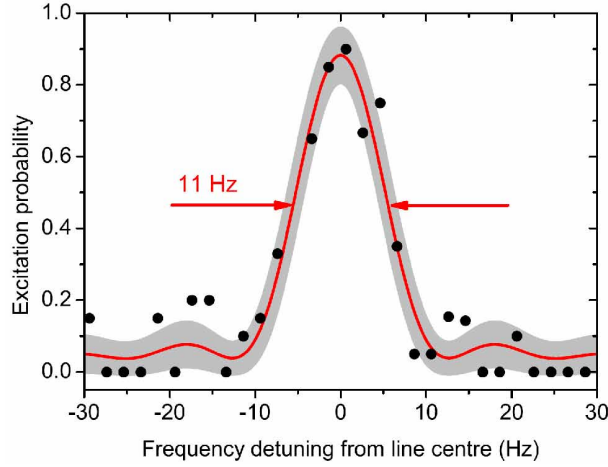


Fig. 28. – Line profile of the $^{171}\text{Yb}^+$ octupole transition taken with a 100 ms probe time. The fitted lineshape shows a linewidth close to the 9-Hz Fourier limit [211].

the systematic uncertainty from the Yb^+ ion was 0.31 Hz (4.5×10^{-16}).

7.5. $^{171}\text{Yb}^+$ octupole clock. – The $^{171}\text{Yb}^+$ single ion is especially interesting in that it has another optical clock transition, namely the extremely weak 467 nm $^2\text{S}_{1/2} - ^2\text{F}_{7/2}$ octupole (E3) transition between the ion ground state and the long-lived $^2\text{F}_{7/2}$ level with a measured lifetime of ~ 6 years [209], and corresponding natural width in the nanohertz range and line Q of 10^{23} . With such a narrow natural width, the observable clock transition linewidth will be set by the Fourier-limited linewidth corresponding to the clock-pulse interrogation period, and this will reflect on the attainable Q and stability. This offers an improved quantum limit compared to those typical for quadrupole transitions where natural decay can foreshorten interrogation periods, and thereby lead to reduced stabilities. The advantage of increased interrogation periods approaching a second is better stability achievable with shorter averaging periods. This in turn allows systematic frequency shift investigations to be made at reduced levels (*e.g.* at the 10^{-17} level) at a faster rate. Cold ion octupole linewidths in the range ~ 7 Hz to 11 Hz for near transform-limited probe pulses have been observed [210, 211] (see fig. 28).

Similar to the $^{171}\text{Yb}^+$ quadrupole case, laser cooling is effected by cycling on the $^2\text{S}_{1/2} (F = 1) - ^2\text{P}_{1/2} (F = 0)$ 369 nm dipole transition with repumping at 935 nm. It is also possible to induce spontaneous Raman transitions to $^2\text{S}_{1/2} (F = 0)$ as a result of weakly driving the $^2\text{S}_{1/2} (F = 0) - ^2\text{P}_{1/2} (F = 1)$ transition in the wing of the cooling light profile. In order to counter this, a 14.7 GHz sideband is generated by electro-optic modulation to drive the $^2\text{S}_{1/2} (F = 0) - ^2\text{P}_{1/2} (F = 1)$ transition to recover the ion from the $^2\text{S}_{1/2} (F = 0)$ level to the cooling cycle. Finally, a further 369 nm sideband at 2.1 GHz is used to state prepare the ion in $^2\text{S}_{1/2} (F = 0)$ in preparation for driving the $^2\text{S}_{1/2} (F = 0) - ^2\text{F}_{7/2} (F = 3)$ octupole (E3) transition at 467 nm. As with the quadrupole case, the long $^2\text{F}_{7/2}$ lifetime is also a problem for the cooling and probing pulse sequence, in that the metastable level acts as a sink for the ion. During the stepped frequency interrogation of the octupole transition, it is necessary to quickly recover the ion from the F -state back to the $^2\text{S}_{1/2}$ ground state using 638 nm or 760 nm clear-out

lasers.

The $^{171}\text{Yb}^+$ odd isotope has a low nuclear spin of $I = 1/2$ resulting in a fairly simple hyperfine structure, and the octupole transition also has an $m_F = 0 \rightarrow m_F = 0$ magnetic-field insensitive transition with no first-order Zeeman effect. The second-order Zeeman shift has been measured [212] to be $-1.72(3) \times \text{mHz/mT}^2$ for the octupole transition. Operational fields of $20 \mu\text{T}$ are typical. Loss of fluorescence at close-to-zero magnetic fields due to dark state formation (coherent population trapping) in the ground state is prevented by fast polarisation switching of the cooling light. The small magnetic field applied is sufficient to prevent similar coherent population trapping in the $^2\text{D}_{3/2}$ level during the cooling cycle.

Until recently, the dominant shift associated with the $^{171}\text{Yb}^+$ octupole transition has been the AC Stark shift owing to the large 467 nm probe laser intensity needed to drive the transition, with typical coefficient of *e.g.* $48(10) \mu\text{Hz W}^{-1}\text{m}^2$ [213], dependent on the probe beam wave-vector angle to the quantization axis. Measurement strategies to deal with this are based on extrapolation of the probe intensity to zero intensity by accurate measurement of intensity ratios for two power levels during the probe sequence. Further improvement could be made by reduction in probe laser linewidth, giving rise to reduced spectral spread and improved efficiency of overlap with the octupole transition. In addition, a technique of hyper-Ramsey excitation has been reported, where the phase and pulse length of the second Ramsey pulse are varied, with the effect of suppressing the AC Stark shift by two orders of magnitude or more [214].

The electric quadrupole shift of the octupole transition can be nulled by measuring the transition frequency in three orthogonal magnetic fields, whereby the shift averages to zero [215]. This nulling is made all the more easier by the magnitude of the electric quadrupole moment, which has been measured to be $-0.041 ea_0^2$ [210]. This is nearly two orders of magnitude smaller than the quadrupole moments measured for the quadrupole clock transitions. The other major systematic frequency shift is the blackbody radiation shift. Calculated blackbody shift coefficients [205] give rise to uncertainties of a few $\times 10^{-18} \text{ K}^{-1}$ at room temperature. Recently, a total systematic uncertainty of 7×10^{-17} was reported for the octupole transition [210]. Independent absolute frequency measurements at PTB and NPL show excellent agreement within the combined 1σ value of the individual uncertainties of 8×10^{-16} [210] and 1×10^{-15} [211] respectively. The agreement is even better when account is taken of the individual fountain clocks relative to the International Atomic Time (TAI).

7.6. $^{27}\text{Al}^+$ quantum logic clock. – The ion species that has demonstrated the leading optical clock performance to date is the $^{27}\text{Al}^+$ ion, which has a $^1\text{S}_0 - ^3\text{P}_0$ weak clock transition at 267 nm with 8 mHz natural width corresponding to a 20 s lifetime of the upper clock state [16]. It also has extremely low or zero sensitivities to environmental fields, giving rise to an advantageous systematic frequency-shift uncertainty budget. For example, it has no electric quadrupole shift, and its sensitivity to blackbody radiation is the lowest of all clock species currently under consideration. However, the major issue with this ion is that its cooling wavelength is ~ 169 nm in the vacuum ultraviolet region of the spectrum, and thus is technically very difficult to produce and transmit between source and ion trap. Researchers at NIST have overcome this problem by separating clock and laser cooling/preparation functionality between two different-species ions in the same linear rf ion trap. The logic ion ($^9\text{Be}^+$ or $^{25}\text{Mg}^+$ have been used to date) is directly laser cooled in the conventional way via accessible cooling radiation (313 nm for $^9\text{Be}^+$, or 280 nm for $^{25}\text{Mg}^+$). The $^{27}\text{Al}^+$ clock ion is sympathetically cooled by

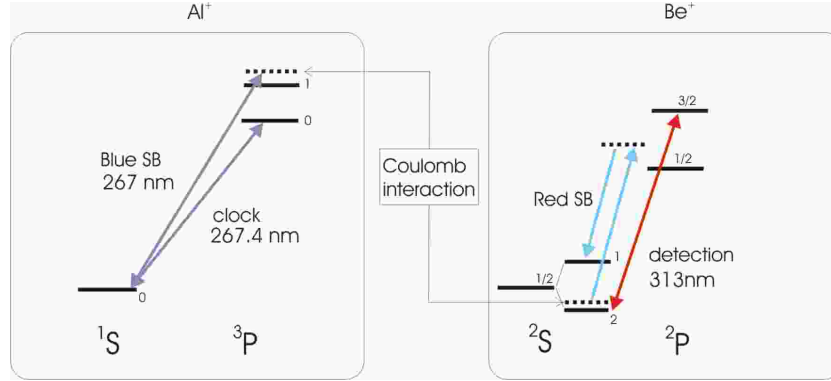


Fig. 29. – Schematic of the quantum logic clock state read-out algorithm; reprinted from [216].

virtue of the combined motional mode set up via the coulombic interaction between the two logic and clock ions in the linear trap. The Al^+ ion is then probed on the 267 nm clock transition. However, there is an additional complexity here in that there is no Al^+ cooling fluorescence available with which to observe clock transition quantum jumps. This is overcome by making use of coherent manipulation techniques developed previously for quantum information research at NIST, whereby the quantum jump clock transition profile data is mapped back to the logic ion, again via the collective 2-ion vibration motional state.

In very brief detail, the pulse sequence to achieve this sympathetic cooling and $1S_0 - 3P_0$ clock transition read out is as follows. The combined ion motion is prepared close to its motional ground state by a combination of Doppler cooling and sideband cooling via the logic ion cooling wavelengths. The clock transition is driven (or not), and the result is mapped to the 267 nm $^{27}\text{Al}^+ 1S_0 - 3P_1$ coupled transition [216], as shown in fig. 29. By means of a blue sideband π pulse on this transition followed by a red sideband π pulse on the logic ion Raman cooling transition, which are interconnected through their common motional mode, the clock drive result is then read out on the logic ion fluorescence. Typical clock probe pulses of 100 to 150 ms have been used, but the subsequent clock state readout algorithm can be executed remarkably quickly in ~ 2 ms. Overall duty cycles of 65 % have been achieved where the dead-time is primarily due to state preparation and read-out plus other interleaved parameter switching in order to minimise micro-motion. Of order ten interrogation pulse / read-out sequences would be made at each frequency step across the clock transition profile. This technique has resulted in an observed 2.7 Hz clock transition FWHM linewidth [16], which corresponds to a Q of 4.2×10^{14} , the highest recorded Q to date.

As mentioned earlier, $1S_0 - 3P_0$ transitions are free from quadrupole shift, on account of the $J = 0$ value for both lower and upper levels. There is, however, a linear magnetic field dependence of order several $\times 10$ Hz (μT^{-1}) for the outermost Zeeman components. This is eliminated in the same way as with the even isotope quadrupole transitions, by measuring Zeeman component pair frequencies and taking the average value. The second-order Zeeman shift is measured to be -70 Hz/ mT^2 [216].

In a recent comparison between two Al^+ clocks (where each clock made use of a different logic ion species, see fig. 30), the better of the clock realizations had a total

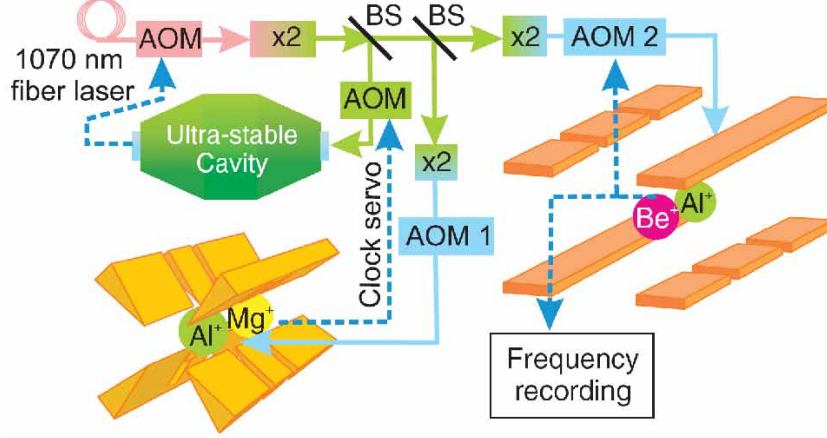


Fig. 30. – Experimental arrangement for comparing two $^{27}\text{Al}^+$ quantum logic clocks at NIST [16].

systematic-shift fractional uncertainty of 8.6×10^{-18} [16]. This was dominated by second-order Doppler shifts due to residual secular motion and excess micromotion, which are likely to be larger than in the single ion case, partly due to the lighter mass of the ion (see Table VI). The relative frequency stability between the clocks was observed to be $2.8 \times 10^{-15} \tau^{-1/2}$ ($50 \text{ s} < \tau < 2000 \text{ s}$). The relative frequency difference between the clocks was measured to be -1.8×10^{-17} .

7.7. $^{115}\text{In}^+$ clock. – $^{115}\text{In}^+$ is another ion species with a weak $^1\text{S}_0 - ^3\text{P}_0$ clock transition at 236 nm, with natural linewidth of 0.8 Hz [217]. It also has a relatively small blackbody coefficient. There is no accessible strong cooling transition, but direct bi-chromatic cooling has been performed via the weak $^1\text{S}_0 - ^3\text{P}_0$ intercombination transition at 230 nm [218]. As a result, this direct cooling is not greatly efficient, and other possibilities such as sympathetic cooling eg by Yb^+ are under investigation. Previously, the clock transition has been measured to an absolute uncertainty of 230 Hz ($\sim 2 \times 10^{-13}$ fractional

TABLE VI. – *Uncertainty budget for Al^+ clock [16].*

Effect	Shift (10^{-18})	Uncertainty (10^{-18})
Excess micromotion	-9	6
Secular motion	-16.3	5
Blackbody radiation shift	-9	3
Cooling laser Stark shift	-3.6	1.5
Quad. Zeeman shift	-1079.9	0.7
Linear Doppler shift	0	0.3
Clock laser Stark shift	0	0.2
Background-gas collisions	0	0.5
AOM freq. error	0	0.2
Total	-1117.8	8.6

uncertainty), but this remains inconsistent with a later measurement [217, 219].

There are other cold ion systems that have been researched as a possible standard over the past two decades, such as the $^{135}\text{Ba}^+ \ ^2\text{S}_{1/2} - \ ^2\text{D}_{5/2}$ infra-red transition at $1.762 \ \mu\text{m}$. In the latter case, no high accuracy frequency measurements have been made at this time to our knowledge.

Table VII shows the current trapped ion optical clock systems where state-of-the-art systematic uncertainties have been reported. In a number of cases, these uncertainties can be seen to be lower than the systematic uncertainties achieved for the best cold caesium fountain primary standards ($\sim 2 \times 10^{-16}$).

8. – Future prospects

8.1. High accuracy remote optical clock comparisons. – Throughout this survey we have seen the rapid rate of progress with optical atomic clocks both in terms of instability and absolute uncertainty. The best clocks now achieve an instability of less than 2×10^{-18} in only six hours of averaging time, while the most accurate clocks have uncertainties of less than 6 parts in 10^{18} . Moreover, we anticipate that these values will be reduced still considerably more in the near future as no fundamental limitations loom at this point. However, there still exists one potential roadblock that could limit progress on a global scale, namely, our inability to compare clocks separated by long distance. There are now dozens of clocks under development on five continents, but we are severely limited in our ability to compare them, which ultimately is a critical step from the perspective of the development of future standards. Up to now, remote comparisons have largely been performed indirectly, for example, as we saw in the case of the Sr lattice clock, through comparison to the local Cs microwave standards. Such comparisons are usually limited, however, by the microwave standards, and as the optical standards move well beyond their microwave counterparts in terms of performance, other techniques will be required that can be used in both shorter-range and longer-range comparisons. The challenge here is to find dissemination techniques that can transfer the clock signal without significantly compromising its performance.

This problem has been first solved over short distances (e.g., less than tens of km) by the use of phase-noise-compensated optical fibres [220]. This technique is used in almost all optical labs today to transmit light from one lab to another (or even from one part of the experiment to another) by means of optical fibre without adding phase noise. As a result optical and microwave clocks within one institute or even between institutes in the same city can be readily compared [163]. For longer-distance frequency comparisons, however, today links mediated by satellites are employed. The exchange of coded microwave signals for TWSTFT links (Two Way Satellite Time and Frequency Transfer), or the use of the phase of the received signals in the GPS carrier phase method, enables frequency comparisons on the global scale at a fractional uncertainty of 10^{-15} for a measurement period of several days, which is far noisier than required by present-day (and near-future) atomic clocks. Even though these techniques may improve to the 10^{-16} level in a few years, it is already clear that the achievable stability of a microwave link will not be competitive with the current demonstrated stability of optical clocks. One new approach has been to extend the phase-noise-compensated fibre technique to longer distances with repeater stations as needed [221]. This all-optical method has already been demonstrated on scales up to 920 km (as realized, for example, in Germany between the PTB and Max Planck Institute laboratories), and the best results have

TABLE VII. – Trapped ion optical clock species showing their associated state-of-the-art systematic uncertainties reported in the literature. The penultimate column gives the lowest cold ion clock transition linewidths observed to date; in general, these observed linewidths are Fourier-limited widths dominated by the clock laser probe pulse width.

Ion	Nuclear spin	λ_{cool} (nm)	Clock. trans.	λ_{clock} (nm)	Natural linewidth $\Delta\nu$ (Hz)	obs. linewidth $\Delta\nu_{obs}$ (Hz)	rel. uncertainty
$^{27}\text{Al}^+$	5/2	279.5 ($^{25}\text{Mg}^+$)	$^1\text{S}_0\text{-}^3\text{P}_0$	267	0.008	2.7	8.6×10^{-18} [16]
$^{40}\text{Ca}^+$	7/2	397	$^2\text{S}_{1/2}\text{-}^2\text{D}_{5/2}$	729	0.2	30	2.4×10^{-15} [196]
$^{88}\text{Sr}^+$	0	422	$^2\text{S}_{1/2}\text{-}^2\text{D}_{5/2}$	674	0.4	5	2.1×10^{-17} [206]
$^{115}\text{In}^+$	9/2	231	$^1\text{S}_0\text{-}^3\text{P}_0$	236	0.8	43	2×10^{-13} [217]
$^{171}\text{Yb}^+$ (oct.)	1/2	370	$^2\text{S}_{1/2}\text{-}^2\text{F}_{7/2}$	467	10^{-9}	7	7.1×10^{-17} [212]
$^{171}\text{Yb}^+$ (quad.)	1/2	370	$^2\text{S}_{1/2}\text{-}^2\text{D}_{3/2}$	436	3.1	10	4.5×10^{-16} [96]
$^{199}\text{Hg}^+$	1/2	194	$^2\text{S}_{1/2}\text{-}^2\text{D}_{5/2}$	282	1.7	6.7	1.9×10^{-17} [6]

shown frequency instabilities as low as 5×10^{-15} at 1 s (reaching 10^{-18} in less than 1000 s), with an estimated accuracy within 4×10^{-19} [222]. This method today is the only known way to make comparisons between optical clocks at high stability, and there is a growing interest in realizing optical-fibre links between European metrology institutes to test the link instabilities over distances of more than 1000 km [222]. Ultimately this approach could lead to all of the optical clocks in Europe being directly connected by optical fibre. Similar efforts are also underway in Japan, where optical clocks spread throughout multiple institutes have been connected by optical fibre [223] and in Italy, where a 630 km-long fiber link between INRIM laboratories in Torino and LENS-UNIFI laboratories in Firenze is currently under test [224].

While this approach will bear considerable fruit since it enables true remote optical clock comparisons, it is not clear how it could be extended further to enable intercontinental clock comparisons. Such comparisons will be necessary as the field moves inexorably towards a redefinition of the SI second and will enable a variety of experiments including tests of fundamental physics (see the subsequent section). The most likely solution will be some type of optical version of the microwave TWSTFT links, but issues such as atmospheric turbulence and limited connection time (e.g., due to cloud cover), which are much more serious for optical signals, will need to be addressed. Nonetheless, experiments along these lines are already underway with some encouraging initial results (see [225] and references therein). We can envision that one day such optical links in combination with a high-performance clock located in space (e.g., on a dedicated satellite or the International Space Station) to minimize terrestrial effects could enable a global high-performance clock environment for realization of the SI second, relativistic geodesy, and tests of fundamental physics [170, 106]. Indeed, feasibility projects such as the European Space Agency's "Space Optical Clock" Program (SOC) [170] and "Space-Time Explorer and Quantum Equivalence Principle Space Test" (STE-QUEST) [226] or the National Aeronautics and Space Agency's "Deep Space Optical Clock Mission" [227] are already underway, although it may be a decade or more before we see optical clocks in Space.

8'2. Practical applications and tests of fundamental physics with high accuracy/stability optical clocks. – To this point the bulk of the research in the field of optical atomic clocks has focused on the development of optical clock systems and the advancement of their performance rather than on the construction of field-able systems. Indeed, given the relative youth of the field (the first optical clock demonstrations complete with femtosecond-laser combs occurred about 12 years ago, at the time of this writing), it is reasonable to anticipate that the most powerful applications of optical clocks still remain to be identified and developed, much the way the microwave atomic-clock-based GPS positioning revolution followed decades after the demonstrations of the first Cs clocks. Nonetheless, we expect that the most powerful applications will lie in fields that have traditionally exploited precision clocks, such as navigation, communications, and signal synchronization and timing. Given their high performance level, these clocks will probably be used in more extreme cases such as deep-space navigation and ultra-low noise secure communications. In fact, we already have seen glimpses of such applications on the horizon. The world's quietest microwave signals are now generated from down-converted optical signals [228], and referenced optical frequency combs are used for precision calibration of astronomical spectrographs in searches for exo-planets [229]. Moreover, discussions are taking place at national standards institutions about a possible redefinition of the SI second in terms of an optical transition (either in an ion- or neutral atom-based system). Finally,

the pre-eminence of the second, in terms of being (by far) the most precisely measurable physical quantity, has already enabled significant tests of fundamental physics, with more possibilities on the horizon.

Historically, physicists have sought the best ways to use time, perhaps our most sensitive probe of nature, to test some of our most fundamental theories including Quantum Electrodynamics and General Relativity. Given the more recent challenges posed by dark energy and dark matter, there is renewed urgency to find ways to exploit the possibilities raised by the advances in clock performance. Since these clocks can offer eighteen digits of performance at energies orders of magnitude lower than those of particle physics experiments, we see that the clocks offer the possibility of making measurements that would be complementary to those of high energy physics. The first contributions of optical clock measurements to our understanding of fundamental physics have come from direct comparisons between optical-clock transition frequencies over time periods of several years. Since different transitions can have different dependencies on fundamental physical constants such as α , the fine-structure constant, tests for drifts of transition frequencies can test for drifts in the fundamental constants themselves (note that such tests require small absolute uncertainties for the clock systems). The most sensitive test to date was a comparison between two trapped ion clock systems, based on Hg^+ and Al^+ , over the period of a year, which constrained the present day fractional drift in α to be $-1.6 \pm 2.3 \times 10^{-17}/\text{year}$ [6]. Similarly by tracking such a ratio over space (e.g., as the Earth orbits the sun), one can put limitations on spatial dependencies of gravitational coupling constants. A comparison between Sr lattice clocks and Cs microwave clocks spanning a year of Earth orbit was able to test local position invariance and set the tightest limits on gravitational coupling constants for the fine-structure constant, the electron-proton mass ratio, and the light-quark mass [230].

Another way to perform tests of gravitation would be to make precision tests of the gravitational redshift via its effect upon the clock frequency (recall sect. 4.6). An early rocket-based experiment demonstrated the power of this technique to track changes in the acceleration of gravity [104] (through the use of a microwave H maser), and a more recent terrestrial demonstration by Chou et al. [103] used optical clocks to resolve altitude differences of less than 30 cm. Eventually we anticipate clock-based terrestrial altitude sensitivities at the 1 mm level, which would enable the prospect of using a portable clock in conjunction with a fixed clock (maybe even one in a microgravity environment) to map out the Earth geoid with high sensitivity over large areas, thereby taking advantage of both the high stability and low uncertainty of optical clocks.

Methods developed for optical clocks can be extended also to other fields. A noticeable case is atom interferometry that has strong conceptual and technical connections with atomic clocks (for a review on atom interferometry see [231, 232]). For example, an atom interferometry scheme was recently proposed [233] based on the clock transition of alkaline-earth atoms with possible applications ranging from gravimetry to the detection of gravitational waves [234].

8.3. Clocks of the future. – Here we close this review article with a look toward the future of atomic clock design. To be sure, the remarkable progress (and lack of obvious barriers to further improvements) of optical clocks has not kept scientists from seeking what might be the next breakthrough in atomic clock technology. From the discussions in sect. 2 and 3, the clear path forward would be to base new clocks on atomic transitions with higher frequencies and smaller inherent environmental sensitivities. Higher frequency electronic transitions could be accessed in highly charged atoms [235, 236], per-

haps excited by higher harmonics of stabilized femtosecond frequency combs [237, 238]. For reduced sensitivity to the environment, however, we might be better served to look to nuclear transitions, for which the inherent shielding of the nucleus could yield a clock with extremely small uncertainty. While precision spectroscopy of typical nuclear transitions will have to wait for stabilized MeV sources, scientists have identified one anomalous nuclear transition in the VUV part of the spectrum. This transition, the isomeric $3/2^+$ (631) \rightarrow $5/2^+$ (633) magnetic nuclear dipole transition in $^{229}\text{Th}^+$ has a transition energy of 7.8 ± 0.5 eV, which corresponds to a wavelength around 160 (10) nm, making it, in principle, accessible with existing spectroscopic tools (e.g., VUV frequency combs). This transition has a quality factor, $Q \sim 10^{20}$ and could support a fractional frequency uncertainty of $\sim 10^{-19}$ [239]. Several groups have proposed to excite this transition in various ways [240, 241, 242], and very recently one group claimed the first direct de-excitation of the $^{229}\text{Th}^+$ transition, thereby confirming the first indirect wavelength estimate and measuring a transition half-life of 6 ± 1 h [243]. While this result is still to be confirmed, it will be interesting to see how it compares with other possible excitation schemes including observation in a doped solid-state, high-band-gap crystal or via NEET, that is, nuclear excitation through an electronic transition [244]. Although the challenges facing the construction of a clock based on this transition in thorium are formidable, the transition offers a sensitivity to fundamental constant variation six orders of magnitude greater than do electronic transitions, and thus is likely to continue to attract considerable attention as an extremely inviting target for scientists.

* * *

N. P. acknowledges support from Italian Ministry of Research and Education (under contract PRIN 2009 - prot.2009ZJJBLX). We also acknowledge financial support from the European Union Seventh Framework Programme (FP7/2007-2013 grant agreement 263500, project “Space Optical Clocks”). C. O. acknowledges support from the Defense Advanced Research Projects Agency Quantum Assisted Sensing and Readout program, NASA Fundamental Physics, and NIST. We thank N. Hinkley and N. Phillips for their careful reading of the manuscript.

REFERENCES

- [1] HALL J. L., *Rev. Mod. Phys.*, **78** (2006) 1279.
- [2] HÄNSCH T. W., *Rev. Mod. Phys.*, **78** (2006) 1297.
- [3] WINELAND D. J., *Rev. Mod. Phys.*, **85** (2013) 1103.
- [4] DOW J. M., NEILAN R. E. and RIZOS C., *J. Geod.*, **83** (2009) 191.
- [5] NORMILE D. and CLERY D., *Science*, **333** (2011) 1820, 1823.
- [6] ROSEN BAND T., HUME D. B., SCHMIDT P. O., CHOU C. W., BRUSCH A., LORINI L., OSKAY W. H., DRULLINGER R. E., FORTIER T. M., STALNAKER J. E., DIDDAMS S. A., SWANN W. C., NEWBURY N. R., ITANO W. M., WINELAND D. J. and BERGQUIST J. C., *Science*, **319** (2008) 1808.
- [7] HOLLBERG L., DIDDAMS S., BARTELS A., FORTIER T. and KIM K., *Metrologia*, **42** (2005) S105.
- [8] EVENSON K. M., WELLS J. S., PETERSEN F. R., DANIELSON B. L., DAY G. W., BARGER R. L. and HALL J. L., *Phys. Rev. Lett.*, **29** (1972) 1346.
- [9] SCHNATZ H., LIPPHARDT B., HELMCKE J., RIEHLE F. and ZINNER G., *Phys. Rev. Lett.*, **76** (1996) 18.
- [10] UDEM T., HUBER A., GROSS B., REICHERT J., PREVEDELLI M., WEITZ M. and HÄNSCH T., *Phys. Rev. Lett.*, **79** (1997) 2646.

- [11] TOUAHRI D., ACEF O., CLAIRON A., ZONDY J.-J., FELDER R., HILICO L., DE BEAUVOIR B., BIRABEN F. and NEZ F., *Opt. Commun.*, **133** (1997) 471.
- [12] BERNARD J. E., MADEJ A. A., MARMET L., WHITFORD B. G., SIEMSEN K. J. and CUNDY S., *Phys. Rev. Lett.*, **82** (1999) 3228.
- [13] UDEM T., REICHERT J., HOLZWARTH R. and HÄNSCH T. W., *Opt. Lett.*, **24** (1999) 881.
- [14] UDEM T., REICHERT J., HOLZWARTH R. and HÄNSCH T. W., *Phys. Rev. Lett.*, **82** (1999) 3568.
- [15] BIZE S., LAURENT P., ABGRALL M., MARION H., MAKSIMOVIC I., CACCIAPUOTI L., GRUNERT J., VIAN C., DOS SANTOS F., ROSENBUSCH P., LEMONDE P., SANTARELLI G., WOLF P., CLAIRON A., LUITEN A., TOBAR M. and SALOMON C., **38** (2005) .
- [16] CHOU C. W., HUME D. B., KOELEMELJ J. C. J., WINELAND D. J. and ROSENBERG T., *Phys. Rev. Lett.*, **104** (2010) 070802.
- [17] BLOOM B. J., NICHOLSON T. L., WILLIAMS J. R., CAMPBELL S. L., BISHOP M., ZHANG X., ZHANG W., BROMLEY S. L. and YE J., preprint, arXiv:1309.1137. Accepted for publication in Nature (2013).
- [18] TINO G. M., CACCIAPUOTI L., BONGS K., BORDE C. J., BOUYER P., DITTUS H., ERTMER W., GOERLITZ A., INGUSCIO M., LANDRAGIN A., LEMONDE P., LAMMERZAHN C., PETERS A., RASEL E., REICHEL J., SALOMON C., SCHILLER S., SCHLEICH W., SENGSTOCK K., STERR U. and WILKENS M., *Nucl. Phys. B-Proc. Suppl.*, **166** (2007) 159.
- [19] PARKER T. E., *Metrologia*, **47** (2010) 1.
- [20] ITANO W. M., BERGQUIST J. C., BOLLINGER J. J., GILLIGAN J. M., HEINZEN D. J., MOORE F. L., RAIZEN M. G. and WINELAND D. J., *Phys. Rev. A*, **47** (1993) 3554.
- [21] HINKLEY N., SHERMAN J. A., PHILLIPS N. B., SCHIOPPO M., LEMKE N. D., BELOY K., PIZZOCARO M., OATES C. W. and LUDLOW A. D., *Science*, **341** (2013) 1215.
- [22] HOLZWARTH R., UDEM T., HÄNSCH T. W., KNIGHT J. C., WADSWORTH W. J. and RUSSELL P. S., *Phys. Rev. Lett.*, **85** (2000) 2264.
- [23] JONES D. J., DIDDAMS S. A., RANKA J. K., STENZ A., WINDELER R. S., HALL J. L. and T. C. S., *Science*, **288** (2000) 635.
- [24] RANKA J. K., WINDELER R. S. and STEINZ A. J., *Opt. Lett.*, **25** (2000) 25.
- [25] MA L.-S., BI Z., BARTELS A., ROBERTSSON L., ZUCCO M., WINDELER R. S., WILPERS G., OATES C. W. and DIDDAMS S. A., *Science*, **303** (2004) 1843.
- [26] DIDDAMS S. A., UDEM T., BERGQUIST J. C., CURTIS E. A., DRULLINGER R. E., HOLLBERG L., ITANO W. M., LEE W. D., OATES C. W., VOGEL K. R. and WINELAND D. J., *Science*, **293** (2001) 825.
- [27] DIDDAMS S. A., *J. Opt. Soc. Am. B*, **27** (2010) B51.
- [28] KIPPENBERG T. J., HOLZWARTH R. and DIDDAMS S. A., *Science*, **332** (2011) 555.
- [29] KERSTEN P., MENSING F., STERR U. and RIEHLE F., *Appl. Phys. B*, **68** (1999) 27.
- [30] SHIRLEY J. H., *IEEE Trans. Instr. Meas.*, **46** (1997) 117.
- [31] CHU S., *Rev. Mod. Phys.*, **70** (1998) 685.
- [32] PHILLIPS W., *Rev. Mod. Phys.*, **70** (1998) 721.
- [33] COHEN-TANNOUJJI C., *Rev. Mod. Phys.*, **70** (1998) .
- [34] ANDERSON M. H., ENSHER J. R., MATTHEWS M. R., WIEMAN C. E. and CORNELL E. A., *Science*, **269** (1995) 198.
- [35] DEMARCO B. and JIN D. S., *Science*, **285** (1999) 1703.
- [36] KREMS R., FRIEDRICH B. and STWALLEY W., *Cold Molecules* (CRC Press Inc.) 2009.
- [37] HUMMON M. T., YEO M., STUHL K., COLLOPY A. L., XIA Y. and YE J., *Phys. Rev. Lett.*, **110** (2013) 143001.
- [38] WINELAND D. J., *Science*, **226** (1984) 395.
- [39] WINELAND D. J. and ITANO W. M., *Phys. Today*, **40** (1987) 2.
- [40] DICKE R. H., *Phys. Rev.*, **89** (1953) 472.
- [41] BERGQUIST J. C., ITANO W. M. and WINELAND D. J., *Phys. Rev. A*, **36** (1987) 428.
- [42] SCHIOPPO M., *Development of a transportable strontium optical clock*, Ph.D. thesis, Dipartimento di Fisica e Astronomia, Università di Firenze, Firenze (Dec. 2010).
URL <http://coldatoms.lens.unifi.it/>

- [43] PHILLIPS W. D. and METCALF H., *Phys. Rev. Lett.*, **48** (1982) 596.
- [44] RAAB E. L., PRENTISS M., CABLE A., CHU S. and PRITCHARD D. E., *Phys. Rev. Lett.*, **59** (1987) 2631.
- [45] KUROSU T. and SHIMIZU F., *Jpn. J. Appl. Phys.*, **29** (1990) L2127.
- [46] PHILLIPS W. D., PRODAN J. V. and METCALF H. J., *J. Opt. Soc. Am. B*, **2** (1985) 1751.
- [47] KATORI H., TAKAMOTO M., PAL'CHIKOV V. and OVSIANNIKOV V., *Phys. Rev. Lett.*, (2003) 173005.
- [48] TAKAMOTO M. and KATORI H., *Phys. Rev. Lett.*, **91** (2003) 223001.
- [49] SALOMON C., HILS D. and HALL J. L., *J. Opt. Soc. Am. B*, **5** (1988) 1576.
- [50] YOUNG B., CRUZ F. C., BERGQUIST J. C. and ITANO W. M., *Phys. Rev. Lett.*, **82** (1980) 3799.
- [51] NUMATA K., KEMERY A. and CAMP J., *Phys. Rev. Lett.*, **93** (2004) 250602.
- [52] COLE G. D., ZHANG W., MARTIN M. J., YE J. and ASPELMEYER M., *Nat. Phot.*, **7** (2013) 644.
- [53] KESSLER T., HAGEMANN C., GREBING C., LEGERO T., STERR U., RIEHLE F., MARTIN M. J., CHEN L. and YE J., *Nat. Photonics*, **6** (2012) 687.
- [54] POLI N., DRULLINGER R. E., FERRARI G., PREVEDELLI M., SORRENTINO F., TARALLO M. G. and TINO G. M., *Proc. of SPIE*, **6673** (2007) 66730F.
- [55] DICK G., *Local oscillator induced instabilities in trapped ion frequency clock*, in proc. of *Precise Time and Time Intervals, Redondo Beach (USNO)* 1987, p. 133.
URL <http://tycho.usno.navy.mil/ptti/index.html>
- [56] SANTARELLI G., AUDOIN C., MAKDISSI A., LAURENT P., DICK G. J. and CLAIRON A., *IEEE Trans. Ultrason. Ferroelectr. Freq. Control.*, **45** (1998) 887.
- [57] QUESSADA A., KOVACICH R. P., SANTARELLI G. and LEMONDE P., *J. Opt. B*, **5** (2003) S150.
- [58] KÉFÉLIAN F., JIANG H., LEMONDE P. and SANTARELLI G., *Opt. Lett.*, **34** (2009) 914.
- [59] DREVER R. W. P., HALL J. L., KOWALSKI F. V., HOUGH J., FORD G. M., MUNLEY A. J. and WARD H., *Applied Physics B Photophysics and Laser Chemistry*, **31** (1983) 97.
- [60] FOX R. W., OATES C. W. and HOLLBERG L. W., *Experimental Methods in the Physical Sciences*, **40** (2003) 1.
- [61] CHEN Q. F., NEVSKY A. and SCHILLER S., *Appl. Phys. B*, **107** (2012) 679.
- [62] LUDLOW A., HUANG X. and NOTCUTT M., *Opt. Lett.*, **32** (2007) 641.
- [63] WEBSTER S. and GILL P., *Opt. Lett.*, **36** (2011) 3572.
- [64] LEIBRANDT D. R., THORPE M. J., NOTCUTT M., DRULLINGER R. E., ROSEN BAND T. and BERGQUIST J. C., *Opt. Expr.*, **19** (2011) 3471.
- [65] ARGENCE B., PREVOST E., LÉVEQUE R., LE GOFF R., BIZE S., LEMONDE P. and SANTARELLI G., *Opt. Expr.*, **20** (2012) 25409.
- [66] THORPE M. J., LEIBRANDT D. R. and FORTIER T. M., *Opt. Expr.*, **18** (2010) 18744.
- [67] JIANG Y. Y., LUDLOW A. D., LEMKE N. D., FOX R. W., SHERMAN J. A., MA L. and OATES C. W., *Nat. Phys.*, **5** (2011) 158.
- [68] LODEWYCK J., WESTERGAARD P. G. and LEMONDE P., *Phys. Rev. A*, **79** (2009) 061401(R).
- [69] TAKAMOTO M., TAKANO T. and KATORI H., *Nature Photonics*, **5** (2011) 288.
- [70] BIEDERMANN G. W., TAKASE K., WU X., DESLAURIERS L., ROY S. and KASEVICH M. A., *Phys. Rev. Lett.*, **111** (2013) 170802.
- [71] THORPE M. J., RIPPE L., FORTIER T. M., KIRCHNER M. S. and ROSEN BAND T., *Nat. Phot.*, **5** (2011) 688.
- [72] FOX R. W., SHERMAN J., DOUGLAS W., OLSON J. B., LUDLOW A. D. and OATES C. W., *A high stability optical frequency reference based on thermal calcium atoms*, in proc. of *IEEE International Frequency Control Symposium, IFCS 2012*, pp. 404–406.
- [73] RICHARD J. P. and HAMILTON J. J., *Rev. Sci. Instrum.*, **62** (1991) 2375.
- [74] SEEL S., STORZ R., RUOSO G., MLYNEK J. and SCHILLER S., *Phys. Rev. Lett.*, **78** (1997) 4741.
- [75] KESSLER T., LEGERO T. and STERR U., *J. Opt. Soc. Am. B*, **29** (2012) 178.

- [76] KATORI H., TAKAMOTO M., TAKANO T., USHIJIMA I., OHKUBO T., YAMANAKA K., OHMAE N., ASO Y., SHODA A., USHIBA T., THOUMANY P., DAS M., CHRISTENSEN B. T. R. and AKATSUKA T., *Proc. 2012 IEEE Int. Freq. Control Symp.*, (2012) 56.
- [77] MADEJ A. A. and BERNARD J. E., *Single-ion optical frequency standards and measurement of their absolute optical frequency*, in *Frequency measurement and control: advanced techniques and future trends*, edited by LUITEN A. N., Vol. 79 of *Top. Appl. Phys.* (Springer-Verlag, Berlin) 2000, pp. 153–194.
- [78] MADEJ A., BERNARD J., DUBÉ P., MARMET L. and WINDELER R., *Phys. Rev. A*, **70** (2004) 012507.
- [79] BERKELAND D., MILLER J., BERGQUIST J., ITANO W. and WINELAND D., *Phys. Rev. Lett.*, **80** (1998) 2089.
- [80] VANIER J. and AUDOIN C., *The quantum physics of atomic frequency standards* (IOP Publishing Ltd) 1989.
- [81] DEMTRÖDER W., *Laser Spectroscopy* (Springer) 2008.
- [82] BORDÉ C. J., SALOMON C., AVRILLER S., VAN LERBERGHE A., BREANT C., BASSI D. and SCOLES G., *Phys. Rev. A*, **30** (1984) 1836.
- [83] DEGENHARDT C., STOEHR H., LISDAT C., WILPERS G., SCHNATZ H., LIPPHARDT B., NAZAROVA T., POTTIE P.-E., STERR U., HELMCKE J. and RIEHLE F., *Phys. Rev. A*, **72** (2005) 062111.
- [84] OATES C., WILPERS G. and HOLLBERG L., *Phys. Rev. A*, **71** (2005) 023404.
- [85] DIEDRICH F., BERGQUIST J., ITANO W. and WINELAND D., *Phys. Rev. Lett.*, **62** (1989) 403.
- [86] OSKAY W. H., DIDDAMS S. A., DONLEY E. A., FORTIER T. M., HEAVNER T. P., HOLLBERG L., ITANO W. M., JEFFERTS S. R., DELANEY M. J., KIM K., LEVI F., PARKER T. E. and BERGQUIST J. C., *Phys. Rev. Lett.*, **97** (2006) 020801.
- [87] MIDDELMANN T., FALKE S., LISDAT C. and STERR U., *Phys. Rev. Lett.*, **109** (2012) 263004.
- [88] LUDLOW A., SHERMAN J., LEMKE N., BELOY K., HINKLEY N., PIZZOCARO M., FOX R. and OATES C., *Blackbody effects in the Yb optical lattice clock*, in *proc. of IEEE International Frequency Control Symposium, IFCS 2012*, pp. 311–313.
- [89] SHERMAN J. A., LEMKE N. D., HINKLEY N., PIZZOCARO M., FOX R. W., LUDLOW A. D. and OATES C. W., *Phys. Rev. Lett.*, **108** (2012) 153002.
- [90] FARLEY J. W. and WING W. H., *Phys. Rev. A*, **23** (1981) 23972424.
- [91] PORSEV S. and DEREVIANKO A., *Phys. Rev. A*, **74** (2006) 020502.
- [92] SAFRONOVA M., KOZLOV M. and CLARK C., *Precision calculation of blackbody radiation shifts for metrology at the 18th decimal place*, in *proc. of Conference on Lasers and Electro-Optics: Laser Science to Photonic Applications, CLEO 2011*, pp. 56–61.
- [93] SAFRONOVA M. S., KOZLOV M. G. and CLARK C. W., *IEEE Transactions on Ultrasonics, Ferroelectrics, and Frequency Control*, **59** (2012) 439.
- [94] HACHISU H., MIYAGISHI K., PORSEV S., DEREVIANKO A., OVSIANNIKOV V., PAL'CHIKOV V., TAKAMOTO M. and KATORI H., *Phys. Rev. Lett.*, **100** (2008) 053001.
- [95] JIANG D., ARORA B., SAFRONOVA M. S. and CLARK C. W., *Journal of Physics B: Atomic, Molecular and Optical Physics*, **42** (2009) 154020.
- [96] TAMM C., WEYERS S., LIPPHARDT B. and PEIK E., *Phys. Rev. A*, **80** (2009) 043403.
- [97] HOSAKA K., WEBSTER S. A., STANNARD A., WALTON B. R., MARGOLIS H. S. and GILL P., *Phys. Rev. A*, **79** (2009) 033403.
- [98] KATORI H., TAKAMOTO M., TAKANO T., USHIJIMA I., OHKUBO T., YAMANAKA K., OHMAE N., ASO Y., SHODA A., USHIBA T., THOUMANY P., DAS M., CHRISTENSEN B. and AKATSUKA T., *Prospects for frequency comparison of sr and hg optical lattice clocks toward 10^{-18} uncertainties*, in *proc. of 2012 IEEE International Frequency Control Symposium, IFCS 2012* 2012, pp. 56–61.
- [99] JEFFERTS S., SHIRLEY J., PARKER T., HEAVNER T., MEEKHOF D., NELSON C., LEVI F., COSTANZO G., DEMARCHI A., DRULLINGER R., HOLLBERG L., LEE W. and WALLS F., *Metrologia*, **39** (2002) 321.
- [100] FREDIN-PICARD S., *Metrologia*, **26** (1989) 235.

- [101] STERR U., DEGENHARDT C., STOEHR H., LISDAT C., SCHNATZ H., HELMCKE J., RIEHLE F., WILPERS G., OATES C. and HOLLBERG L., *C.R. Acad. Sci. Paris*, **5** (2004) 845.
- [102] AKATSUKA T., TAKAMOTO M. and KATORI H., *Nat. Phys.*, **4** (2008) 954.
- [103] CHOU C. W., HUME D. B., ROSEN BAND T. and WINELAND D. J., *Science*, **329** (2010) 1630.
- [104] VESSOT R. F. C., LEVINE M. W., MATTISON E. M., BLOMBERG E. L., HOFFMAN T. E., NYSTROM G. U., FARREL B. F., DECHER R., EBY P. B., BAUGHER C. R., WATTS J. W., TEUBER D. L. and WILLS F. D., *Phys. Rev. Lett.*, **45** (1980) 2081.
- [105] KLEPPNER D., *Phys. Today*, **59** (2006) 10.
- [106] SCHILLER S., TINO G. M., GILL P., SALOMON C., STERR U., PEIK E., NEVSKY A., GRITZ A., SVEHLA D., FERRARI G., POLI N., LUSANNA L., KLEIN H., MARGOLIS H., LEMONDE P., LAURENT P., SANTARELLI G., CLAIRON A., ERTMER W., RASEL E., MILLER J., IORIO L., LÄMMERZAHN, DITTUS C. H., GILL, ROTHACHER E. M., FLECHNER F., SCHREIBER U., FLAMBAUM V., NI W., LIU L., CHEN X., CHEN J., GAO K., CACCIAPUOTI L., HOLZWARTH R., HE M. P. and SCHFER W., *Exp. Astron.*, **23** (2009) 573.
- [107] WILPERS G., OATES C. W., DIDDAMS S. D., BARTELS A., FORTIER T. M., OSKAY W. H., BERGQUIST J. C., JEFFERTS S. R., HEAVNER T. P., PARKER T. E. and HOLLBERG L., *Metrologia*, **44** (2007) 146.
- [108] HOLLBERG L., OATES C. W., WILPERS G., HOYT C. W., BARBER Z. W., DIDDAMS S. A., OSKAY W. H. and BERGQUIST J. C., *J. Phys. B*, **38** (2005) S469.
- [109] FRIEBE J., RIEDMANN M., WÜBBENA, PAPE A., KELKAR H., ERTMER W., TERRA O., STERR U., WEYERS S., GROSCHE G., SCHNATZ H. and RASEL E. M., *New J. Phys.*, **13** (2011) 125010.
- [110] HALL J. L., HOLLBERG L., BAER T. and ROBINSON H., *Appl. Phys. Lett.*, **39** (2005) 680.
- [111] YE J., MA L.-S. and HALL J. L., *Phys. Rev. Lett.*, **87** (2001) 270801.
- [112] RAMSEY N. F., *Phys. Rev.*, **76** (1949) 996.
- [113] LETOKHOV V. S. and PAVLIK B. D., *Opt. Spectrosc.*, **32** (1972) 455.
- [114] BAKLANOV Y. V., CHEBOTAYEV V. P. and DUBETSKII B. Y., *Appl. Phys. Lett.*, **11** (1976) 201.
- [115] BERGQUIST J. C., LEE S. A. and HALL J. L., *Phys. Rev. Lett.*, **38** (1976) 159.
- [116] BORDÉ C. J., *Phys. Lett. A*, **140** (1989) 10.
- [117] BORDÉ C. J., SALOMON C., AVRILLIER S., VAN LERBERGHE A., BREANT C., BASSI D. and SCOLES G., *Phys. Rev. A*, **30** (1984) 1836.
- [118] RIEHLE F., WITTE A., KISTERS T. and HELMCKE J., *Appl. Phys. B*, **54** (1992) 333.
- [119] HALL J. L., BORDÉ C. J. and UEHARA K., *Phys. Rev. Lett.*, **37** (1976) 1339.
- [120] MORINAGA A., RIEHLE F., ISHIKAWA J. and HELMCKE J., *Appl. Phys. B*, **48** (1989) 165.
- [121] KISTERS T., ZEISKE K., RIEHLE F. and HELMCKE J., *Appl. Phys. B*, **59** (1994) 89.
- [122] PARTHEY C. G., MATVEEV A., ALNIS J., BERNHARDT B., BEYER A., HOLZWARTH R., MAISTROU A., POHL R., PREDEHL K., UDEM T., WILKEN, T. KOLACHEVSKY N., ABGRALL M., ROVERA D., SALOMON C., LAURENT P. and HÄNSCH T. W., *Phys. Rev. Lett.*, **107** (2011) 203001.
- [123] MATVEEV A., PARTHEY C. G., PREDEHL K., ALNIS J., BEYER A., HOLZWARTH R., UDEM T., WILKEN T., KOLACHEVSKY N., ABGRALL M., ROVERA D., SALOMON C., LAURENT P., GROSCHE G., TERRA O., LEGERO T., SCHNATZ H., WEYERS S., ALTSCHUL B. and HÄNSCH T. W., *Phys. Rev. Lett.*, **110** (2013) 230801.
- [124] KATORI H., IDO T., ISOYA Y. and KUWATA-GONOKAMI M., *Phys. Rev. Lett.*, **82** (1999) 1116.
- [125] VOGEL K. R., DINEEN T. P., GALLAGHER A. and HALL J. L., *IEEE Trans. Instrum. Meas.*, **48** (1999) 618.
- [126] BINNEWIES T., WILPERS G., STERR U., RIEHLE F., HELMCKE J., MEHLSTAÜBLER T., RASEL E. M. and ERTMER W., *Phys. Rev. Lett.*, **87** (2001) 123002.
- [127] CURTIS E. A., OATES C. W. and HOLLBERG L., *J. Opt. Soc. Am. B*, **20** (2003) 977.

- [128] BARGER R. L., BERGQUIST J. C., ENGLISH T. C. and GLAZE D. J., *Appl. Phys. Lett.*, **34** (2003) 850.
- [129] BARGER R. L., *Opt. Lett.*, **6** (1980) 145.
- [130] ZIBROV A. S., FOX R. W., ELLINGSEN R., WEIMER C. S., VELICHANSKY V. L., TINO G. M. and HOLLBERG L., *Appl. Phys. B*, **59** (1994) 327.
- [131] MORINAGA A., ITO N. and SAKURAI T., *Appl. Phys. B*, **54** (1992) 29.
- [132] KRAFT S., VOGT F., APPEL O., RIEHLE F. and STERR U., *Phys. Rev. Lett.*, **103** (2009) 130401.
- [133] OATES C. W., CURTIS E. A. and HOLLBERG L., *Opt. Lett.*, **25** (2000) 1603.
- [134] ITANO W. M., BERGQUIST J. C., HULET R. G. and WINELAND D. J., *Phys. Rev. Lett.*, **59** (1987) 2732.
- [135] OATES C. W., BONDU F., FOX R. W. and HOLLBERG L., *Eur. Phys. J. D*, **7** (1999) 449.
- [136] XIE X.-P., ZHUANG W. and CHEN J.-B., *Chin. Phys. Lett.*, **27** (2010) .
- [137] STERR U., SENGSTOCK K., MÜLLER J. H., BETTERMANN D. and ERTMER W., *Appl. Phys. B*, **54** (1992) 341.
- [138] KEUPP J., DOUILLET A., MEHLSTAÜBLER T. E., REHBEIN N., RASEL E. M. and ERTMER W., *Eur. Phys. J. D*, **36** (2005) 289.
- [139] MEHLSTAÜBLER T. E., MOLDENHAUER K., RIEDMANN M., REHBEIN N., FRIEBE J., RASEL E. M. and ERTMER W., *Phys. Rev. A*, **77** (2008) 021402(R).
- [140] RÜHMANN S., RIEDMANN M., WÜBBENA T., KULOSA A., PAPE A., FIM D., ZIPFEL K., LAMPMANN B., FRIEBE J., KEIKAR H., ERTMER W. and RASEL E. M., *Towards a magnesium optical lattice clock*, presented at *CLEO Europe/EQEC* 2011.
- [141] NICHOLSON T. L., MARTIN M. J., WILLIAMS J. R., BLOOM B. J., SWALLOWS M., CAMPBELL S. L. and YE J., *Phys. Rev. Lett.*, **109** (2012) 230801.
- [142] PORSEV S. G., DEREVIANKO A. and FORTSON E. N., *Phys. Rev. A*, **69** (2004) 021403(R).
- [143] TAKAMOTO M., KATORI H., MARMO S. I., OVSIANNIKOV V. D. and PAL'CHIKOV V. G., *Phys. Rev. Lett.*, **102** (2009) 063002.
- [144] KATORI H., *Nature Photonics*, **5** (2011) 203.
- [145] BRUSCH A., LE TARGAT R., BAILLARD X., FOUCHÉ M. and LEMONDE P., *Phys. Rev. Lett.*, **96** (2006) 103003.
- [146] TAICHENACHEV A. V., YUDIN V. I., OVSIANNIKOV V. D., PAL'CHIKOV V. G. and OATES C. W., *Phys. Rev. Lett.*, **101** (2008) 193601.
- [147] TAICHENACHEV A. V., YUDIN V. I., OATES C. W., HOYT C. W., BARBER Z. W. and HOLLBERG L., *Phys. Rev. Lett.*, **96** (2006) 083001.
- [148] TINO G. M., BARSANTI M., DE ANGELIS M., GIANFRANI L. and INGUSCIO M., *Appl. Phys. B*, **55** (1992) 397.
- [149] FERRARI G., CANCIO P., DRULLINGER R., GIUSFREDI G., POLI N., PREVEDELLI M., TONINELLI C. and TINO G. M., *Phys. Rev. Lett.*, **91** (2003) 243002.
- [150] LOFTUS T. H., IDO T., BOYD M. M., LUDLOW A. D. and YE J., *Phys. Rev. A*, **70** (2004) 063413.
- [151] MUKAIYUMA T., KATORI H., IDO T., LI Y. and KUWATA-GONOKAMI M., *Phys. Rev. Lett.*, **90** (2003) 113002.
- [152] BAILLARD X., FOUCHÉ M., LE TARGAT R., WESTERGAARD P. G., LECALLIER A., CHAPELET F., ABGRALL M., ROVERA G. D., LAURENT P., ROSENBUSCH P., BIZE S., SANTARELLI G., CLAIRON A., LEMONDE P., GROSCHE G., LIPPARDT B. and SCHNATZ H., *Eur. Phys. J. D*, **48** (2008) 11.
- [153] POLI N., TARALLO M. G., SCHIOPPO M., OATES C. W. and TINO G. M., *Appl. Phys. B*, **97** (2009) 27.
- [154] CLAIRON A., LAURENT P., SANTARELLI G., GHEZALI S., LEA S. and BAHOURA M., *IEEE Trans. Instr. Meas.*, **44** (1995) 128.
- [155] WINELAND D. J., ITANO W. M., BERGQUIST J. C. and HULET R. G., *Phys. Rev. A*, **36** (1987) 2220.
- [156] BOYD M. M., ZELEVINSKY T., LUDLOW A. D., BLATT S., ZANON-WILLETTE T., FOREMAN S. M., CAMPBELL G. K. and YE J., *Phys. Rev. A*, **76** (2007) 022510.

- [157] LE TARGAT R., LORINI L., LE COQ Y., ZAWADA M., GUENA J., ABGRALL M., GUROV M., ROSENBUSCH P., ROVERA D. G., NAGORNY B., GARTMAN R., WESTERGAARD P. G., TOBAR M. E., LOURS M., SANTARELLI G., CLAIRON A., BIZE S., LAURENT P., LEMONDE P. and LODEWYCK J., *Nat. Commun.*, **4** (2013) 2109.
- [158] CAMPBELL G. K., LUDLOW A. D., BLATT S., THOMSEN J. W., MARTIN M. J., DE MIRANDA M. H. G., ZELEVINSKY T., BOYD M. M., YE J., DIDDAMS S. A., HEAVNER T. P., PARKER T. E. and JEFFERTS S. R., *Metrologia*, **45** (2008) 539.
- [159] HONG F.-L., MUSHI M., TAKAMOTO M., INABA H., YANAGIMACHI S., TAKAMIZAWA A., WATABE K., IKEGAMI T., IMAE M., FUJII Y., AMEMIYA M., NAKAGAWA K., UEDA K. and KATORI H., *Opt. Lett.*, **34** (2009) 692.
- [160] YAMAGUCHI A., SHIGA N., NAGANO S., LI Y., ISHIJIMA H., HACHISU H., KUMAGAI M. and IDO T., *Appl. Phys. Expr.*, **5** (2012) 022701.
- [161] FALKE S., SCHNATZ H., WINFRED J. S. R. V., MIDDELMANN T., VOGT S., WEYERS S., LIPPHARDT B., GROSCHE G., RIEHLE F., STERR U. and LISDAT C., *Metrologia*, **48** (2011) 399.
- [162] BAILLARD X., FOUCHÉ M., LE TARGAT R., WESTERGAARD P. G., LECALLIER A., LE COQ Y., ROVERA G. D., BIZE S. and LEMONDE P., *Opt. Lett.*, **32** (2007) 1812.
- [163] LUDLOW A. D., ZELEVINSKY T., CAMPBELL G. K., BLATT S., BOYD M. M., DE MIRANDA M. H. G., MARTIN M. J., THOMSEN J. W., FOREMAN S. M., YE J., FORTIER T. M., STALNAKER J. E., DIDDAMS S. A., LE COQ Y., BARBER Z. W., POLI N., LEMKE N. D., BECK K. M. and OATES C. W., *Science*, **319** (2008) 1805.
- [164] YAMAGUCHI A., FUJIEDA M., KUMAGAI M., HACHISU H., NAGANO S., LI Y., IDO T., TAKANO T., TAKAMOTO M. and KATORI H., *Appl. Phys. Expr.*, **4** (2011) 082203.
- [165] WESTERGAARD P., LODEWYCK J., LORINI L., LECALLIER A., BURT E., ZAWADA M., MILLO J. and LEMONDE P., *Phys. Rev. Lett.*, **106** (2011) 210801.
- [166] LISDAT C., VELLORE WINFRED J. S. R., MIDDELMANN T., RIEHLE F. and STERR U., *Phys. Rev. Lett.*, **103** (2009) 090801.
- [167] CAMPBELL G. K., BOYD M. M., THOMSEN J. W., MARTIN M. J., BLATT S., SWALLOWS M. D., NICHOLSON T. L., FORTIER T., OATES C. W., DIDDAMS S. A., LEMKE N. D., NAIDON P., JULIENNE P., YE J. and LUDLOW A. D., *Science*, **324** (2009) 360.
- [168] BISHOP M., LIN Y., SWALLOWS M. D., GORSHIKOV A. V., YE J. and REY A. M., *Phys. Rev. Lett.*, **106** (2011) 250801.
- [169] SAFRONOVA M. S., PORSEV S. G., SAFRONOVA U. I., KOZLOV M. G. and CLARK C. W., *Phys. Rev. A*, **87** (2013) 012059.
- [170] SCHILLER S., GRITZ A., NEVSKY A., ALIGHANBARI S., VASILYEV S., ABOU-JAUDEH C., MURA G., FRANZEN T., STERR U., FALKE S., LISDAT C., RASEL E., KULOSA A., BIZE S., LODEWYCK J., TINO G. M., POLI N., SCHIOPPO M., BONGS K., SINGH Y., GILL P., BARWOOD G., OVCHINNIKOV Y., STUHLER J., KAENDERS W., BRAXMAIER C., HOLZWARTH R., DONATI A., LECOMTE S., CALONICO D. and LEVI F., *The space optical clocks project: Development of high-performance transportable and breadboard optical clocks and advanced subsystems*, in *Lets embrace space*, edited by UNION E., Vol. II (European Union, Luxembourg: Publications Office of the European Union, 2012) 2012, Ch. 45, pp. 452–463.
- [171] TSIGUTKIN K., DOUNAS-FRAZER D., FAMILY A., STALNAKER J. E., YASHCHUK V. V. and BUDKER D., *Phys. Rev. Lett.*, **103** (2009) 071601.
- [172] FUKUHARA T., SUGAWA S. and TAKAHASHI Y., *Phys. Rev. A*, **76** (2007) 051604.
- [173] PARK C. Y. and YOON T. H., *Phys. Rev. A*, **68** (2003) 055401.
- [174] MARUYAMA R., WYNAR R. H., ROMALIS M. V., ANDALKAR A., SWALLOW M. D., PEARSON C. E. and FORTSON E. N., *Phys. Rev. A*, **68** (2003) 011403.
- [175] HOYT C. W., BARBER Z. W., OATES C. W., FORTIER T. M., DIDDAMS S. D. and HOLLBERG L., *Phys. Rev. Lett.*, **95** (2005) 083003.
- [176] KOHNO T., YASUDA M., HOSAKA K., INABA H., NAKAJIMA Y. and HONG F.-L., *Appl. Phys. Expr.*, **2** (2009) 072501.

- [177] NEVSKY A. Y., BRESSEL U., ERNSTING I., EISELE C., OKHAPKIN M., SCHILLER S., GUBENKO A., LIVSHITS D., MIKHRIN S., KRESTNIKOV I. and KOVSH A., *Appl. Phys. B*, **92** (2008) 501.
- [178] PIZZOCARO M., COSTANZO G., GODONE A., LEVI F., MURA A., ZOPPI M. and CALONICO D., *IEEE Trans. Ultrason. Ferroelectr. Freq. Control.*, **59** (2012) 426.
- [179] JIANG H., LI G. and XU X., *Opt. Express*, **17** (2009) 16073.
- [180] BARBER Z. W., HOYT C. W., OATES C. W. and HOLLBERG L., *Phys. Rev. Lett.*, **96** (2006) 083002.
- [181] POLI N., BARBER Z. W., LEMKE N. D., OATES C. W., MA L. S., STALNAKER J. E., FORTIER T. M., DIDDAMS S. A., HOLLBERG L., BERGQUIST J. C., BRUSCH A., JEFFERTS S., HEAVNER T. and PARKER T., *Phys. Rev. A*, **77** (2008) 050501.
- [182] LEMKE N. D., LUDLOW A. D., BARBER Z. W., FORTIER T. M., DIDDAMS S. A., JIANG Y., JEFFERTS S. R., HEAVNER T. P., PARKER T. E. and OATES C. W., *Phys. Rev. Lett.*, **103** (2009) 063001.
- [183] PARK C. Y., YU D. H., LEE W. K., PARK S. E., KWON T. Y., BUM S.-B. and MUN J., *Development of ¹⁷¹Yb optical lattice clock at KRISS*, in proc. of *Conference of Precision Electromagnetic Measurements* (IEEE, 345 E 47TH ST, NEW YORK, NY 10017 USA) 2012, pp. 616–617.
- [184] BARBER Z. W., STALNAKER J. E., LEMKE N. D., POLI N., OATES C. W., FORTIER T. M., DIDDAMS S. D., HOLLBERG L. and HOYT C. W., *Phys. Rev. Lett.*, **100** (2008) 103002.
- [185] LEMKE N. D., VON STECHER J., SHERMAN J. A., REY A. M., OATES C. W. and LUDLOW A. D., *Phys. Rev. Lett.*, **107** (2011) 103902.
- [186] LUDLOW A. D., LEMKE N. D., SHERMAN J. A., OATES C. W., QUÉMÉNER G., VON STECHER J. and REY A. M., *Phys. Rev. Lett.*, **107** (2011) 103902.
- [187] BELOY K., LEMKE N. D., HINKLEY N., FOX R. W., LUDLOW A. D. and OATES C. W., *Phys. Rev. A*, **86** (2012) 051404(R).
- [188] SAFRONOVA M. S., PORSEV S. G. and CLARK C. W., *Phys. Rev. Lett.*, **109** (2012) 230802.
- [189] SANTARELLI C., LAURENT P., LEMONDE P., CLAIRON A., MANN A., CHANG S., LUITEN A. and SALOMON C., *Phys. Rev. Lett.*, **82** (1999) 4619.
- [190] MCFERRAN J., YI L., MEJRI S., DI MANNO S., ZHANG W., GUÉNA J., LE COQ Y. and BIZE S., *Phys. Rev. Lett.*, **108** (2012) 1.
- [191] YI L., MEJRI S., MCFERRAN J. J., LE COQ Y. and BIZE S., *Phys. Rev. Lett.*, **106** (2011) 073005.
- [192] MCFERRAN J. J., MAGALHAES D. V., MANDACHE C., MILLO J., ZHANG W., LE COQ Y., SANTARELLI G. and BIZE S., *Opt. Lett.*, **37** (2012) 3477.
- [193] FISCHER E., *Z. Phys.*, **156** (1959) 1.
- [194] SCHRAMA C., PEIK E., SMITH W. and WALTHER H., *Opt. Commun.*, **101** (1993) 32.
- [195] PRESTAGE J. D., DICK G. J. and MALEKI L., *J. Appl. Phys.*, **66** (1989) 1013.
- [196] CHWALLA M., BENHELM J., KIM K., KIRCHMAIR G., MONZ T., RIEBE M., SCHINDLER P., VILLAR A., HÄNSEL W., ROOS C., BLATT R., ABGRALL M., SANTARELLI G., ROVERA G. and LAURENT P., *Phys. Rev. Lett.*, **102** (2009) 023002.
- [197] WILPERS G., SEE P., GILL P. and SINCLAIR A. G., *Nat. Nanotechnol.*, **7** (2012) 572.
- [198] BROWNNUTT M., LETCHUMANAN V., WILPERS G., THOMPSON R., GILL P. and SINCLAIR A., *Appl. Phys. B*, **87** (2007) 411.
- [199] DEHMELT H. G., *IEEE Trans. Instrum. Meas.*, **M-31** (1982) 83.
- [200] BARWOOD G. P., GILL P., HUANG G. and KLEIN H. A., *Meas. Sci. Tech.*, **23** (2012) 055201.
- [201] STALNAKER J., DIDDAMS S., FORTIER T., KIM K., HOLLBERG L., BERGQUIST J., ITANO W., DELANY M., LORINI L., OSKAY W., HEAVNER T., JEFFERTS S., LEVI F., PARKER T. and SHIRLEY J., *Appl. Phys. B*, **89** (2007) 167.
- [202] BARWOOD G., GILL P., HUANG G. and KLEIN H., *IEEE Trans. Instrum. Meas.*, **56** (2007) 226.
- [203] DUBÉ P., MADEJ A. A., ZHOU Z. and BERNARD J. E., *Phys. Rev. A*, **87** (2013) 023806.

- [204] DUBÉ P., MADEJ A., BERNARD J., MARMET L., BOULANGER J.-S. and CUNDY S., *Phys. Rev. Lett.*, **95** (2005) 033001.
- [205] MITROY J., SAFRONOVA M. S. and CLARK C. W., *J. Phys. B: At. Mol. Opt. Phys.*, **43** (2010) 202001.
- [206] MADEJ A. A., DUBÉ P., ZHOU Z., BERNARD J. E. and GERTSVOLF M., *Phys. Rev. Lett.*, **109** (2012) 203002.
- [207] MARGOLIS H. S., BARWOOD G. P., HUANG G., KLEIN H. A., LEA S. N., SZYMANIEC K. and GILL P., *Science*, **306** (2004) 1355.
- [208] MATSUBARA K., HACHISU H., LI Y., NAGANO S., LOCKE C., NOGAMI A., KAJITA M., HAYASAKA K., IDO T. and HOSOKAWA M., *Opt. Expr.*, **20** (2012) 22034.
- [209] ROBERTS M., TAYLOR P., BARWOOD G. P., ROWLEY W. R. C. and GILL P., *Phys. Rev. A*, **62** (2000) 020501.
- [210] HUNTEMANN N., OKHAPKIN M., LIPPHARDT B., WEYERS S., TAMM C. and PEIK E., *Phys. Rev. Lett.*, **108** (2012) 090801.
- [211] KING S. A., GODUN R. M., WEBSTER S. A., MARGOLIS H. S., JOHNSON L. A. M., SZYMANIEC K., BAIRD P. E. G. and GILL P., *New J. Phys.*, **14** (2012) 013045.
- [212] HOSAKA K., WEBSTER S., BLYTHE P., STANNARD A., BEATON D., MARGOLIS H., LEA S. and GILL P., *IEEE Trans. Instrum. Meas.*, **54** (2005) 759.
- [213] BLYTHE P. J., WEBSTER S., HOSAKA K. and GILL P., *J. Phys. B: At. Mol. Opt. Phys.*, **36** (2003) 981.
- [214] HUNTEMANN N., LIPPHARDT B., OKHAPKIN M., TAMM C., PEIK E., TAICHENACHEV A. V. and YUDIN V. I., *Phys. Rev. Lett.*, **109** (2012) 213002.
- [215] ITANO W. M., *J. Res. Nat. Inst. Stand. Technol.*, **105** (2000) 829.
- [216] ROSEN BAND T., SCHMIDT P., HUME D., ITANO W., FORTIER T., STALNAKER J., KIM K., DIDDAMS S., KOELEMEL J., BERGQUIST J. and WINELAND D., *Phys. Rev. Lett.*, **98** (2007) 220801.
- [217] VON ZANTHIER J., BECKER T., EICHENSEER M., NEVSKY A. Y., SCHWEDES C., PEIK E., WALTHER H., HOLZWARTH R., REICHERT J., UDEM T., HÄNSCH T. W., POKASOV P. V., SKVORTSOV M. N. and BAGAYEV S. N., *Opt. Lett.*, **25** (2000) 1729.
- [218] BECKER T., ZANTHIER J. and NEVSKY A., *Phys. Rev. A*, **63** (2001) 051802.
- [219] LIU T., WANG Y. H., ELMAN V., STEJSKAL A., ZHAO Y. N., ZHANG J., LU Z. H., WANG L. J., DUMKE R., BECKER T. and WALTHER H., *Proc. 2010 IEEE Int. Freq. Control Symp.*, (2007) 407.
- [220] MA L.-S., JUNGNER P., YE J. and HALL J. L., *Opt. Lett.*, **19** (1994) 1777.
- [221] DAUSSY C., LOPEZ O. and AMY-KLEIN A., *Phys. Rev. Lett.*, **94** (2005) 203904.
- [222] PREDEHL K., GROSCHE G., RAUPACH S. M. F., DROSTE S., TERRA O., ALNIS J., LEGERO T., HÄNSCH T. W., UDEM T., HOLZWARTH R. and SCHNATZ H., *Science*, **336** (2012) 441.
- [223] FUJIEDA M., KUMAGAI M., NAGANO S., YAMAGUCHI A., HACHISU H. and IDO T., *Opt. Expr.*, **19** (2011) 16498.
- [224] LEVI F., AMBROSINI R., CALONICO D., CALOSSO C. E., CLIVATI C., COSTANZO G., DENATALE P., GALZERANO G., MAZZOTTI D., MURA A., POLI N., TINO G. M. and ZUCCO M., *LIFT: The italian fiber network for frequency and time distribution*, in proc. of *Joint UFFC, EFTF and PFM Symposium, 21-25 July, Prague (CZ)* (IEEE, 345 E 47TH ST, NEW YORK, NY 10017 USA), pp. 477–480.
- [225] GIORGETTA F. R., SWANN W. C., SINCLAIR L. C., BAUMANN E., CODDINGTON I. and NEWBURY N. R., *Nat. Photon.*, **7** (2011) 434.
- [226] See for example the STE-QUEST Mission Proposal document.
URL <http://sci.esa.int/ste-quest/>
- [227] See for example the mission web site.
URL http://www.nasa.gov/mission_pages/tdm/clocks/
- [228] FORTIER T. M., KIRCHNER M. S., QUINLAN F., TAYLOR J., BERGQUIST J. C., ROSEN BAND T., LEMKE N., LUDLOW A., JIANG Y., OATES C. W. and DIDDAMS S. D., *Nat. Phot.*, **5** (2011) 425.

- [229] YCAS G. G., QUINLAN F., DIDDAMS S. D., OSTERMAN S., MAHADEVAN S., REDMAN S., TERRIEN R., RAMSEY L., BENDER C. F., BOTZER B. and SIGURDSSON S., *Opt. Express*, **20** (2012) 6631.
- [230] BLATT S., LUDLOW A. D., CAMPBELL G. K., THOMSEN J. W., ZELEVINSKY T., BOYD M. M., YE J., BAILLARD X., FOUCHÉ M., LE TARGAT R., BRUSCH A., LEMONDE P., TAKAMOTO M., HONG F.-L., KATORI H. and FLAMBAUM V. V., *Phys. Rev. Lett.*, **100** (2008) 140801.
- [231] CRONIN A. D., SCHMIEDMAYER J. and PRITCHARD D., *Rev. Mod. Phys.*, **81** (2009) 1051.
- [232] TINO G. M. and KASEVICH M. A. (Eds.), *Atom Interferometry*, Proceedings of the International School of Physics “Enrico Fermi”, Course CLXXXVIII, Varenna 2013 (Società Italiana di Fisica and IOS Press) To be published.
- [233] GRAHAM P. W., HOGAN J. M., KASEVICH M. A. and RAJENDRAN S., *Phys. Rev. Lett.*, **110** (2013) 171102.
- [234] *Special issue on “Gravitational waves detection with atom interferometry”*, in *Gen. Relativ. Gravit.*, edited by TINO G. M., VETRANO F. and LÄMMERZAHN C., Vol. 43 2011, pp. 1901–2088.
- [235] DZUBA V. A., DEREVIANKO A. and FLAMBAUM V. V., *Phys. Rev. A*, **86** (2012) 054501.
- [236] BERENGUT J. C., DZUBA V. A., FLAMBAUM V. V. and ONG A., *Phys. Rev. Lett.*, **109** (2012) .
- [237] KANDULA D., GOHLE C., PINKERT T., UBACHS W. and EIKEMA K., *Phys. Rev. Lett.*, **105** (2010) .
- [238] ÇINGÖZ A., YOST D. C., ALLISON T. K., RUEHL A., FERMANN M. E., HARTL I. and YE J., *Nature*, **482** (2012) 68.
- [239] CAMPBELL C. J., RADNAEV A. G., KUZMICH A., DZUBA V. A., FLAMBAUM V. V. and DEREVIANKO A., *Phys. Rev. Lett.*, **108** (2012) 120802.
- [240] PEIK E. and TAMM C., *EuroPhys. Lett.*, **61** (2003) 181.
- [241] RELLERGERT W. G., DEMILLE D., GRECO R. R., HEHLEN M. P., TORGERSON J. R. and HUDSON E. R., *Phys. Rev. Lett.*, **104** (2010) 200802.
- [242] KAZAKOV G. A., LITVINOV A. N., ROMANENKO V. I., YATSENKO L. P., ROMANENKO A. V., SCHREITL M., WINKLER G. and SCHUMM T., *New Jour. Phys.*, **14** (2012) 083019.
- [243] ZHAO X., MARTINEZ DE ESCOBAR Y. N., RUNDBERG R., BOND E. M., MOODY A. and VIEIRA D. J., *Phys. Rev. Lett.*, **109** (2012) 160801.
- [244] PORSEV S. G., FLAMBAUM V. V., PEIK E. and TAMM C., *Phys. Rev. Lett.*, **105** (2010) 182501.